Forests through the Eye of a Satellite: Understanding regional forest-cover dynamics using Landsat Imagery

By

Matthias Baumann

A dissertation submitted in partial fulfillment of

the requirements for the degree of

Doctor of Philosophy

(Forestry)

at the

UNIVERSITY OF WISCONSIN-MADISON

2013

Date of final oral examination: 12/06/2013

The dissertation is approved by the following members of the Final Oral Committee:
Mutlu Ozodgan, Assistant Professor, Forestry
Volker C. Radeloff, Professor, Forestry
Stith T. Gower, Professor, Forestry
Murray K. Clayton, Professor, Plant Pathology
Chengquan Huang, Assistant Professor, University of Maryland, Geography

Acknowledgements

My name is the only one that is written on the front page of this dissertation, but there are so many people I have to thank because without their support finishing this thesis would not have been possible.

Mutlu Ozdogan and *Volker Radeloff*, who guided me with patience and enthusiasm through the past years. Thank you for always letting me develop my own research interests and for all your countless scientific and non-scientific advice you gave me over the past years. *Mutlu*, thank you for your support in developing as a scientist with attention to detail and your excitement for new ideas to solve the challenges we faced during the past years. I am grateful for all the hours we sat over numbers and distribution which ultimately yielded this dissertation. *Volker*, I can't tell you how much I enjoyed being in your research group and how much I took from our weekly talks, whether they happened in your office or during walks along Lakeshore Path. Thank you for sharing all your scientific experience with me, but even more for your non-scientific advice, especially when things did not went so smoothly for me. It is hard to find words for how much that meant to me.

My committee members *Chengquan Huang, Murray Clayton* and *Tom Gower*. Thank you for joining me on the PhD journey and I am thankful for the valuable discussions and feedback you provided.

The *SILVIS-Lab*, for providing me a great environment. *Dave, Shelley* and *Glen*: thank you for always being there no matter how small the problem was, and also for not kicking me out when I came into your office to talk about non-work-related things.

Eric, *Brooke, Jess, Nick, Sebastian, Sarah, Catalina, Naparat*: thank you for all the fun we had at work or over many alcoholic beverages. *Van Butsic*, for all I learned from you while working with you in the Congo, but even more over adult beverages and at the Bierkie.

Dima Aksenov, *Elena Esipova* and the crew from *Greenpeace Russia* for data exchange and for your support during field visits

My parents, *Helga* and *Peter Baumann*, and my sisters *Kirsten, Katrin* and *Judith Baumann*, who were sitting on the other side of the Atlantic Ocean. Without their love and their understanding for me to be that far away for so long it would have been hard to finish this.

Chris and *James*, my two true friends during my time here in Madison. From day one, going to work was even more exciting knowing that there will be a lot of laughter at work. *Chris*, except for signing up for the Ironman you joined me for almost everything no matter how stupid the idea was; and on top of that you provided me a home here in Madison. I hope I can host you in my hometown Berlin soon and take you for a travel around Germany. *James*, I will miss your world-class fantasy Smack Talk and your dislike of good German Pilsener. I'm thankful to have you as my friend and office mate and I'm glad I could introduce you a little into my world of working.

Nils and Jens Vortmann, my best friends in Germany who came to visit me here in Madison and always kept me up-to-date with everything that happens in Germany. I am looking forward living closer to you and being able to visit you more frequently.

Siegfried Schmidt, who always made sure my work would not take over my life but who encouraged me to compete twice in the Ironman here in Madison.

Tobias Kuemmerle, who was a main factor why I pursued this PhD at UW-Madison. Thanks for all our discussions and I am looking forward working with you again and also revive our soccer rivalries.

Lastly, I would like to express my gratefulness to the person, who made my life here in Madison so much better. *Erica*: things haven't worked out yet how we were dreaming initially. But I am looking forward to what's to come and no matter what it will be I want you to know that without you my time here in Madison would not have been nearly as nice and enjoyable and this thesis not as good. Thank you!

Table of Contents:

List of Figures: ix

List of Tables: xiii

Forests through the Eye of a Satellite: Exploring the Forests in Russia and the United States using Landsat imagery. 1

Introduction 1

Background chapter 1: Socio-economic shocks and forest-cover change 2

Background chapter 2: Disturbance type mapping with remote sensing 5

Background chapter 3: Remote sensing of green-leaf phenology 7

Executive summaries 9

Chapter 1: Using the Landsat record to detect forest-cover changes during and after the collapse of the Soviet Union in the temperate zone of European Russia 9

Chapter 2: Landsat remote sensing of forest windfall disturbance. 12

Chapter 3: Modeling green-leaf phenology using Dynamic Time Warping and all available Landsat data 15

Overall Significance 17

References 19

Chapter 1: Using the Landsat record to detect forest-cover changes during and after the collapse of the Soviet Union in the temperate zone of European Russia 33

Abstract: 33
Introduction 35
Study Area 40
Data and Methods 41
Data and pre-processing 41
Training and image classification 43
Analysis of forest-cover change 48
Results 49
Discussion 52
Conclusions 58
References 60
Figure Captions 69
Tables 71
Chapter 2: Landsat remote sensing of forest windfall disturbance 87
Abstract: 87
Introduction 89
Methods 92
Study Area 92
Image pre-processing 93

Forest/Non-Forest classification 94

Forest disturbance detection 96

Detecting windfall disturbance 97

Accuracy assessment 99

Results 100

Discussion 103

References 108

Figure Captions 119

Tables 121

Chapter 3: Modeling green-leaf phenology using Dynamic Time Warping and all available Landsat data 139

Abstract: 139

Introduction 141

Methods 146

Study area and datasets 146

Dynamic Time Warping to create a Landsat phenology 146

Time-series comparison 149

Results 150

Discussion 152

References 157

Figure Captions 164

Tables 167

List of Figures:

Figure 1: The temperate zone of European Russia with its administrative deviation, and the Landsat footprints, selected for classification.

Figure 2: Area estimates, summarized and averaged across all 12 footprints. The top diagram indicates the overall area at each time step in km2, including the absolute areas of forest disturbance and forest recovery. The bottom diagram shows the net change of forested areas in km2 to the previous time-step.

Figure 3: Forest area estimates for each footprint. The top diagram indicates the overall area at each time step in km2, including the absolute areas of forest disturbance and forest recovery. The bottom diagram shows the net change of forested areas in km2 to the previous time-step.

Figure 4: Rates of forest disturbance and forest recovery per time period (left and middle column), and relative net change (RNC) of forested area over the entire observation period, aggregated at the district level.

Figure 5: Difference in classification accuracies after adding a winter-image when image acquisition was sub-optimal.

Figure 6: Forest-cover change map for footprint 176021 (Vladimir region) for 1985-2010

Figure 7: Locations where the windfall classification method was tested. Study site 1 is located in the temperate zone of European Russia; study site 2 is located in the Greater Border Lake Region in northeast Minnesota (USA).

Figure 8: Schematic representation training data collection strategy for the windfall classification. The data in the histogram represent values of the validation data of the Russian study site for the band-5 reflectance.

Figure 9: Classification results for the Russia site (left) and the U.S. site (right). For both study locations, examples are presented of areas characterized primarily by windfall disturbance (177019A and 026027A), and areas primarily characterized by clear-cut harvest (177019B and 026027B).

Figure 10: Validation of the training data to classify disturbance areas into 'windfall' and 'clear-cut harvest' in the spectral feature space in which they were generated.

Figure 11: Proportion of correctly classified disturbance patches by patch size for the two classes, 'windfall' and 'clear-cut harvest', and the two classes combined. The top row represents the Russian site (footprint 177019), the bottom row the U.S. site (footprint 026027). The data presented are binned data with a bin width of 0.5 ha. Every bin was subdivided into six groups with 0.09 ha increments in patch size (i.e., increments of one Landsat pixel). The point represent the mean proportion correctly classified polygons across sub-groups in each bin, the error bars represent the standard deviation. The colors represent the number of polygons in every bin.

Figure 12: Misclassified disturbance site. Classification results suggest that the disturbance is caused by harvest. Validation data reveal that the site is caused by windfall.

Figure 13: Example of the three phenology-profiles (Landsat, PhenoCam and MODIS) and the estimation strategy of the keydates. The top row represents the EVI/ExGm time

series, whereas the middle and bottom row represent the first and second derivative of the phenology-profiles. The keydates are (chronologically with the year): green-up date (GU, red line), Start-of-Season date (SoS, blue line), Maturity date (Mat, orange line), Senescence date (Sen, green line), the End-of-Season date (EoS, light blue line), and Dormancy date (Dorm, yellow line). The example represents the Mammothcave study site for the year 2012.

Figure 14: Comparison of the Landsat-time series 'unwarped' vs. 'warped', the example is the Mammothcave study site for the year 2012. The red dots are Landsat EVI values from 2012, the grey dots indicate Landsat EVI data from all other years that got time-warped to the reference year. The black line represents the MODIS EVI from the reference year 2012.

Figure 15: Scatterplots and correlation coefficients to assess the differences in the keydates between Landsat and PhenoCam time series (top), and Landsat and MODIS time series (bottom). All points represent one year of analysis at one study site. The colors represent the different study sites.

Figure 16: Differences in estimated keydates at the different study sites. The top row represents the Landsat-MODIS comparison, the bottom row the Landsat-PhenoCam comparison. The points describe the mean difference in estimated keydates across all years that were analyzed at each particular study sites. The error bars show the standard deviation of the keydate estimations.

Figure 17: Example of daily EVI time series between 2003 and 2012 at the Mammothcave study site. The EVI maps represent a 500x500 pixel subset around the

location of the PhenoCam on day of year 200. The EVI curves represent the modeled phenology for Landsat and PhenoCam at the PhenoCam location.

Figure 18: Comparison of the MODIS phenology and the newly generated Landsat phenology. Presented are the estimated keydates GU, SoS, Mat (left column top to bottom) and Sen, EoS and Dorm (right column). In addition, the phenology at the approximate location of the PhenoCam is presented. The example shows the case of the Mammothcave study region for the year 2012

List of Tables:

Table 1: Classified footprints and average classification accuracies. All values represent percentages, except for the kappa-values, which range between 0 and 1, and were obtained by 10-fold cross-validation.

Table 2: Accuracy measures for six randomly selected change-maps. Presented are overall accuracy, kappa for the entire change map; for the classes F (persistent forest), NF (persistent non-forest), D (disturbance) and R (regrowth) user's and producer's accuracy are provided. All values represent percentages, except the kappa values, which range between 0 and 1.

Table 3: Image acquisition dates for the Landsat imagery used in this analysis. The images for footprint Path/Row 177/019 are ranked in the order they were used to create the image composite.

Table 4: Area-weighted classification accuracies for our Landsat-based change-maps. Presented are the overall accuracies, kappa, user's and producer's accuracies for the three classes 'Constant Forest (F)', 'Constant Non-Forest (NF)' and 'Disturbance (D)'.

Table 5: Accuracy measures for the separation of the disturbance polygons into 'windfall' (W) and 'clear-cut harvest' (CC). Presented are the overall accuracy, the kappa statistics as well as user's and producer's accuracy.

Table 6: Study sites and datasets, used in the study. Years indicate the years with complete phenology in the PhenoCam-data.

Forests through the Eye of a Satellite: Exploring the Forests in Russia and the United States using Landsat imagery.

Introduction

Forests are changing at an alarming pace worldwide (Hansen et al. 2013). Forests are an important provider of ecosystem services that contribute to human wellbeing (Global Land Project 2005), including the provision of timber and non-timber products (Millenium Ecosystem Assessment 2005), habitat for biodiversity (DeFries et al. 2004; Laurance 1999; Wood et al. 2012), recreation amenities (Tyrvainen and Miettinen 2000). Most prominently, forests serve as a sink for atmospheric carbon dioxide (Asner et al. 2010; Kauppi et al. 2006; Luyssaert et al. 2008; Valentini et al. 2000) that ultimately helps to mitigate changes in the global climate (Bonan 2008). It is thus important to understand *where*, *how* and *why* forests change worldwide.

My dissertation provides answers to these questions. The overarching goal of my dissertation is to improve our understanding of regional forest-cover dynamics by analyzing Landsat satellite imagery. I answer *where* forests change following drastic socio-economic shocks by using the breakdown of the Soviet Union as a natural experiment. My dissertation provides innovative algorithms to answer *why* forests change – because of human activities or because of natural events such as storms. Finally, I will show *how* dynamic forests are within one year by providing ways to characterize green-leaf phenology from satellite imagery. With my findings I directly contribute to a better understanding of the processes on the Earth's surface and I

highlight the importance of satellite imagery to learn about regional and local forest-cover dynamics.

My dissertation answers these questions in three chapters. I first provide background information for each chapter. After that I present the three chapters as summaries to highlight their scientific contribution at a greater detail, including a discussion of the overall significance of the dissertation research. Finally, I present the three chapters in full.

Background chapter 1: Socio-economic shocks and forest-cover change

Observing where forest-cover changes occur is among the most important components of the global environmental change research (Foley et al. 2005), because of their potential to help mitigating changes in the global climate (Bonan 2008; Global Land Project 2005). It is also important to understand the observed pattern, for example of forest loss, because this ultimately might allow for a better understanding on the decision making that causes forest-cover changes in particular, and land-use/land-cover changes in general (Geist and Lambin 2002; Lambin and Geist 2006). The general assumption is that land-use systems usually transition from one state into another (Foley et al. 2005), and that transition is strongly correlated to the overall economic development of a country.

The forest transition theory is one conceptual model for such a gradual model (Mather 1992; Rudel et al. 2005). The theory suggests that while a gradual demographic shifts and economic development initially leads to deforestation and net forest-cover loss in a certain country, eventually the trend gets reverted and forest-cover increases. The turning point from net forest-area loss to net forest-area gain is then called the 'forest transition' (Rudel 1998). The mechanisms behind the transition are divided into two pathways: the first path is the *economic development path*, which describes the reforestation of previously cleared land for agricultural purposes. With general economic development of a country farmer's wages raise. This overall diminishes the farming profitability, leading to abandoned fields that eventually get reforested. The second path is the *forest scarcity path*. It describes raising prices for forest resources in countries with growing population and little ability to import forest products, making it profitable for land owners to plant trees instead of agricultural crops. Depending on the region and the political institutions, a country can go through one or more forest transitions (Meyfroidt and Lambin 2008; Meyfroidt and Lambin 2011). Overall, the theory suggests a gradual transition of a country's forest cover, independently of the mechanism behind it.

However, land-use transitions, and thus forest transitions, can also be described as rapid shifts from one period of relative stability into a new period of relative stability (DeFries et al. 2004; Meyfroidt et al. 2010). Such shifts can be triggered by drastic socio-economic transformations, for example revolutions (Müller et al. 2009), economic shocks (Sunderlin 1999; Sunderlin and Pokam 2002), technical breakthroughs (Schulz et al. 2011; Zak et al. 2008) or armed conflicts (Machlis and Hanson 2008; Stevens et al. 2011).

The breakdown of the Soviet Union can be seen as such a socio-economic shift and the question is thus whether the implications on forest-cover changes were equally drastic? The time period after 1991 was characterized by decreasing agricultural land-use (Alcantara et al. 2012; Baumann et al. 2011; Kuemmerle et al. 2008; Müller et al. 2009; Prishchepov et al. 2012), mostly because of declining farming profitability following the introduction of market economy principals (Lerman 1999 ; Mathijs and Swinnen 1998) including price liberalization (Ioffe and Nefedova 2004), budget constraints and the removal of guaranteed markets (Lerman et al. 2004; Turnock 1998). However, the strong decline in agricultural intensity was not uniform across the entire former Soviet Union. Instead, some countries experienced only little farmland abandonment (e.g., Belarus). This underlines the importance of institutions and policies for land-use change during times of socio-economic disturbance (Alcantara et al. 2012).

The question is whether changes in institutions also triggered regionally different pattern of forest cover change? In Ukraine and Romania, as examples of two former Soviet countries, the socio-economic and political turmoil after 1991 yielded strongly increasing forest disturbance rates that in many cases could be linked directly to changes in forest legislations (Griffiths et al. 2012; Knorn et al. 2012; Kuemmerle et al. 2009; Kuemmerle et al. 2007). Whether the pattern are similar and homogenous across space in the much larger country Russia is unclear, but multiple changes in forest management and forest policies indicate that the temperate forests indeed underwent substantial changes as well (Wendland et al. 2011). For example, after the collapse of the Soviet Union, forest management and administration were decentralized, the timber industry privatized (Eikeland et al. 2004) and the forestry sector was opened for foreign competitors. During the first years of the transition, Russia's temperate forests were characterized by highly inefficient wood utilization and poorly managed forest areas and illegal logging (Krott et al. 2000, Torniainen and Saastamoinen 2007). In 2004, the forests were recentralized due to a governmental incentive to re-gain control over regions (Torniainen et al. 2006), followed in 2007 by another decentralization of decision-making powers to regional authorities. Likewise, forest ownership rights changed substantially. For example forest harvesting leases were extended up to 99 years (Torniainen and Saastamoinen 2007). The bottom-line is thus, that during the first twenty years since the breakdown of the Soviet Union, Russia's forest legislation repeatedly changed, but what this overall meant for regional differences in how the temperate forests were used, remains unclear.

Background chapter 2: Disturbance type mapping with remote sensing

Understanding why forests change is an important issue for many research disciplines. For example, econometric analyses that study the drivers of timber harvest often use remote sensing based forest disturbance maps (Chomitz and Gray 1996; Wendland et al. 2011). Likewise, assessments of the effectiveness of protected areas focus on harvesting activities inside and outside of protected areas (Knorn et al. 2012; Sieber et al. 2013). The problem with these studies is, that they often only have limited access to information by what kind of event the forest disturbance was caused. As a result, harvested areas might be overestimated in many of the studies above, reducing the significance of drivers of timber harvest, or leading to misinterpretation the effectiveness of protected areas. From an ecological point of view, information on the type of forest disturbance is important for biomass estimations and for the prediction of post-disturbance successions (Scheller and Mladenoff 2004). For example, more living biomass remains in a place following a windfall event, compared to a harvest, which can hinder the establishment of early successional species (Peterson 2000; Webb and Scanga 2001). The bottom-line is that understanding whether forest disturbance is human-made or the result of a natural event, such as windfall, insect defoliation or fire, is crucial for research disciplines that use remote-sensing derived disturbance maps.

The most common natural disturbances affecting forests are fire, insect defoliation and windfall (FAO 2005, 2010). Fire and insect defoliation can already be mapped well (French et al. 2008; Garcia-Haro et al. 2001; Roder et al. 2008; Schroeder et al. 2011; Townsend et al. 2012), and are for the MODIS sensor already available as a standard product that provides online-information about fires globally at almost real-time (Giglio et al. 2003). Windfall mapping of continental storms such as the Boundary Water Blowdown in the Greater Border Lakes Region (USA) in 1999, on the other hand, is more challenging (Rich et al. 2010; Stueve et al. 2011), and to-date there is no universal algorithm available to map post-storm damages in forest ecosystems.

With the continuation of the Landsat program and successful launch of the Landsat Data Continuity Mission (LDCM, later Landsat 8) there will be an extension of the already longest continuous data record. At the same time, processing steps have become routinely enough that all new data and most archived data will be online available as pre-processed data products. Such data products currently include monthly global surface reflectance mosaics, but with complementing missions Landsat 9 and Landsat 10 in the future (Loveland and Dwyer 2012), observation density will potentially increase to a degree that will allow for the routinely generation of user-friendly data products similar to what has been available from MODIS. This will require algorithms that are simple, do not require user input and, probably most importantly, are performing equally good across the world. As such, finding algorithms that map any kind of disturbance type, should meet such requirements to potentially serve future product developments.

Background chapter 3: Remote sensing of green-leaf phenology

Characterizing green leaf phenology is an important measure to describe the development of vegetation over the year and thus offers ways to characterize the interaction between climate and the biosphere (Wolfe et al. 2005; Zhang et al. 2006). Information about seasonal events has been collected for centuries to characterize changes in growing season length, for example as cherry blossom observations (Chmielewski and Rotzer 2001; Menzel and Fabian 1999). Nowadays, digital camera photography (PhenoCam network; primarily consisting of stations in the United States but it extends to other study regions worldwide) allows for a much more detailed observation of the dynamics of vegetation phenology (Richardson et al. 2009; Richardson et al. 2007; Sonnentag et al. 2012).

Phenological information can improve our understanding of Earth-atmosphere interactions for example by serving as input for the calculation of net primary production (Goward et al. 1985), or annual evapotranspiration (Sun et al. 2004). However, the research needs of characterizing green-leaf phenology across large areas, limits the use of ground-based phenological information. Remote sensing can provide phenological information across large spatial scales in an accurate manner (Zhang et al. 2006; Zhang et al. 2003), for example to characterize growing season dynamics including shifts in the timing of bud burst, leaf development, senescence and changes in growing season length (Cleland et al. 2007; Ganguly et al. 2010). Since the early 2000s, data from MODIS provide the data basis for global scale studies on surface phenology (Ahl et al. 2006) at a spatial resolution of 500m.

One basic requirement to describe surface phenology throughout a year is a sufficiently high temporal resolution (also called a short repetition cycle). MODIS meets this requirement (daily observations, 8 day repetition at 500m spatial resolution). Ecological applications, such as the detection of migration bird habitat or the characterization of mixed forests, would benefit from a higher spatial resolution, such as provided by Landsat satellites (30m). Though, information about one year phenological dynamics from Landsat satellites is not available. Probably the major reason for that is the relatively coarse temporal resolution, i.e., the frequency with which any point of the Earth gets captured. Landsat satellites have a theoretical repetition cycle of 16 days, but this interval often is not met due to cloud contamination, broken archives or other technical issues. As a consequence phenological research with

Landsat to-date has been limited to the characterization of mean phenologies over years (Fisher et al. 2006) or changes in seasonal events (Melaas et al. 2013). A single-year phenology from Landsat, however, is not available; and an approach to generate such a product would primarily have to overcome the issue of low temporal resolution.

Executive summaries

Chapter 1: Using the Landsat record to detect forest-cover changes during and after the collapse of the Soviet Union in the temperate zone of European Russia.

Understanding what drives deforestation and forest area changes is an issue of global concern. Most theories assume a gradual forest-cover change over time, but forest transitions might also occur over a short period of time triggered by drastic institutional and socio-economic changes. That raises the question on the spatial rates and patterns of forest-cover changes during such turbulent times. The political breakdown of the Soviet Union provides a great opportunity to learn about how drastic socio-economic changes shape the forest landscape across large areas. Multiple changes in forest legislation and foreign competition over forest use rights suggest that the temperate forests in European Russia underwent substantial changes since 1991. At the same time though, turbulent times often do not allow for the evaluation of rich statistical datasets about forest ownership and forest resource use. Remote sensing offers a valuable alternative to gather information on how forests change during socio-economic times when statistical information is not available.

The goal of this chapter was to provide an understanding on how the temperate forests of European Russia changed during the transition period after the collapse of the Soviet Union. Landsat imagery formed the basis of the analysis, which I examined in five year intervals from 1985 to 2010. I first quantified the changes in forested areas and forest disturbance rates across the entire analyzed area, and then summarized the results at the local administrative level. I also examined forest recovery areas, i.e., areas that were not forested in 1985 but became forest during any analyzed time period afterwards. I then compared my findings to those of other Eastern European countries.

I used a state-of-the art classification technique involving Support-Vector Machines that allowed for an efficient extraction of forest-area changes and forest disturbance rates over time. Despite the free and rich Landsat archives, the processing capabilities and data availability did not allow for a wall-to-wall mapping approach. Instead, I selected a sample of overall 12 Landsat footprints. This sample was further stratified into five forest-cover categories, ranging from 'low forest cover' to 'very high forest cover'. The strata were based on the 2005 MODIS Vegetation Continuous Field (VCF), and compromised general image availability, cloud contamination, location within the growing season and homogeneity of acquisition-day-of-year. However, for some regions no optimal images were available, but had to be acquired from earlier in the year (e.g., early to mid May). Images from such dates often yield class confusions in forest classifications, especially between forest areas and neighboring agricultural fields. Such class confusions likely bias the results. To overcome this issue of sub-optimal data availability, I additionally included winter imagery (i.e., images that show presence of snow), which greatly improved the classification results. I thus added a methodological component to this chapter that highlights the value of winter images for forest classifications.

My results suggested that during the early post-socialist years, forest area in the temperate zone of European Russia decreased. This confirmed findings from other former Soviet countries such as Ukraine, Slovakia or Poland. However, for the time after 2000 I observed a strong increase in overall forest area. I attributed this to (a) the recovery of formerly harvested areas, and (b) the re-growth of forests on abandoned agricultural fields, which were widespread across the study region. At the same time, the results substantially varied between different regions. Some regions (e.g., Yaroslav region) showed no or only little changes in forest area throughout the analyzed time period, whereas other regions (e.g., Smolensk region) showed strong differences. The same was observed for forest disturbance rates. These regional differences suggest, that (a) the decentralization of Russia's forest administration after 1991, and (b) the foundation of timber harvesting in Russia's forest sector on the balance of relative costs and benefits resulted in the regional differences I observed.

Overall, the findings suggest two things. First, rapid socio-economic disturbances such as the collapse of the Soviet Union can have substantial impact of the forest area overall, and the role of forest administration and legislation resulted in strong regional differences of forest-cover change. Second, the overall increase in forest cover due to forest regrowth on abandoned agricultural fields indicate that the region potentially could turn into a large carbon sink in the future.

Chapter 2: Landsat remote sensing of forest windfall disturbance.

Understanding whether forest disturbance is human-made or the result of a natural event, such as windfall, insect defoliation, or fire, is crucial for carbon cycle assessments, econometric analyses of timber harvesting, and other research questions. The problem is, that forest-disturbance maps derived from satellites rarely discriminate among the different types of forest disturbance. The most common natural disturbances affecting forests are fire, insect defoliation and windfall. Fire and insect defoliation can be mapped well with remote sensing and standardized products exist. However, for identifying windfall disturbance a specialized and potentially universal method is missing.

The goal of this chapter was thus to develop an algorithm that separates windfall disturbance areas from disturbance areas caused by clear-cut harvests in Landsat classifications. In addition, the algorithm had to be efficient in terms of user input and processing requirements, and had to behave robust across different study locations. To make the algorithm as efficient as possible, I based the algorithm on simple z-transformed image histograms that helped isolating the spectral characteristics of both disturbance types. To possibly make it robust across study regions, I transformed the Landsat bands into Tasseled-Cap indices, which in other classification schemes perform equally well across different forest biomes. Once, the algorithm was developed, I tested it in the temperate zone of European Russia, and the southern boreal forests of the United States.

In a first step, I extracted all areas of forest disturbance using the dark object method and the Disturbance Index. The challenge was then to generate a representative training data sample of either class of interest (i.e., 'windfall' and 'clear-cut'). To do this I selected image bands and image band transformations that carry distinct spectral characteristics of either type of disturbance, and applied a standard z-transformation to these bands. These bands were (a) the Tasseled-Cap Brightness which is a measure of the soil proportion in the spectral signal, (b) the Tasseled-Cap Wetness and (c) the band-5-reflectance which both can be interpreted as measure of moisture content at a disturbance site. Within the histograms of the z-transformed bands I targeted the areas in which I expected pixel-clusters of either disturbance type. For example, after a recent-clear cut harvest, soil is often exposed and shadows are rare leading to high brightness values. Contrary, after a windfall event, remaining biomass at the site reduces soil reflectance and maintains shadows. In other words, 'on average' a clear-cut site thus could be expected to have higher brightness values than a windfall site. In a z-transformed histogram, representative training samples of either class thus could be expected to be located on the far left side (windfall) and on the far right side (clear-cut harvest). Using this rule set I extracted the pixels in these histogram areas and used them as training samples for the disturbance type classification.

The results suggested an overall accuracy of over 75% between windfall and clear-cut harvest, and this accuracy was consistent between the two study sites. This was lower compared to other recent studies that divided fire disturbance and clear-cut harvest, and likely a remnant of the automation inherent in the algorithm. The results also suggested that the classification accuracy increased with the size of a disturbance site, with a general tendency towards commission errors. Such errors were likely a result of (a) mixed pixel problems along edges at small and narrow disturbance sites, and (b) confusion with partial harvest, which underlines the need for a thorough understanding of harvesting practices before attributing disturbance types.

Overall, the algorithm design met the a-priori requirements: (a) it is a fast processing algorithm that does not need any ancillary information; (b) it is applicable to any type of Landsat-based disturbance and can be seen as a stand-alone approach; and (c) performs equally well across different forest biomes. The increased level of categorical information produced as a result of this work is of great value especially for research that requires information about changes in forest area. Further, the algorithm also contributes to the ongoing research on the provision of remote-sensing map products from Landsat satellites.

Chapter 3: Modeling green-leaf phenology using Dynamic Time Warping and all available Landsat data

Green leaf phenology is an important measure to describe the development of vegetation over the year and thus offers ways to characterize the interaction between climate and the biosphere. Remote sensing can characterize green leaf phenology well and there are standardized products available at a spatial resolution of 500m. However, other applications such as the detection of bird migration stopover habitat or a detailed classification of mixed forests would benefit from a higher spatial resolution. Landsat satellites provide images at a higher spatial resolution (30m), but there is no product available that describes the phenological dynamics throughout a single year. One reason for that might be imperfect temporal resolution of Landsat satellites. Technically, every point of the earth gets revisited in a 16-day cycle. However, cloud contamination, broken archives or other technical issues cause that for many regions of the world a true 16-day repeat cycle is not achieved. As a result, fitting a phenologically meaningful function through observations of one single year is challenging if not impossible.

The goal of this chapter was thus to find a way to increase the temporal resolution of Landsat observations that allows for the simulation of green leaf phenology product using Landsat satellites. In addition, the product of the novel method was compared to (a) green leaf phenology from MODIS and (b) ground-based phenology observations from the PhenoCam network.

The main idea that helped solving the problem of insufficient number of imagery was to generate a dense time series of Landsat imagery that consisted of all available images between 2002 and 2012. Yet, the challenge here was to find a way that allowed for the adjustment of different phenologies across years. I made the adjustment by applying Dynamic Time Warping (DTW) to MODIS Enhanced Vegetation Index (EVI) time series of different years. For example given a reference phenology (e.g., for the year 2005) and the phenology of a second, different year (e.g., 2007), the use of DTW enabled me to find for each day in the 2007-phenology the corresponding day of year in the reference phenology. Such corresponding years can be interpreted, for example, that May 15th of the year 2007 corresponds phenologically to May 25th of the reference year (2005). Using this information, I re-ordered the Landsat observations and created a new, synthetic, very dense Landsat time series, of which I then modeled green leaf phenology. This new phenology I then compared to the original MODIS phenology as well as to the PhenoCam phenology by comparing the timing of green-up, start-of-season, maturity, senescence, end-of-season and dormancy which are easy to extract from the first and second derivative of the phenology function. I repeated all steps across multiple different years (based on the availability of PhenoCam data) and across different study sites to test the robustness of the approach.

On average our Landsat time series consisted of 274 images. The Landsat green-up date was on average 0.6 days later than the green-up in the PhenoCam and 1.7 days later than in the MODIS reference time series, the start-of-season 9.1 days later (1.6 days), the end-of-season 1.5 days later. The differences in the days were stronger driven by the years of analysis compared to the study site, suggesting that the method is more sensitive to the year of analysis but relatively robust across study regions. While the approach certainly seems being successful in describing phenological dynamics of one year, there are some limitations to it, such as (a) the sensitivity to changes in land-cover such as harvests and (b) the dependence on external data products during the re-alignment process which makes this approach not a stand-alone method.

Overall, the presented phenology product can be seen as a considerable alternative to existing remote sensing based products, though at a much higher spatial resolution. Further, the study also can be seen as another application that makes use of the entire rich Landsat archives, highlighting the large potential of these archives.

Overall Significance

Forests are of important value but they are changing at an alarming pace in many regions worldwide. Understanding *how*, *why* and *where* forests change is thus among the major priorities in environmental research. In my dissertation I answer these three questions in three chapters.

In chapter one I analyzed *where* forests change during times of rapid and drastic socio-economic changes, and I used the collapse of the Soviet Union as example. My research uncovered vast regional differences of forest-cover change and for the region as a whole a net forest-cover gain. Two main implications rose from the research: (1) in a large country like Russia, regional forest legislation and forest management seem to be stronger drivers forest-cover changes compared to overall national policy changes. (2) A regime-shift seems to offer an opportunity for a region to turn into a net carbon sink, highlighting the importance of understanding regime-shifts in a comprehensive way.

In chapter two I developed ways to find out *why* forests change. I presented an algorithm that allows for the accurate classification of forest disturbance into 'windfall' and 'clear-cut harvest' sites. Currently, one major research direction in Landsat-based remote sensing is headed towards the automation of image processing chains with the goal to facilitate standardized global map products. The presented research here stands in line with the trend. It provides a way to inform about the processes behind observed forest-cover change, and as such contributes to our understanding of how the Earth's surface changes.

In chapter three, I presented *how* dynamic forests are. I did this in a detail that has not been available before. However, the high detail will be beneficial to other ecological applications. Forests are a dynamic system, both across years, but also within years. So far, our understanding of the dynamics within years was limited by technical restrictions. With the research presented here I provide a way towards a deeper understanding of these dynamics at the local scale. In conjunction with other research disciplines my research will thus directly contributes to a better understanding of climate-biosphere interactions.

References

1. Ahl, D.E., Gower, S.T., Burrows, S.N., Shabanov, N.V., Myneni, R.B., & Knyazikhin, Y. (2006). Monitoring spring canopy phenology of a deciduous broadleaf forest using MODIS. *Remote Sensing of Environment*, 104, 88-95
2. Alcantara, C., Kuemmerle, T., Prishchepov, A.V., & Radeloff, V.C. (2012). Mapping abandoned agriculture with multi-temporal MODIS satellite data. *Remote Sensing of Environment*, 124, 334-347
3. Asner, G.P., Powell, G.V.N., Mascaro, J., Knapp, D.E., Clark, J.K., Jacobson, J., Kennedy-Bowdoin, T., Balaji, A., Paez-Acosta, G., Victoria, E., Secada, L., Valqui, M., & Hughes, R.F. (2010). High-resolution forest carbon stocks and emissions in the Amazon. *Proceedings of the National Academy of Sciences*, 107, 16738-16742
4. Baumann, M., Kuemmerle, T., Elbakidze, M., Ozdogan, M., Radeloff, V.C., Keuler, N.S., Prishchepov, A.V., Kruhlov, I., & Hostert, P. (2011). Patterns and drivers of post-socialist farmland abandonment in Western Ukraine. *Land Use Policy*, 28, 552-562
5. Bonan, G.B. (2008). Forests and climate change: Forcings, feedbacks, and the climate benefits of forests. *Science*, 320, 1444-1449
6. Chmielewski, F.M., & Rotzer, T. (2001). Response of tree phenology to climate change across Europe. *Agricultural and Forest Meteorology*, 108, 101-112
7. Chomitz, K.M., & Gray, D.A. (1996). Roads, land use, and deforestation: A spatial model applied to belize. *World Bank Economic Review*, 10, 487-512

8. Cleland, E.E., Chuine, I., Menzel, A., Mooney, H.A., & Schwartz, M.D. (2007). Shifting plant phenology in response to global change. *Trends in Ecology & Evolution*, 22, 357-365
9. DeFries, R.S., Foley, J.A., & Asner, G.P. (2004). Land-use choices: balancing human needs and ecosystem function. *Frontiers in Ecology and the Environment*, 2, 249-257
10. Eikeland, S., Eythorsson, E., & Ivanova, L. (2004). From management to mediation: Local forestry management and the forestry crisis in post-socialist Russia. *Environmental Management*, 33, 285-293
11. FAO (2005). Global Forest Ressource Asessment 2005. In FAO (Ed.), Forestry Papers. Rome, Italy Food and Agriculture Organization of the United Nations
12. FAO (2010). Global Forest Ressource Assessment 2010. In Food and Agriculture Organization of the United Nations (Ed.) (p. 378)
13. Fisher, J.I., Mustard, J.F., & Vadeboncoeur, M.A. (2006). Green leaf phenology at Landsat resolution: Scaling from the field to the satellite. *Remote Sensing of Environment*, 100, 265-279
14. Foley, J.A., DeFries, R., Asner, G.P., Barford, C., Bonan, G., Carpenter, S.R., Chapin, F.S., Coe, M.T., Daily, G.C., Gibbs, H.K., Helkowski, J.H., Holloway, T., Howard, E.A., Kucharik, C.J., Monfreda, C., Patz, J.A., Prentice, I.C., Ramankutty, N., & Snyder, P.K. (2005). Global consequences of land use. *Science*, 309, 570-574
15. Folke, C., Carpenter, S.R., Walker, B., Scheffer, M., Chapin, T., & Rockstrom, J. (2010). Resilience Thinking: Integrating Resilience, Adaptability and Transformability. *Ecology and Society*, 15

16. French, N.H.F., Kasischke, E.S., Hall, R.J., Murphy, K.A., Verbyla, D.L., Hoy, E.E., & Allen, J.L. (2008). Using Landsat data to assess fire and burn severity in the North American boreal forest region: an overview and summary of results. International *Journal of Wildland Fire*, 17, 443-462

17. Ganguly, S., Friedl, M.A., Tan, B., Zhang, X.Y., & Verma, M. (2010). Land surface phenology from MODIS: Characterization of the Collection 5 global land cover dynamics product. *Remote Sensing of Environment*, 114, 1805-1816

18. Garcia-Haro, F.J., Gilabert, M.A., & Melia, J. (2001). Monitoring fire-affected areas using Thematic Mapper data. *International Journal of Remote Sensing*, 22, 533-549

19. Geist, H.J., & Lambin, E.F. (2002). Proximate causes and underlying driving forces of tropical deforestation. *Bioscience*, 52, 143-150

20. Giglio, L., Descloitres, J., Justice, C.O., & Kaufman, Y.J. (2003). An enhanced contextual fire detection algorithm for MODIS. *Remote Sensing of Environment*, 87, 273-282

21. Global Land Project (2005). Science plan and implemantation strategy. IGBP Report Number 53/IHDP Report Number 1.19. *International Geosphere-Biosphere Programme*, Stockholm, Sweden.

22. Goward, S.N., Tucker, C.J., & Dye, D.G. (1985). North-American Vegetation Patterns Observed with the Noaa-7 Advanced Very High-Resolution Radiometer. *Vegetatio*, 64, 3-14

23. Griffiths, P., Kuemmerle, T., Kennedy, R.E., Abrudan, I.V., Knorn, J., & Hostert, P. (2012). Using annual time-series of Landsat images to assess the effects of forest restitution in post-socialist Romania. *Remote Sensing of Environment*, 118, 199-214

24. Griffiths, P., van der Linden, S., Kuemmerle, T., & Hostert, P. (2013). A Pixel-Based Landsat Compositing Algorithm for Large Area Land Cover Mapping. Ieee Journal of *Selected Topics in Applied Earth Observations and Remote Sensing*, PP, 1-14

25. Hansen, M.C., & DeFries, R.S. (2004). Detecting long-term global forest change using continuous fields of tree-cover maps from 8-km advanced very high resolution radiometer (AVHRR) data for the years 1982-99. *Ecosystems*, 7, 695-716

26. Hansen, M.C., Potapov, P.V., Moore, R., Hancher, M., Turubanova, S.A., Tyukavina, A., Thau, D., Stehman, S.V., Goetz, S.J., Loveland, T.R., Kommareddy, A., Egorov, A., Chini, L., Justice, C.O., & Townshend, J.R.G. (2013). High-Resolution Global Maps of 21st-Century Forest Cover Change. *Science*, 342, 850-853

27. Huang, C., Goward, S.N., Masek, J.G., Thomas, N., Zhu, Z., & Vogelmann, J.E. (2010). An automated approach for reconstructing recent forest disturbance history using dense Landsat time series stacks. Remote Sensing of Environment, 114, 183-198

28. Ioffe, G., & Nefedova, T. (2004). Marginal farmland in European Russia. *Eurasian Geography and Economics*, 45, 45-59

29. Kauppi, P.E., Ausubel, J.H., Fang, J.Y., Mather, A.S., Sedjo, R.A., & Waggoner, P.E. (2006). Returning forests analyzed with the forest identity. *Proceedings of the National Academy of Sciences of the United States of America*, 103, 17574-17579

30. Kennedy, R.E., Yang, Z., & Cohen, W.B. (2011). Detecting trends in forest disturbance and recovery using yearly Landsat time series: 1. LandTrendr -- Temporal segmentation algorithms. *Remote Sensing of Environment*, 114, 2897-2910

31. Knorn, J., Kuemmerle, T., Radeloff, V.C., Szabo, A., Mindrescu, M., Keeton, W.S., Abrudan, I., Griffiths, P., Gancz, V., & Hostert, P. (2012). Forest restitution and protected area effectiveness in post-socialist Romania. *Biological Conservation*, 146, 204-212

32. Krott, M., Tikkanen, I., Petrov, A., Tunystsya, Y., Zheliba, B., Sasse, V., Rykounina, I., & Tynytsya, T. (2000). Policies for Sustainable Forestry in Belarus, Russia and Ukraine. In, European Forest Institute Research Report No. 9. . Koninklijke Brill NV, Leiden.

33. Kuemmerle, T., Chaskovskyy, O., Knorn, J., Radeloff, V.C., Kruhlov, I., Keeton, W.S., & Hostert, P. (2009). Forest cover change and illegal logging in the Ukrainian Carpathians in the transition period from 1988 to 2007. *Remote Sensing of Environment*, 113, 1194-1207

34. Kuemmerle, T., Hostert, P., Radeloff, V.C., Perzanowski, K., & Kruhlov, I. (2007). Post-socialist forest disturbance in the Carpathian border region of Poland, Slovakia, and Ukraine. *Ecological Applications*, 17, 1279-1295

35. Kuemmerle, T., Hostert, P., Radeloff, V.C., van der Linden, S., Perzanowski, K., & Kruhlov, I. (2008). Cross-border Comparison of Post-socialist Farmland Abandonment in the Carpathians. *Ecosystems*, 11, 614-628

36. Lambin, E.F., & Geist, H. (2006). Land-Use and Land-Cover Change. Berlin: Springer Verlag

37. Lambin, E.F., Geist, H.J., & Lepers, E. (2003). Dynamics of land-use and land-cover change in tropical regions. *Annual Review of Environment and Resources*, 28, 205-241

38. Laurance, W.F. (1999). Reflections on the tropical deforestation crisis. Bio*logical Conservation*, 91, 109-117

39. Lerman, Z. (1999). Land reform and farm restructuring in Ukraine. *Problems of Post-Communism*, 46, 42-55

40. Lerman, Z., Csaki, C., & Feder, G. (2004). Evolving farm structures and land use patterns in former socialist countries. *Quarterly Journal of International Agriculture*, 43, 309-335

41. Loveland, T.R., & Dwyer, J.L. (2012). Landsat: Building a strong future. *Remote Sensing of Environment,* 122, 22-29

42. Luyssaert, S., Schulze, E.D., Borner, A., Knohl, A., Hessenmoller, D., Law, B.E., Ciais, P., & Grace, J. (2008). Old-growth forests as global carbon sinks. *Nature*, 455, 213-215

43. Machlis, G.E., & Hanson, T. (2008). Warfare ecology. *Bioscience*, 58, 729-736

44. Mather, A.S. (1992). The Forest Transition. *Area*, 24, 367-379

45. Mathijs, E., & Swinnen, J.F.M. (1998). The economics of agricultural decollectivization in East Central Europe and the former Soviet Union. *Economic Development and Cultural Change*, 47, 1-26

46. Melaas, E.K., Friedl, M.A., & Zhu, Z. (2013). Detecting interannual variation in deciduous broadleaf forest phenology using Landsat TM/ETM data. *Remote Sensing of Environment*, 132, 176-185

47. Menzel, A., & Fabian, P. (1999). Growing season extended in Europe. *Nature*, 397, 659-659

48. Meyfroidt, P. (2013). Environmental Cognitions, Land Change and Social-Ecological Feedbacks: Local Case Studies of Forest Transition in Vietnam. *Human Ecology*, 41, 367-392

49. Meyfroidt, P., & Lambin, E.F. (2008). Forest transition in Vietnam and its environmental impacts. *Global Change Biology*, 14, 1319-1336

50. Meyfroidt, P., & Lambin, E.F. (2011). Global Forest Transition: Prospects for an End to Deforestation. *Annual Review of Environment and Resources*, 36

51. Meyfroidt, P., Rudel, T.K., & Lambin, E.F. (2010). Forest transitions, trade, and the global displacement of land use. *Proceedings of the National Academy of Sciences*, 107, 20917-20922

52. Millenium Ecosystem Assessment (2005). Ecosystems and Human Well-Being: Volume 2 Scenarios: Findings of the Scenarios Working Group (Millennium Ecosystem Assessment Series): Island Press

53. Müller, D., Kuemmerle, T., Rusu, M., & Griffiths, P. (2009). Lost in transition: determinants of post-socialist cropland abandonment in Romania. *Journal of Land Use Science*, 4, 109 - 129

54. Nelson, B.W., Kapos, V., Adams, J.B., Wilson, J.O., & Braun, O.P.G. (1994). Forest Disturbance by Large Blowdowns in the Brazilian Amazon. *Ecology*, 75, 853-858

55. Peterson, C.J. (2000). Damage and recovery of tree species after two different tornadoes in the same old growth forest: a comparison of infrequent wind disturbances. *Forest Ecology and Management*, 135, 237-252

56. Potapov, P., Turubanova, S., & Hansen, M.C. (2011). Regional-scale boreal forest cover and change mapping using Landsat data composites for European Russia. *Remote Sensing of Environment*, 115, 548-561

57. Potapov, P.V., Turubanova, S.A., Hansen, M.C., Adusei, B., Broich, M., Altstatt, A., Mane, L., & Justice, C.O. (2012). Quantifying forest cover loss in Democratic Republic of the Congo, 2000–2010, with Landsat ETM+ data. *Remote Sensing of Environment*, 122, 106-116

58. Prishchepov, A., V., Radeloff, V., C., Baumann, M., Kuemmerle, T., & Müller, D. (2012). Effects of institutional changes on land use: agricultural land abandonment during the transition from state-command to market-driven economies in post-Soviet Eastern Europe. *Environmental Research Letters*, 7, 024021

59. Rich, R.L., Frelich, L., Reich, P.B., & Bauer, M.E. (2010). Detecting wind disturbance severity and canopy heterogeneity in boreal forest by coupling high-spatial resolution satellite imagery and field data. *Remote Sensing of Environment*, 114, 299-308

60. Richardson, A.D., Braswell, B.H., Hollinger, D.Y., Jenkins, J.P., & Ollinger, S.V. (2009). Near-surface remote sensing of spatial and temporal variation in canopy phenology. *Ecological Applications*, 19, 1417-1428

61. Richardson, A.D., Jenkins, J.P., Braswell, B.H., Hollinger, D.Y., Ollinger, S.V., & Smith, M.L. (2007). Use of digital webcam images to track spring green-up in a deciduous broadleaf forest. *Oecologia*, 152, 323-334

62. Roder, A., Hill, J., Duguy, B., Alloza, J.A., & Vallejo, R. (2008). Using long time series of Landsat data to monitor fire events and post-fire dynamics and identify driving factors. A case study in the Ayora region (eastern Spain). *Remote Sensing of Environment*, 112, 259-273

63. Rudel, T.K. (1998). Is there a forest transition? Deforestation, reforestation, and development. *Rural Sociology*, 63, 533-552

64. Rudel, T.K., Coomes, O.T., Moran, E., Achard, F., Angelsen, A., Xu, J.C., & Lambin, E. (2005). Forest transitions: towards a global understanding of land use change. *Global Environmental Change*, 15, 23-31

65. Scheffer, M., Carpenter, S., Foley, J.A., Folke, C., & Walker, B. (2001). Catastrophic shifts in ecosystems. *Nature*, 413, 591-596

66. Scheller, R.M., & Mladenoff, D.J. (2004). A forest growth and biomass module for a landscape simulation model, LANDIS: design, validation, and application. *Ecological Modelling*, 180, 211-229

67. Schroeder, T.A., Wulder, M.A., Healey, S.P., & Moisen, G.G. (2011). Mapping wildfire and clearcut harvest disturbances in boreal forests with Landsat time series data. *Remote Sensing of Environment*, 115, 1421-1433

68. Schulz, J.J., Cayuela, L., Rey-Benayas, J.M., & Schroder, B. (2011). Factors influencing vegetation cover change in Mediterranean Central Chile (1975-2008). *Applied Vegetation Science*, 14, 571-582

69. Sieber, A., Kuemmerle, T., Prishchepov, A.V., Wendland, K.J., Baumann, M., Radeloff, V.C., Baskin, L.M., & Hostert, P. (2013). Landsat-based mapping of post-Soviet land-use change to assess the effectiveness of the Oksky and Mordovsky protected areas in European Russia. *Remote Sensing of Environment*, 133, 38-51

70. Skole, D., & Tucker, C. (1993). Tropical Deforestation and Habitat Fragmentation in the Amazon - Satellite Data from 1978 to 1988. *Science*, 260, 1905-1910

71. Sonnentag, O., Hufkens, K., Teshera-Sterne, C., Young, A.M., Friedl, M., Braswell, B.H., Milliman, T., O'Keefe, J., & Richardson, A.D. (2012). Digital repeat photography for phenological research in forest ecosystems. *Agricultural and Forest Meteorology*, 152, 159-177

72. Stevens, K., Campbell, L., Urquhart, G., Kramer, D., & Qi, J. (2011). Examining complexities of forest cover change during armed conflict on Nicaragua's Atlantic Coast. *Biodiversity and Conservation*, 20, 2597-2613

73. Stueve, K.M., Perry, C.H., Nelson, M.D., Healey, S.P., Hill, A.D., Moisen, G.G., Cohen, W.B., Gormanson, D.D., & Huang, C.Q. (2011). Ecological importance of

intermediate windstorms rivals large, infrequent disturbances in the northern Great Lakes. *Ecosphere*, 2, art2

74. Sun, R., Gao, X., Liu, C.M., & Li, X.W. (2004). Evapotranspiration estimation in the Yellow River Basin, China using integrated NDVI data. *International Journal of Remote Sensing*, 25, 2523-2534
75. Sunderlin, W.D. (1999). Between danger and opportunity: Indonesia and forests in an era of economic crisis and political change. *Society & Natural Resources*, 12, 559-570
76. Sunderlin, W.D., & Pokam, J. (2002). Economic crisis and forest cover change in Cameroon: The roles of migration, crop diversification, and gender division of labor. *Economic Development and Cultural Change*, 50, 581-606
77. Torniainen, T.J., & Saastamoinen, O.J. (2007). Formal and informal institutions and their hierarchy in the regulation of the forest lease in Russia. *Forestry*, 80, 489-501
78. Torniainen, T.J., Saastamoinen, O.J., & Petrov, A.P. (2006). Russian forest policy in the turmoil of the changing balance of power. *Forest Policy and Economics*, 9, 403-416
79. Townsend, P.A., Singh, A., Foster, J.R., Rehberg, N.J., Kingdon, C.C., Eshleman, K.N., & Seagle, S.W. (2012). A general Landsat model to predict canopy defoliation in broadleaf deciduous forests. *Remote Sensing of Environment*, 119, 255-265
80. Turnock, D. (1998). Introduction. In D. Turnock (Ed.), Privatization in Rural Eastern Europe. The Process of Restitution and Restructuring (pp. 1-48). Cheltenham: Edward Elgar
81. Tyrvainen, L., & Miettinen, A. (2000). Property prices and urban forest amenities. *Journal of Environmental Economics and Management*, 39, 205-223

82. Valentini, R., Matteucci, G., Dolman, A.J., Schulze, E.D., Rebmann, C., Moors, E.J., Granier, A., Gross, P., Jensen, N.O., Pilegaard, K., Lindroth, A., Grelle, A., Bernhofer, C., Grunwald, T., Aubinet, M., Ceulemans, R., Kowalski, A.S., Vesala, T., Rannik, U., Berbigier, P., Loustau, D., Guomundsson, J., Thorgeirsson, H., Ibrom, A., Morgenstern, K., Clement, R., Moncrieff, J., Montagnani, L., Minerbi, S., & Jarvis, P.G. (2000). Respiration as the main determinant of carbon balance in European forests. *Nature*, 404, 861-865

83. Webb, S.L., & Scanga, S.E. (2001). Windstorm Disturbance without patch dynamics: Twelve Years of Change in a Minnesota forest. *Ecology*, 82, 893-897

84. Wendland, K.J., Lewis, D.J., Alix-Garcia, J., Ozdogan, M., Baumann, M., & Radeloff, V.C. (2011). Regional- and district-level drivers of timber harvesting in European Russia after the collapse of the Soviet Union. *Global Environmental Change*, 21, 1290-1300

85. Wolfe, D.W., Schwartz, M.D., Lakso, A.N., Otsuki, Y., Pool, R.M., & Shaulis, N.J. (2005). Climate change and shifts in spring phenology of three horticultural woody perennials in northeastern USA. *International Journal of Biometeorology*, 49, 303-309

86. Wood, E.M., Pidgeon, A.M., Liu, F., & Mladenoff, D.J. (2012). Birds see the trees inside the forest: The potential impacts of changes in forest composition on songbirds during spring migration. *Forest Ecology and Management*, 280, 176-186

87. Woodcock, C.E., Allen, R., Anderson, M., Belward, A., Bindschadler, R., Cohen, W., Gao, F., Goward, S.N., Helder, D., Helmer, E., Nemani, R., Oreopoulos, L., Schott, J.,

Thenkabail, P.S., Vermote, E.F., Vogelmann, J., Wulder, M.A., & Wynne, R. (2008). Free access to Landsat imagery. *Science*, 320, 1011-1011

88. Wulder, M.A., Masek, J.G., Cohen, W.B., Loveland, T.R., & Woodcock, C.E. (2012). Opening the archive: How free data has enabled the science and monitoring promise of Landsat. *Remote Sensing of Environment*, 122, 2-10
89. Zak, M.R., Cabido, M., Caceres, D., & Diaz, S. (2008). What drives accelerated land cover change in central Argentina? Synergistic consequences of climatic, socioeconomic, and technological factors. *Environmental Management*, 42, 181-189
90. Zhang, X.Y., Friedl, M.A., & Schaaf, C.B. (2006). Global vegetation phenology from Moderate Resolution Imaging Spectroradiometer (MODIS): Evaluation of global patterns and comparison with in situ measurements. *Journal of Geophysical Research,* 111
91. Zhang, X.Y., Friedl, M.A., Schaaf, C.B., Strahler, A.H., Hodges, J.C.F., Gao, F., Reed, B.C., & Huete, A. (2003). Monitoring vegetation phenology using MODIS. *Remote Sensing of Environment*, 84, 471-475

Chapter 1: Using the Landsat record to detect forest-cover changes during and after the collapse of the Soviet Union in the temperate zone of European Russia

Co-Authors: Mutlu Ozdogan, Tobias Kuemmerle, Kelly J. Wendland, Elena Esipova, Volker C. Radeloff

Remote Sensing of Environment 124, 174-184

Abstract:

The political breakdown of the Soviet Union in 1991 provides a rare case of drastic changes in social and economic conditions, and as such a great opportunity to investigate the impacts of socioeconomic changes on the rates and patterns of forest harvest and regrowth. Our goal was to characterize forest-cover changes in the temperate zone of European Russia between 1985 and 2010 in 5-year increments using a stratified random sample of 12 Landsat footprints. We used Support Vector Machines and post-classification comparison to monitor forest area, disturbance and reforestation. Where image availability was sub-optimal, we tested whether winter images help to improve classification accuracy. Our approach yielded accurate mono-temporal maps (on average > 95% overall accuracy), and change maps (on average 93.5%). The additional use of winter imagery improved classification accuracy by about 2%. Our results suggest that Russia's temperate forests underwent substantial changes during the observed period. Overall, forested areas increased by 4.5%, but the changes in forested area varied over time: a decline in forest area between 1990 and 1995 (-1%) was followed by an increase in overall forest area in recent years (+1.4%, 2005-2010), possibly caused in part by forest regrowth on abandoned farmlands. Disturbances varied greatly among administrative regions, suggesting that differences in socioeconomic conditions strongly influence disturbance rates. While portions of Russia's temperate forests experienced high disturbance rates, overall forest area is expanding. Our use of a stratified random sample of Landsat footprints, and of summer and winter images, allowed us to characterize forest dynamics across a large region over a long time period, emphasizing the value of winter imagery in the free Landsat archives, especially for study areas where data availability is limited.

Keywords: Forest-cover change, SVM, temperate forests, Central and Eastern Europe, Post-Soviet land-use change, logging, winter imagery, Landsat, stratified random sample

Introduction

Land-cover and land-use-change (LCLUC) is one of the most important components of global environmental change (Foley et al. 2005). Among the different land cover classes, changes in forests are particularly important because of their ability to sequester atmospheric carbon sequestration and their potential to help mitigating climate change (Bonan 2008; FAO 2010). Remote sensing has played a key role in monitoring forest change at multiple scales and in different regions of the world (Hansen et al. 2008; Kennedy et al. 2011; Potapov et al. 2011).

LCLUC is often linked to socio-economic changes, leading to conceptual models that describe LCLUC as a function of a country's economic development (e.g., Lambin et al. 2003, Foley et al. 2005). However, these conceptual models usually assume relatively continuous development of political and economic conditions, and it is less clear how drastic and rapid changes in political and economic decisions affect land use. A prime example of a drastic change is the collapse of the Soviet Union in 1991. The switch from a state-controlled economy towards an open market system, and the institutional transformation in Russia resulted in major changes in forest legislation, and the privatization of both the timber industry (Turnock 1998; Wendland et al. 2011) and the agricultural sector, which had substantial influences on agricultural intensity (Lerman 2009, Prishchepov et al. 2012).

Forest cover changed markedly in many parts of Eastern Europe after the collapse of the Soviet Union, and remote sensing has played a key role in mapping these changes. For example, analyses of Landsat Thematic Mapper (TM) and Enhanced

Thematic Mapper Plus (ETM+) data in the Carpathians revealed that the transition period after the breakdown of the Soviet Union was partially characterized by widespread forest harvests (Main-Knorn et al. 2009; Griffiths et al. 2012; Knorn et al. 2012), including illegal logging (Kuemmerle et al. 2009). In European Russia's boreal forest, harvesting rates were about 1.5% between 2000 and 2005 according to a wall-to-wall analysis of Landsat data (Potapov et al. 2011). In addition to Landsat based studies, European Russia was also part of studies that investigated global forest-cover changes using the Moderate Resolution Imaging Spectroradiometer (MODIS) (Hansen et al. 2010; Potapov et al. 2008). However, past studies either focused on a large area over a short and recent time period, or they analyzed long-term change, but were geographically limited to a smaller study area. What is lacking is a study of the temperate forests of European Russia that analyzes a long time series in the entire region.

One reason that such a study has not been undertaken previously is the quality and volume of data that is needed, in both the spatial and temporal domain. While MODIS imagery provides very frequent information for large areas, these observations are made at moderate spatial resolution (250 to 500m), which limits their utility for small scale landscape changes. Moreover, since MODIS only started recording the Earth's surface in 2000, the timeframe of available data is too short to analyze forest-cover changes during the last years of socialism and the early post-socialist period. On the other hand, Landsat sensors (especially TM and ETM+) provide high-resolution data (30 m) that are available continuously from 1984 to the present, which makes them ideal for addressing questions of post-Socialist forest-cover change. However, Landsat sensors' relatively narrow swath width (approximately 185 km) makes Landsat data more challenging to use wall-to-wall across large areas. The lower temporal repeat cycle (16 days, 8 days when considering the overlap areas to neighboring footprints in higher latitudes) as one consequence of the narrow swath width and frequent obstructions by clouds lead in some regions of the world to a maximum of 1-2 suitable images per growing season at best, making wall-to-wall-coverage across large areas impossible. An alternative approach for describing forest dynamics across a larger region is to statistically sample a subset of Landsat footprints, greatly reducing the amount of data needed. Such an approach has been used for the United States as part of the North American Forest Dynamics (NAFD) project (Goward et al. 2008) in which 23 footprints were selected and analyzed using Landsat Time Series Stacks (LTSS; Huang et al. 2009a). Similarly, agricultural expansion on expense of intact forests has been investigated in the tropics (Gibbs et al. 2010). Achard et al. (2002) studied the world's humid tropical forests in the TREES-2 project using a sample of overall 100 Landsat scenes (quarters and full scenes). These scenes were selected using a deforestation risk map, which had been created previously based on expert knowledge, and considered higher sampling probabilities in deforestation hot spot areas. The FAO Forest Resources Assessment 1990 used a stratified sample of 117 Landsat TM scenes in the tropics containing at least 10,000 km2 land surface (FAO 1996) to assess forest cover. For an analysis of the European Union using a sample of Landsat TM scenes, Gallego (2005) selected his sample based on Thiessen polygons and a stratification process. Stehman

(2005) generally showed that focusing on a sample rather than on the entire population yields better estimates, when the improvement of error during the analysis of the sample outweighs the introduction of the sampling error. As such, in the present study, we focused on a sample of Landsat footprints rather than on a wall-to-wall coverage. Our study also focuses on capturing local and regional forest-cover changes which, we assume, vary across the entire region. Caused by the low data availability that did not allow us to cover the region wall-to-wall for our entire time period of interest, we used a stratified random sample and selected 12 Landsat footprints across the temperate zone of European Russia.

While the use of a statistical sample reduces the number of footprints necessary to study, it does not completely eliminate the problem that cloud-free imagery during the growing season is often limited. Leaf-off imagery in spring and fall can result in classification errors between deciduous trees and non-forested vegetation classes (Reese et al. 2002). We hypothesized that the additional use of a winter image can help overcome this issue, especially for the accurate delineation of forest boundaries. Landsat imagery from the winter season can be useful because of the strong radiance contrast in these areas during the winter (Peterson et al. 2004, Liira et al. 2004). Grasslands and open spaces are completely covered with snow during the winter, leading to high visible reflectance while deciduous and needle leaf forests have a lower reflectance due to branches and shadows. In other words, adding a second image from the winter period of the same year may possibly increase the overall accuracy of the classification by helping to distinguish grass areas from deciduous forests. The use of winter imagery has been successfully shown in the past: their addidional use led to an accuracy of 89% for quantification of bamboo understory growth in a mixed forest area (Wang et al. 2009). Winter imagery use was also reported providing an alternative to hyperspectral data for mapping forest wildlife habitat in the central and southern Appalachians (Tirpak and Giuliano 2010). In the most recent study, Stueve et al. (2011) tested snow-covered Landsat imagery in North America and found that they reduce commission errors of disturbance areas by nearly 28%. Based on these prior findings, we decided to investigate if winter imagery can also improve forest/non-forest-classifications in the temperate region of Russia.

Another shortcoming of most prior studies in European Russia is that they examined only permanent forests and forest disturbances, while ignoring forest recovery (defined here as forest regeneration on disturbance sites, as well as forest expansion onto land that was not forested at the beginning of the Landsat record). Rates of forest recovery are of paramount importance for studies of carbon sequestration both above ground (Houghton 2005, Böttcher et al. 2008) and in the soil (Guo and Gifford 2002). Forest recovery is particularly important in the former Soviet Union and Eastern Europe (Vuichard et al. 2008). For example, widespread farmland abandonment (as documented by Baumann et al. 2011; Kuemmerle et al. 2008; Prishchepov et al. 2012) suggests that large areas of former farmland are reverting to forests, which creates a large carbon storage potential (Kuemmerle et al. 2011; Olofsson et al. 2011). However, the extent and the intensity of forest recovery in the temperate zone of European Russia is not well known.

The overarching goal of our study was therefore to characterize regional differences of post-socialist forest-cover changes in the temperate region of European Russia using a representative sample of Landsat footprints. More specifically, our objectives were to:

- quantify the changes in forested areas in 5-year-increments from 1985 to 2010 across a stratified random sample of 12 Landsat footprints,
- determine forest recovery rates in these footprints before and after the collapse of the Soviet Union and compare these patterns with those in other eastern European countries, and
- test whether the inclusion of a winter image increases classification accuracy.

Study Area

Our study region included three Russian federal districts, 27 federal districts (hereafter: 'regions'), which are subdivided into 821 municipal districts (Figure 1). The two largest cities of European Russia, St. Petersburg and Moscow, were located in our study region. Russia contains 20% of the world's forests (about 809 million ha; FAO 2010), and in the temperate region, temperate coniferous, broadleaf, and mixed forests dominate the landscape.

European Russia's forest sector and forest legislation underwent several substantial changes since 1991, including privatization of the timber industry, and changing decentralizations and re-centralizations of the forest administration between federal, local and regional administrators (Eikeland et al. 2004, Wendland et al. 2011). Based on the 1993 Principles of Forest Legislation, forest management and administration were decentralized to local forest administrators, giving them responsibility for forest management activities, including sanitary cuts, thinning, and reforestation. Concurrent privatization of logging enterprises and wood processing centers did not stop highly inefficient wood utilization and poor management of forest areas that was present during Soviet times (Krott et al. 2000). In 1997, Russia issued its first forest code, which recentralized the decision making authority first to the regional level, and later to the federal level, and one aim was to stop illegal harvesting activities (Torniainen et al. 2006). In the latest version of the Forest Code, Russia again decentralized decision-making to the regional level, while at the same time designating responsibilities for forest resource use to private timber firms (Torniainen and Saastamoinen 2007).

Similar to the forest sector, the agricultural sector underwent substantial changes after 1991. The introduction of a market-driven economy resulted in the end of most agricultural subsidies. Together with rural population decline wide areas of agricultural land were abandoned (Lerman 2009), many of which are now reverting back to forests (Prishchepov et al., 2012).

Data and Methods

Data and pre-processing

We used a stratified random sample of 12 Landsat footprints that we were confident of being able to represent the variability of forest areas and forest-area changes across the temperate region of European Russia. To select a representative sample we stratified our study area by forest cover, and selected a random sample of footprints from each stratum. We stratified the Landsat footprints by forest cover using the 2005 MODIS vegetation continuous field (VCF; Hansen et al. 2006), to ensure that our sample contained areas of higher and lower proportion of forest cover in the landscape. Our interest was to analyze the differences among administrative regions and these differences affect forest-cover patterns. Thus we calculated the mean value of the mean tree canopy cover for each administrative region, and divided the regions into five forest cover categories of approximately even size. We then attached the Landsat footprints that overlaps each region and randomly selected two footprints from each category and one additional footprint from the two categories with the highest forest cover. With this method, a Landsat footprint always contained the information of the administrative region it overlaps with most (Figure 1). This way we were able to capture the variability of forest cover within the study region with extra attention given to forested areas. This gave a total sample size of 12 Landsat footprints. For each footprint we selected six images, representing 5-year-intervals from 1985 to 2010. We used data from the Landsat sensors TM4 and TM5 as well as from Landsat ETM+ prior to May 2003. We avoided using ETM+ imagery for the time periods after May 2003 because of the scanline corrector (SLC) data gap issue. We selected images that (a) had no or very low cloud contamination, (b) were recorded during the growing season, and (c) were closest to the year of interest (i.e., 1985, 1990, 1995 etc.). 71 out of 76 images were acquired from the United States Geological Survey (USGS 2006) in terrain-corrected quality (L1T) and the remaining images were co-registered to these images using automated tie-point collection (Kuemmerle et al. 2006). We included the Space Shuttle Topography Mission (SRTM) digital elevation model (resampled to 30 m) in the co-registration process to account for relief displacement. The average positional error of the co-registered images was less than 0.20 pixel (or less than 6 m). Some images showed contamination by clouds, which were digitized and masked.

Training and image classification

The task of classifying 72 Landsat scenes (12 footprints with six time steps each) necessitated that we used a training strategy to minimize the overall training effort while maximizing classification accuracy. To do this, we first classified the 2010 image of every footprint using the Iterative Self Organizing Data Analysis Technique (ISODATA) unsupervised classification algorithm into 40 classes and labeled each class either as 'forest' or 'other land cover'. Within both 'forest', and 'other land cover' we randomly sampled 1000 points, ensuring a minimum distance of 2000 m between points to minimize spatial auto-correlation. We then labeled each point as either 'forest' or 'other land cover'. Points were considered 'forest', if they covered at least one Landsat pixel (30x30m) and their tree cover exceeded 60%, corresponding to the category of 'closed tree cover' in the Land Cover Classification system by Di Gregorio (2005). This means that our forest definition included orchards, but not single trees, rows of tree or open shrublands. Our criteria of 60% canopy cover was also more restrictive than the FAO definition where forest is "land with tree crown cover (or equivalent stocking level) of more than 10 percent and an area of more than 0.5 hectares (ha)" (FAO 2010).

To reduce the size of training data, we only considered points that had constant land cover over the entire time period. In other words, rather than labeling training points for each image of a given footprint separately, we analyzed all six images of a footprint simultaneously and considered only points that were consistently characterized as 'forest' or 'other land cover' in all six images (Kuemmerle et al. 2009). We based our decision for each point on the visual interpretation of the Landsat imagery and high resolution Quickbird imagery from Google Earth™. The Quickbird images were only used for confirmation and validation purposes as they were not available for the entire area and their image acquisition varied across our sample. Yet, they also provided useful information when a point was not directly covered by high resolution imagery, because in most cases in the neighborhood of the points high resolution coverage was available and the signature in the Landsat imagery was the same as at the actual point location. This increased the confidence of our labeling decision for each point as it was made based on the best information available. The 'consistency requirement' of our training data dictated that recovering forests be excluded, because no confident decision could be made to determine in every case that the land cover label satisfied our requirement of tree cover exceeding 60%. This strong conservative rule set for each point enabled us to generate one training dataset, which was applicable for each image within a footprint, greatly reducing the time for gathering the training data. At the same time, the pre-stratification using the ISODATA caused that despite these set of rules we had greater than 1750 points on average per footprint available for classification and validation.

We used Support Vector Machines (SVM) to classify our images. SVM fit a linear hyperplane between two classes in a multi-dimensional feature space (Foody and Mathur 2004a) by maximizing the margin between training samples of opposite classes. In the case of two non-linearly separable classes, SVM use kernel functions to transform training data into a higher dimensional feature space where linear separation is possible (Huang et al. 2002). The exclusive focus on pixels at the class boundaries (Foody and Mathur 2004b, 2006), and the ability to handle non-linear separation boundaries, makes SVM very efficient in handling complex class distributions (Huang et al., 2002, Pal and Mather 2005).

In the first step we parameterized a SVM-model using our training dataset and selected as a kernel function a Gaussian radial basis function. This function requires setting two parameters, which are training data dependent and hard to estimate a-priori: γ, describing the kernel width, and the regularization parameter C, that controls the trade-off between maximizing the margin and training error (Pal and Mather 2005). While small C-values tend to ignore outliers, large C-values may lead to overfitted SVM models depending on the variability of the training samples. To find the best γ-C-combination, we tested a wide range of combinations of these parameters and compared all models using cross-validation (Janz et al. 2007; Kuemmerle et al. 2008). We then selected the best performing model and classified each of the 72 Landsat TM/ETM+ images using the six reflective spectral bands and retrieved forest/non-forest maps for each of the six time steps. The changes between these time-steps were finally assessed using post-classification map comparison (Figure 6; Coppin et al. 2004).

Following image classification, we performed an accuracy assessment in three steps. In the first step, we assessed the accuracies for each classification individually. To do this we split our ground truth points into classification and validation points (90% and 10% of the overall points, respectively). Using the validation sample, we then assessed the accuracy of the classification, calculated the error matrix, and derived overall accuracy, user's and producer's accuracy, and the kappa statistic (Congalton 1991; Foody 2002). Additionally we calculated the F-measure that characterizes the overall classification accuracy by calculating weighted mean values of user's and producer's accuracy (van Rijsbergen 1979). For each image, we parameterized ten SVM using different combinations of training and validation points and averaged the resulting accuracy measures to derive robust accuracy estimates for each classification (Steele 2005). The final image classification then was carried out using all ground truth points of our sample, rendering the accuracy measures conservative estimates (Burman 1989). We also corrected our accuracy measures for possible sampling bias (Card 1982) and calculated confidence intervals around the area estimates (Stehman 2012).

In the second step we assessed the accuracy for a subset of our change maps. To do this, we randomly selected six out of the 60 change maps. For each of these change maps we converted the raster-map into polygons. As a reference, we created an image stack of the two reference images (e.g., the 1985 and the 1990 image for a 1985-1990 change map) and segmented the stack using a nested hierarchical scene model segmentation approach (Woodcock and Harward 1992). We then randomly selected 100 polygons of at least 1 ha size (equaling 12 pixels) for each class in the change map and compared it with the segments in the original images. We assigned a validation polygon to the class (constant forest, constant other, forest disturbance, forest recovery) based on visual interpretation of how the majority of the pixels in the polygon developed over time. For each class, we then calculated the same accuracy measures as for the single classifications.

Finally, we compared our classifications for the years 2000 and 2005 with a Landsat classification of the same region, made available by Potapov et al. (2011). This dataset is a wall-to-wall coverage of our study region in 60m resolution. To compare the two classification results, we sampled for every footprint 100 points into each of our two classes and compared the outcome with the classifications by Potapov et al. to derive a measure of agreement.

Some of our initial forest/non-forest classifications were unsatisfactory, mainly when image acquisition dates were either early (e.g., late April/early May) or late (mid to end of October) in the growing season. Detailed analyses of these classifications suggested that most of the classification errors were caused by the confusion between deciduous forest and grassland. We hypothesized that the addition of a second image from the winter season might increase the classification accuracy. We therefore added a winter-season image to the analysis and reran our classifications. We compared the classification results and accuracies of the single image classification with the 2-image stack results, and used the better classification for our analysis. After classifying each image, we applied a majority filter using a minimum mapping unit of 0.5 ha (approximately 6 pixels in a Landsat classification) to remove the salt-and-pepper effect that is typical in raster-based image classifications, but at the same time not omitting smaller scale disturbances.

Analysis of forest-cover change

To understand how forest cover changed in the temperate region, we analyzed our forest maps in two ways. First, we summarized areas of 'forest' for each footprint separately at each time step, and calculated changes in forested areas. To account for our uneven sample, which had a higher sampling density in the more forested regions, we weighted the percentages of change by the number of footprints within each stratum to obtain an accurate measure of forest-area change across the study region. Second, we analyzed forest-cover changes at the district level. We calculated the relative net change (RNC) of forest cover throughout the entire period following Kuemmerle et al (2009) as:

$$RNC = (FC_{2010} / FC_{1985} - 1) * 100$$

with FC as forest cover in km^2 of the described time period. Also at the district level we calculated annual disturbance rates DR for each time period as:

$$DR_j = (D_j / FCBj) * 100 / a$$

where D is the overall area of the disturbed forest during the analyzed time period j, FCB is the forest cover at the beginning of the same time period, and a is the number of years between acquisitions, since our acquisition intervals were not equal across footprints (Table 1).

Finally, we calculated proportion of forest area gain per time period FG_j as:

$$FG_j = (R_j / NF_{1985}) * 100$$

with R as the area not being forested in 1985 but forested in time period j and NF1985 is all non-forested area in 1985 (Kuemmerle et al. 2009).

Results

Our 72 SVM classifications yielded highly accurate forest/non-forest maps for all footprints across all time periods, with an average accuracy of 95.80% (standard deviation 1.51%, maximum 98.28%, minimum 91.16%) and kappa of 0.96 (0.01, 0.98, 0.91;Table 1). The six selected change maps had an average accuracy of 93.52% (standard deviation 1.32%, maximum 94.47%, minimum 90.96%; Table 3) and a kappa of 0.93 (0.01, 0.94, 0.91). The best classes in the change maps were the persistent classes (forest and other land cover), whereas the change classes had moderately lower accuracies (Table 2). Compared to the classifications by Potapov et al. (2011) we found an agreement of 90% between the two classifications.

Our classifications revealed that in 2010 45.53% of the investigated area was forested (Figure 2). The amount of forested areas varied across our study region. The regions with the most forest in 2010 were Kostroma (path/row 175/019; 21,541 km^2, 78.4% of the classified area), Novgorod (path/row 183/019; 18,223 km^2, 64.5% of the classified area), and Vladimir (path/row 176/021; 15,863 km^2, 54.3% of the classified area). The regions with the least forest in 2010 were Tambov (path/row 174/024; 2,962 km^2, 10.4% of the classified area) and Uljanovsk (path/row 171/022; 6,634 km^2, 23.3.% of the classified area).

Forest area changed substantially in our study region through the observed period (Figure 3). Across all 12 footprints, we found a net forest cover increase of 7,492 km², which corresponds to a weighted increase of 4.5% between 1985 and 2010. The regions with the largest net increase between 1985 and 2010 were Smolensk (551.85 km², 9.7%, path/row 181/022) and Kostroma (2257 km², 12.3%, path/row 175/019). Other regions only experienced a moderate net forest cover increase, such as Novgorod (647 km², 3.6%, path/row 183/019) or Kirov (943.43 km², 6.5%, path/row 172/020). In some regions we found a net forest cover decrease between 1985 and 2010, yet the net decreases were smaller than the largest net increases. For example, Uljanowsk (path/row 171/022) and Bashkortostan (path/row 16622) experienced minor decrease in forest area (-215 km² / -3.1% and -245 km² / -2.8%). The strongest net forest loss occurred in Tambov (path/row 174/024) with a loss of 455 km² (-12.2%).

Changes in forest area also varied across regions during the observed time period. For example, for 6 out of the 12 covered regions (Bashkortostan, Perm, Udmurtia, Uljanowsk, Vladimir, Smolensk) we found a net forest area decrease during the early post-Socialist years (period 1990-1995/2000), but a subsequent net increase in forest area. In some regions the net forest area change was strong enough to exceed Socialist forest area (e.g., Vladimir region with an overall gain of 8.1%). Yet, other regions had less forest now than during Soviet times (e.g., Uljanovsk, net loss of -1.3%). Regions that did not lose forest during 1990-1995/2000 either showed minor increase (e.g., Yaroslav, Tambov or Kirov region) or no significant change in forest area (e.g., Kostroma region). For most of the regions within our stratified random sample, we found a net increase of forest cover either over the last 10 years (strongest increase in the regions Vladimir (11.3%), Bryansk (7.1%), Kirov (6.9%)) or over the last 5 years (strongest increase in the regions Yaroslav (3.8%), Uljanovsk 5.1%, Figure 3).

Rates of RNC, disturbance and forest recovery varied substantially over time at the regional level (Figure 4). We found the strongest variation in Bashkortosan (Landsat path/row 166022) during the period 1985-1990 with a standard deviation of 9.42% (max 12.54%, min 2.62%), the lowest within-region variation was 0.10% (0.45%, 0.00%) in Smolensk (path/row 181022). Of all the districts, the highest disturbance rate occurred in a district in Uljanovsk (14.44% period 1985-1990), followed by a district in Kirov (13.11% period 1990-1995), and then Bashkortosan (19.54% period 1985-1990). On the other hand, there were also districts with essentially no disturbance (e.g., in Novgorod 1985-1990, Bryansk 179023, and Uljanovsk 2000-2005). Within-region variation (i.e., different disturbance rates among districts within one region) changed over time in some regions. The highest changes over time occurred in Bashkortosan (standard deviations of 9.42%, 1.26%, 0.80%, 3.94%, 1.73% for the five change periods), Vladimir (2.70%, 0.85%, 2.48%, 0.87%, 4.30%), and Kirov (3.04%, 3.20%, 7.07%, 0.92%, 5.26%). The variations within all other regions did not change as strongly over time.

Variations at the district level were also observed for the relative net forest area change. For example, in Bryansk, some districts increased by up to 35.20% in forest area, whereas for other districts decreased by up to -21.31%. In Kostroma all districts gained forest area (max 23.38%, min 1.51%). All other regions contained both districts that gained and districts that lost forest area (Figure 4).

When acquisition dates were suboptimal, adding a winter image reduced the classification errors in average from 4.38% to 2.50%. On average, the overall classification accuracy (OCA) increased by 1.95% (standard deviation 1.81%), kappa by 0.04 (0.04) and the F-Measure by 1.97% (1.83%; Figure 5). We found the strongest improvement for 1990 in Landsat footprint 179/023 (increase in overall classification accuracy = 4.08%, Δ kappa = 0.08, Δ F-Measure = 4.13%), and the least improvement in 2000 in footprint 179/023 (increase in overall classification accuracy = 0.22%, Δ kappa = 0.004, Δ F-Measure = 0.23%; Figure 5).

Discussion

Widespread land-use changes have been reported for multiple regions in Eastern Europe for the time period during and after the collapse of the Soviet Union. (Wendland et al. 2011, Kuemmerle et al. 2011). Using a representative subset of 12 Landsat footprints our goal was to analyze regional differences of forest-area changes in the temperate zone of European Russia during and after the collapse of the Soviet Union. The analysis revealed that across our sample forest area initially declined after 1991, but then increased, resulting in a net increase by 2010 of about 6.2% more forest area compared to 1985. However, within our sample, forest-area changes varied substantially over time at both the regional and the district level, sometimes with opposite trends in forest area; suggesting that sub-national differences strongly affect forest cover.

Across samples across the study region, forest cover decreased during the early post-socialist years. This finding matched our expectations, since other Eastern European studies suggested similar patterns of forest-cover changes after 1991 (Kuemmerle et al. 2007, Griffith et al. 2012). Surprising, however, was the strong forest-area increase after 2000, and especially after 2005. This forest area increase is most likely a consequence of forest recovery on former disturbed forest areas and a second major land-use change in this region, farmland abandonment. Vast areas of farmland were abandoned after 1991, following the decline in subsidization, rural outmigration, and ownership changes (Lerman 2009; Mathijs and Swinnen 1998), and many of these former fields are now covered by shrubs and early successional forests or entirely replaced by planted forests (Prishchepov et al. 2012). Furthermore, field visits suggest that even more areas of abandoned farmland may revert to forests in the future, since many abandoned fields exhibit woody vegetation. The high rates of disturbances and forest recovery in some districts may be overestimations, given that our commission errors for these classes in the change maps are relatively high (Table 2).

We found substantial regional and district differences in forest-cover changes over time at the level of single Landsat footprints. For example, our sample includes regions with little or no changes (e.g., Yaroslav) and regions with substantial changes (e.g., Smolensk) in forest cover between 1985 and 2010 including different spatial-temporal pattern. At the same time we found strong within-region variations (i.e., strong differences at the district level within a region) and very homogenous regions and their forest cover. How can we explain these diverse patterns? Assumingly they are a result of the interaction of several factors that involve changing harvesting practices following changing socio-economic and administrative conditions as well as natural forest disturbance such as fires or windfall. From a socio-economic perspective we see the collapse of the Soviet Union as the main driver which led to decentralization of the forest administration from federal to regional levels following the Principles of Forest Legislation in 1993 and changes in the relative costs and benefits of timber harvesting in these regions (Wendland et al. 2011). The partial autonomy of regions to administer their forests might have led to different strategies of forest management and, possibly, to illegal harvesting at different levels in some regions (Torniainen and Saastamoinen 2007). The change in relative costs and benefits of timber harvesting would have influenced where timber harvesting occurred following privatization of the timber industry and changes in the overall economic conditions in Russia. As the other main driver for our forest pattern we emphasize the importance of natural disturbances, such as windfall and fires. Our results suggest different rates and patterns of change compared to official statistics. These statistics report, for example, a drop in harvesting rates between 1988 and 1993. For this divergence we see the different types of assessments being the main reason. More specifically, while in our study we mapped forest cover using remote sensing, assessed change rates using post-classification comparison and summarized them under 'disturbance rates', the official statistics exclusively recorded forest harvests on administrative levels and calculated 'harvesting rates'. In other words, our study included all types of disturbance, whereas the harvesting statistics contain harvests only. Given that fires can cause large declines in forest areas, are usually highly variable in time and space, and are present in Russian forests, this could potentially have caused the differences in the rates and patterns of our study compared to rates of official statistics.

Methodologically, our approach showed that analyzing a stratified random sample of Landsat footprints across a large study region is powerful in highlighting regional differences of forest-cover changes Our stratification based on the MODIS VCF product enabled us to capture the entire range of variability of forest cover which revealed being important for highlighting the regional differences. Our approach is thus particularly well suited to situations, where the main goal is to analyze and highlight spatial-temporal variability of forest area across a larger study area when at the same time data availability does not allow for complete coverage.

Similarly, our approach of post-classification map comparison of six binary forest/non-forest maps yielded accurate change maps. Our approach of gathering training data that did not change over time reduced the amount of overall training data for the classification, and hence the time needed to gather these data. This made it possible to perform a long-term analysis with multiple time steps as a series of bi-temporal post-classification comparisons. Hence, our approach may be viewed as a good compromise between traditional bi-temporal change detection methods (Coppin et al. 2004) and more recent trajectory based land-cover change approaches (Kennedy et al. 2011) which require more frequent data than what may be available in many places (Prishchepov et al., 2012).

The use of winter imagery increased classification accuracy when available image dates were sub-optimal. Stueve et al. (2011) tested winter imagery and found that their use decreased commission errors, leading overall to more accurate classifications. Our results confirmed this. In all cases classification accuracies improved, and in some cases quite substantially so. Despite our already high classification accuracies, we were able to reduce the classification error by over 50% in relative terms. However, our tests were limited to three footprints and only to lower elevation areas (path/row 169/020: mean elevation of 167 m, range between 65 m and 332 m; 179/023: 200 m, 118-287 m; 167/020: 188m, 60-461m). We therefore recommend that more detailed studies be conducted in other forest types. Nevertheless, our results are promising, considering that the Landsat archives contain large amounts of winter imagery that have rarely been used for forest classifications in the past.

Our classification results are in strong agreement with the maps developed by Potapov et al. The small difference in agreement is likely a result of the different resolutions of the two data products (30m in our classification vs. 60m from Potapov et al.) as well the strategy of generating the training data (manually in our case, completely automated by Potapov et al.)

Despite the high single-map accuracies and the improvement using winter images, some classification errors remained. First, the application of our majority filter may have omitted smaller disturbances and re-growth. Yet, we were able to remove salt-and-pepper noise that is common in raster-based classification approaches. We therefore suggest that the application of such a filter likely improved the classification maps more than introducing errors by omitting small-scale disturbances. As we were mainly interested in investigating large-scale forest-cover trends, this form of omissions of small disturbance patches likely only have a very minor effect on the overall results. Second, positional uncertainties in the Landsat images prevented us from labeling points at the forest/non-forest boundaries, which were subsequently excluded from our analysis. These points were also not included in the accuracy assessment, so that classification accuracies in regions where mixed pixels were widespread are possibly overestimated. Third, the positional uncertainties also possibly influenced the quality of the change classes: our training strategy only considered stable 'forest' and 'non-forest' pixels while not explicitly training on the dynamic classes. This possibly introduced classification errors especially in regions of forest recovery, either after forest disturbance or in case of re-growing forests on abandoned agricultural fields. For example, depending on the spectral characteristics of the landscape manifested in the image, young deciduous forest stands on former agricultural fields, may have been assigned to the 'non-forest' category because their reflective spectra were more similar to an agricultural field during the summer than the forest category. In some cases, this might have lead to omissions of forest recovery in certain time steps, but highlighting them in the following time step. In other words, our training design that focused on the constant classes might have caused that the detected forest recovery be assigned to the 'wrong' time step, slightly influencing the spatial-temporal pattern. For the study period and the subset of Landsat footprints (1985-2010) as a whole, however, we are confident of the mapped total area estimates. Finally, the comparison of mono-temporal maps in a time series might have led to an accumulation of classification errors over time. Indeed, the accuracy assessments for our change maps showed accuracy rates that were slightly lower than the theoretical suggestions by Coppin et al. (2004). The validation and the interpretation of accuracy assessments of long classification time series is a problem that has rarely been tackled in the remote sensing literature. Cohen et al. (2010) recently provided a method and tools for the validation and interpretation of dense time stacks. However his framework mainly focuses on time series of annual observations. For many regions of the world, such as the present case, data availability does not allow for annual observations, subsequently leading to other interpretations of detected change. How to handle classification errors that propagate through the time series and how to interpret change products from such analyses, however, has not been investigated yet, despite the fact that this type of analysis will likely gain importance in the future. We therefore suggest that further studies should focus on accuracy measures for long time series that do not consist of annual observations.

Conclusions

In this paper we characterized forest-cover changes between 1985 and 2010 in 5-year-intervals for Russia's temperate forests using a stratified random sample of Landsat footprints. Our results suggest that forest cover decreased after 1991, but since 2000, the region experienced a net forest-cover increase especially so after 2005.

The large variations at the regional and district levels and over time indicate that socioeconomic conditions and the major socioeconomic changes, including changes in forest administration and legislation, that occurred after the collapse of the Soviet Union likely influenced forest cover in the temperate region of European Russia.

The regrowth of forests on abandoned farmlands possibly provide important opportunities for carbon sequestration as suggested from studies in other Eastern European regions (Kuemmerle et al. 2011). The detected widespread farmland abandonment in European Russia and the ongoing and observed onset of forest regrowth on these areas could indicate that the region potentially could turn into a large carbon sink in the future.

From a remote sensing perspective, our study makes two main contributions. First, when available data in space and time are limited, sampling a representative subset of Landsat scenes offers the opportunity to study forest-cover changes across a large area over a long time period and to highlight strong spatial-temporal variations of forest-cover change. Second, our study shows for the temperate zone that winter images can be useful to improve classification accuracy when acquisition dates are suboptimal; and we emphasize the value of winter imagery in forest-cover classifications, given that in some regions of the world data availability is very low.

References

1. Achard, F., Eva, H.D., Stibig, H.J., Mayaux, P., Gallego, J., Richards, T., and Malingreau, J.P. (2002). Determination of deforestation rates of the world's humid tropical forests. *Science*, 297, 999-1002
2. Baumann, M., Kuemmerle, T., Elbakidze, M., Ozdogan, M., Radeloff, V.C., Keuler, N.S., Prishchepov, A.V., Kruhlov, I., and Hostert, P. (2011). Patterns and drivers of post-socialist farmland abandonment in Western Ukraine. *Land Use Policy*, 28, 552-562
3. Bonan, G.B. (2008). Forests and climate change: Forcings, feedbacks, and the climate benefits of forests. *Science*, 320, 1444-1449
4. Böttcher, H., Kurz, W.A., and Freibauer, A. (2008). Accounting of forest carbon sinks and sources under a future climate protocol--factoring out past disturbance and management effects on age-class structure. *Environmental Science and Policy*, 11, 669-686
5. Burman, P. (1989). A Comparative-study of ordinary cross-validation, v-fold cross-validation and the repeated learning-testing methods. Biometrika, 76, 503-514
6. Card, D.H. (1982). Using known map category marginal frequencies to improve estimates of thematic map accuracy. *Photogrammetric Engineering and Remote Sensing*, 48, 431-439
7. Congalton, R.G. (1991). A Review of Assessing the Accuracy of Classifications of Remotely Sensed Data. *Remote Sensing of Environment*, 37, 35-46

8. Coppin, P., Jonckheere, I., Nackaerts, K., Muys, B., and Lambin, E. (2004). Digital change detection methods in ecosystem monitoring: a review. *International Journal of Remote Sensing*, 25, 1565-1596

9. Di Gregorio, A. (2005). Land Cover Classification System Classification (LCCS). Concepts and User Manual Software Version 2. Rome: *Food and Agriculture Organisation of the United Nations*.

10. Eikeland, S., Eythorsson, E., and Ivanova, L. (2004). From management to mediation: Local forestry management and the forestry crisis in post-socialist Russia. *Environmental Management*, 33, 285-293

11. FAO (1996). Forest Resources Assessment 1990. Survey of Tropical Forest Cover and study of Change. *FAO Forestry Paper*, 130

12. FAO (2010). Global Forest Ressource Assessment 2010. (p. 378)

13. Foley, J.A., DeFries, R., Asner, G.P., Barford, C., Bonan, G., Carpenter, S.R., Chapin, F.S., Coe, M.T., Daily, G.C., Gibbs, H.K., Helkowski, J.H., Holloway, T., Howard, E.A., Kucharik, C.J., Monfreda, C., Patz, J.A., Prentice, I.C., Ramankutty, N., and Snyder, P.K. (2005). Global consequences of land use. *Science*, 309, 570-574

14. Foody, G.M. (2002). Status of land cover classification accuracy assessment. *Remote Sensing of Environment*, 80, 185-201

15. Foody, G.M., and Mathur, A. (2004a). A relative evaluation of multiclass image classification by support vector machines. *IEEE Transactions on Geoscience and Remote Sensing*, 42, 1335-1343

16. Foody, G.M., and Mathur, A. (2004b). Toward intelligent training of supervised image classifications: directing training data acquisition for SVM classification. *Remote Sensing of Environment*, 93, 107-117
17. Foody, G.M., and Mathur, A. (2006). The use of small training sets containing mixed pixels for accurate hard image classification: Training on mixed spectral responses for classification by a SVM. *Remote Sensing of Environment*, 103, 179-189
18. Gallego, F.J. (2005). Stratified sampling of satellite images with a systematic grid of points. *ISPRS Journal of Photogrammetry and Remote Sensing*, 59, 369-376
19. Gibbs, H.K., Ruesch, A.S., Achard, F., Clayton, M.K., Holmgren, P., Ramankutty, N., and Foley, J.A. (2010). Tropical forests were the primary sources of new agricultural land in the 1980s and 1990s. *Proceedings of the National Academy of Sciences*, 107, 16732-16737
20. Goward, S.N., Masek, J.G., Cohen, W.B., Moisen, G.G., Collatz, G.J., Healey, S., Houghton, R.A., Huang, C., Kennedy, R.E., Law, B., Powell, S., Turner, D., and Wulder, M.A. (2008). Forest disturbance and North American carbon flux. *Eos Transactions*, 89, 105-116
21. Griffiths, P., Kuemmerle, T., Kennedy, R.E., Abrudan, I.V., Knorn, J., and Hostert, P. (2012). Using annual time-series of Landsat images to assess the effects of forest restitution in post-socialist Romania. *Remote Sensing of Environment*, 118, 199-214
22. Guo, L.B., and Gifford, R.M. (2002). Soil carbon stocks and land use change: a meta analysis. *Global Change Biology*, 8, 345-360

23. Hansen, M., DeFries, R., Townshend, J.R., Carroll, M., Dimiceli, C., and Sohlberg, R. (2006). Vegetation Continuous Fields MOD44B, 2001 Percent Tree Cover, Collection 4. University of Maryland, College Park, Maryland, 2001

24. Hansen, M.C., Stehman, S.V., and Potapov, P.V. (2010). Quantification of global gross forest cover loss. *Proceedings of the National Academy of Sciences*, 107, 8650-8655

25. Hansen, M.C., Stehman, S.V., Potapov, P.V., Loveland, T.R., Townshend, J.R.G., DeFries, R.S., Pittman, K.W., Arunarwati, B., Stolle, F., Steininger, M.K., Carroll, M., and DiMiceli, C. (2008). Humid tropical forest clearing from 2000 to 2005 quantified by using multitemporal and multiresolution remotely sensed data. *Proceedings of the National Academy of Sciences of the United States of America*, 105, 9439-9444

26. Houghton, R.A. (2005). Aboveground forest biomass and the global carbon balance. *Global Change Biology*, 11, 945-958

27. Huang, C., Davis, L.S., and Townshend, J.R.G. (2002). An assessment of support vector machines for land cover classification. *International Journal of Remote Sensing*, 23, 725 - 749

28. Huang, C., Goward, S.N., Masek, J.G., Gao, F., Vermote, E.F., Thomas, N., Schleeweis, K., Kennedy, R.E., Zhu, Z., Eidenshink, J.C., and Townshend, J.R.G. (2009a). Development of time series stacks of Landsat images for reconstructing forest disturbance history. *International Journal of Digital Earth*, 2, 195 - 218

29. Huang, C., Goward, S.N., Masek, J.G., Thomas, N., Zhu, Z., and Vogelmann, J.E. (2010). An automated approach for reconstructing recent forest disturbance history using dense Landsat time series stacks. *Remote Sensing of Environment*, 114, 183-198

30. Huang, C., Goward, S.N., Schleeweis, K., Thomas, N., Masek, J.G., and Zhu, Z. (2009b). Dynamics of national forests assessed using the Landsat record: Case studies in eastern United States. *Remote Sensing of Environment*, 113, 1430-1442

31. Janz, A., van der Linden, S., Waske, B., and Hostert, P. (2007). imageSVM - A user-orientated tool for advanced classification of hyperspectral data using Support Vector Machines. In, *Proceedings of the 5th EARSeL workshop on Imaging Spectroscopy*, Bruges, Belgium

32. Kennedy, R.E., Yang, Z., and Cohen, W.B. (2011). Detecting trends in forest disturbance and recovery using yearly Landsat time series: 1. LandTrendr -- Temporal segmentation algorithms. *Remote Sensing of Environment*, 114, 2897-2910

33. Knorn, J., Kuemmerle, T., Radeloff, V.C., Szabo, A., Mindrescu, M., Keeton, W.S., Abrudan, I., Griffiths, P., Gancz, V., and Hostert, P. (2012). Forest restitution and protected area effectiveness in post-socialist Romania. *Biological Conservation*, 146, 204-212

34. Krott, M., Tikkanen, I., Petrov, A., Tunystsya, Y., Zheliba, B., Sasse, V., Rykounina, I., and Tynytsya, T. (2000). Policies for Sustainable Forestry in Belarus, Russia and Ukraine. In: *European Forest Institute Research Report No. 9.* Koninklijke Brill NV, Leiden.

35. Kuemmerle, T., Chaskovskyy, O., Knorn, J., Radeloff, V.C., Kruhlov, I., Keeton, W.S., and Hostert, P. (2009). Forest cover change and illegal logging in the Ukrainian Carpathians in the transition period from 1988 to 2007. *Remote Sensing of Environment*, 113, 1194-1207

36. Kuemmerle, T., Hostert, P., Radeloff, V.C., van der Linden, S., Perzanowski, K., and Kruhlov, I. (2008). Cross-border Comparison of Post-socialist Farmland Abandonment in the Carpathians. *Ecosystems*, 11, 614-628

37. Kuemmerle, T., Olofsson, P., Chaskovskyy, O., Baumann, M., Ostapowicz, K., Woodcock, C.E., Houghton, R.A., Hostert, P., Keeton, W.S., and Radeloff, V.C. (2011). Post-Soviet farmland abandonment, forest recovery, and carbon sequestration in western Ukraine. *Global Change Biology*, 17, 1335-1349

38. Kuemmerle, T., Radeloff, V.C., Perzanowski, K., and Hostert, P. (2006). Cross-border comparison of land cover and landscape pattern in Eastern Europe using a hybrid classification technique. *Remote Sensing of Environment*, 103, 449-464

39. Lambin, E.F., Geist, H.J., and Lepers, E. (2003). Dynamics of land-use and land-cover change in tropical regions. *Annual Review of Environment and Resources*, 28, 205-241

40. Lerman, Z. (2009). Land reform, farm structure, and agricultural performance in CIS countries. *China Economic Review*, 20, 316-326

41. Liira, J., Pussa, K., and Peterson, U. (2006). The radiance contrast of forest-to-clearcut edges on a medium resolution Landsat Enhanced Thematic Mapper satellite winter image. *International Journal of Remote Sensing*, 27, 2753-2766

42. Main-Knorn, M., Hostert, P., Kozak, J., and Kuemmerle, T. (2009). How pollution legacies and land use histories shape post-communist forest cover trends in the Western Carpathians. *Forest Ecology and Management*, 258, 60-70

43. Mathijs, E., and Swinnen, J.F.M. (1998). The economics of agricultural decollectivization in East Central Europe and the former Soviet Union. *Economic Development and Cultural Change*, 47, 1-26

44. Olofsson, P., Kuemmerle, T., Griffiths, P., Knorn, J., Baccini, A., Gancz, V., Blujdea, V., Houghton, R.A., Abrudan, I.V., and Woodcock, C.E. (2011). Carbon implications of forest restitution in post-socialist Romania. *Environmental Research Letters*, 6, 045202

45. Pal, M., and Mather, P.M. (2005). Support vector machines for classification in remote sensing. *International Journal of Remote Sensing*, 26, 1007-1011

46. Peterson, U., Pussa, K., and Liira, J. (2004). Issues related to delineation of forest boundaries on Landsat Thematic Mapper winter images. *International Journal of Remote Sensing*, 25, 5617-5628

47. Potapov, P., Turubanova, S., and Hansen, M.C. (2011). Regional-scale boreal forest cover and change mapping using Landsat data composites for European Russia. *Remote Sensing of Environment*, 115, 548-561

48. Potapov, P., Yaroshenko, A., Turubanova, S., Dubinin, M., Laestadius, L., Thies, C., Aksenov, D., Egorov, A., Yesipova, Y., Glushkov, I., Karpachevskiy, M., Kostikova, A., Manisha, A., Tsybikova, E., and Zhuravleva, I. (2008). Mapping the World's intact forest landscapes by remote sensing. *Ecology and Society*, 13

49. Prishchepov, A., V., Radeloff, V., C., Baumann, M., Kuemmerle, T., and Müller, D. (2012). Effects of institutional changes on land use: agricultural land abandonment

during the transition from state-command to market-driven economies in post-Soviet Eastern Europe. *Environmental Research Letters*, 7, 024021

50. Reese, H.M., Lillesand, T.M., Nagel, D.E., Stewart, J.S., Goldmann, R.A., Simmons, T.E., Chipman, J.W., and Tessar, P.A. (2002). Statewide land cover derived from multiseasonal Landsat TM data: A retrospective of the WISCLAND project. *Remote Sensing of Environment*, 82, 224-237
51. Serebryanny, L. (2002). Mixed and decidious forests. In M. Shahgedanova (Ed.), The physical geography of northern Eurasia (pp. 234-247): Oxford University Press
52. Steele, B.M. (2005). Maximum posterior probability estimators of map accuracy. *Remote Sensing of Environment*, 99, 254-270
53. Stehman, S.V. (2012). Impact of sample size allocation when using stratified random sampling to estimate accuracy and area of land-cover change. *Remote Sensing Letters*, 3, 111-120
54. Stueve, K.M., Housman, I.W., Zimmerman, P.L., Nelson, M.D., Webb, J.B., Perry, C.H., Chastain, R.A., Gormanson, D.D., Huang, C., Healey, S.P., and Cohen, W.B. (2011). Snow-covered Landsat time series stacks improve automated disturbance mapping accuracy in forested landscapes. *Remote Sensing of Environment*, 115, 3203-3219
55. Tirpak, J.M., and Giuliano, W.M. (2010). Using multitemporal satellite imagery to characterize forest wildlife habitat: The case of ruffed grouse. *Forest Ecology and Management*, 260, 1539-1547

56. Torniainen, T.J., and Saastamoinen, O.J. (2007). Formal and informal institutions and their hierarchy in the regulation of the forest lease in Russia. *Forestry*, 80, 489-501

57. Torniainen, T.J., Saastamoinen, O.J., and Petrov, A.P. (2006). Russian forest policy in the turmoil of the changing balance of power. *Forest Policy and Economics*, 9, 403-416

58. Turnock, D. (1998). Introduction. In D. Turnock (Ed.), Privatization in Rural Eastern Europe. The Process of Restitution and Restructuring (pp. 1-48). Cheltenham: Edward Elgar

59. USGS (2006). USGS Landsat project.

60. van Rijsbergen, C.J. (1979). Information Retrieval. London: Butterworth-Heinemann

61. Vuichard, N., Ciais, P., Belelli, L., Smith, P., and Valentini, R. (2008). Carbon sequestration due to the abandonment of agriculture in the former USSR since 1990. *Global Biogeochemical Cycles*, 22

62. Wang, T., Skidmore, A.K., Toxopeus, A.G., and Liu, X. (2009). Understory bamboo discrimination using a winter image. *Photogrammetric Engineering and Remote Sensing*, 75, 37-47

63. Wendland, K.J., Lewis, D.J., Alix-Garcia, J., Ozdogan, M., Baumann, M., and Radeloff, V.C. (2011). Regional- and district-level drivers of timber harvesting in European Russia after the collapse of the Soviet Union. *Global Environmental Change*, 21, 1290-1300

64. Woodcock, C., and Harward, V.J. (1992). Nested hierarchical scene models and image segmentation. *International Journal of Remote Sensing*, 13, 3167-3187

Figure Captions

Figure 1: The temperate zone of European Russia with its administrative deviation, and the Landsat footprints, selected for classification.

Figure 2: Area estimates, summarized and averaged across all 12 footprints. The top diagram indicates the overall area at each time step in km2, including the absolute areas of forest disturbance and forest recovery. The bottom diagram shows the net change of forested areas in km2 to the previous time-step.

Figure 3: Forest area estimates for each footprint. The top diagram indicates the overall area at each time step in km2, including the absolute areas of forest disturbance and forest recovery. The bottom diagram shows the net change of forested areas in km2 to the previous time-step.

Figure 4: Rates of forest disturbance and forest recovery per time period (left and middle column), and relative net change (RNC) of forested area over the entire observation period, aggregated at the district level.

Figure 5: Difference in classification accuracies after adding a winter-image when image acquisition was sub-optimal.

Figure 6: Forest-cover change map for footprint 176021 (Vladimir region) for 1985-2010

Tables

Table 1: Classified footprints and average classification accuracies. All values represent percentages, except for the kappa-values, which range between 0 and 1, and were

		Overall Accuracy	Kappa	User's Accuracy		Producer's Accuracy		F1-Measure	
				F	NF	F	NF	F	NF
Average accuracies by Path/Row	176021	94.37	0.95	94.46	93.96	95.32	95.72	92.90	94.83
	181022	95.10	0.951	94.92	95.03	95.16	92.98	96.58	93.99
	171022	97.16	0.972	95.99	96.91	97.24	90.95	99.10	93.82
	179023	97.14	0.97	97.02	97.30	97.07	95.68	98.07	96.48
	169020	96.98	0.97	96.97	97.18	96.81	96.97	96.96	0.971
	167020	96.25	0.96	96.24	96.27	96.26	96.18	96.27	96.22
	175019	93.93	0.94	91.92	93.27	96.11	98.73	81.06	95.92
	174024	95.69	0.96	88.14	95.25	95.73	67.26	99.56	78.67
	166022	96.40	0.96	95.83	95.68	96.73	92.97	98.02	94.30
	179019	95.30	0.95	95.29	94.44	96.14	95.88	94.74	95.15
	172020	97.27	0.97	97.27	96.64	97.90	97.76	96.80	97.19
	183019	94.04	0.94	93.47	93.69	94.73	97.16	88.60	95.39
Average accuracies by time-step	1985	95.59	0.96	94.71	95.55	96.03	93.19	94.66	94.14
	1990	95.38	0.95	94.05	94.98	95.73	91.52	95.04	92.78
	1995	95.93	0.96	94.91	95.86	96.18	92.69	95.55	94.02
	2000	95.89	0.96	94.91	95.32	96.50	93.26	95.05	94.12
	2005	95.89	0.96	94.99	95.65	96.30	93.61	94.90	94.44
	2010	96.13	0.96	95.20	95.44	96.85	94.85	94.13	95.02
Accuracies across all classifications	Mean	95.80	0.96	94.79	95.47	96.27	93.19	94.89	94.09
	STD.	1.51	0.01	2.85	1.76	1.35	8.56	5.23	5.21
	Max	98.28	0.98	98.23	98.18	98.76	99.30	99.75	98.30
	Min	91.16	0.91	81.01	90.68	92.08	51.78	76.56	66.01

obtained by 10-fold cross-validation.

Table 2: Accuracy measures for six randomly selected change-maps. Presented are overall accuracy, kappa for the entire change map; for the classes F (persistent forest), NF (persistent non-forest), D (disturbance) and R (regrowth) user's and producer's accuracy are provided. All values represent percentages, except the kappa values, which range between 0 and 1.

Map	Overall Accuracy	Kappa	User's Accuracy				Producer's Accuracy			
			F	NF	D	R	F	NF	D	R
175019 1985-1990	93.49	0.93	95.00	94.00	78.00	80.00	97.95	88.19	69.32	76.15
179023 1985-1990	94.47	0.85	93.00	97.00	80.00	81.00	98.41	94.51	64.77	68.49
176021 1985-1990	94.20	0.94	96.00	93.00	90.00	80.00	98.76	95.59	44.01	49.85
169020 1990-1995	94.45	0.94	94.00	96.00	88.00	77.00	98.28	94.29	100.0	46.66
181022 2000-2005	90.96	0.91	92.00	91.00	80.00	81.00	96.23	96.20	74.20	24.03
183019 2005-2010	93.52	0.94	94.00	97.00	80.00	78.00	98.57	85.50	80.16	100.0

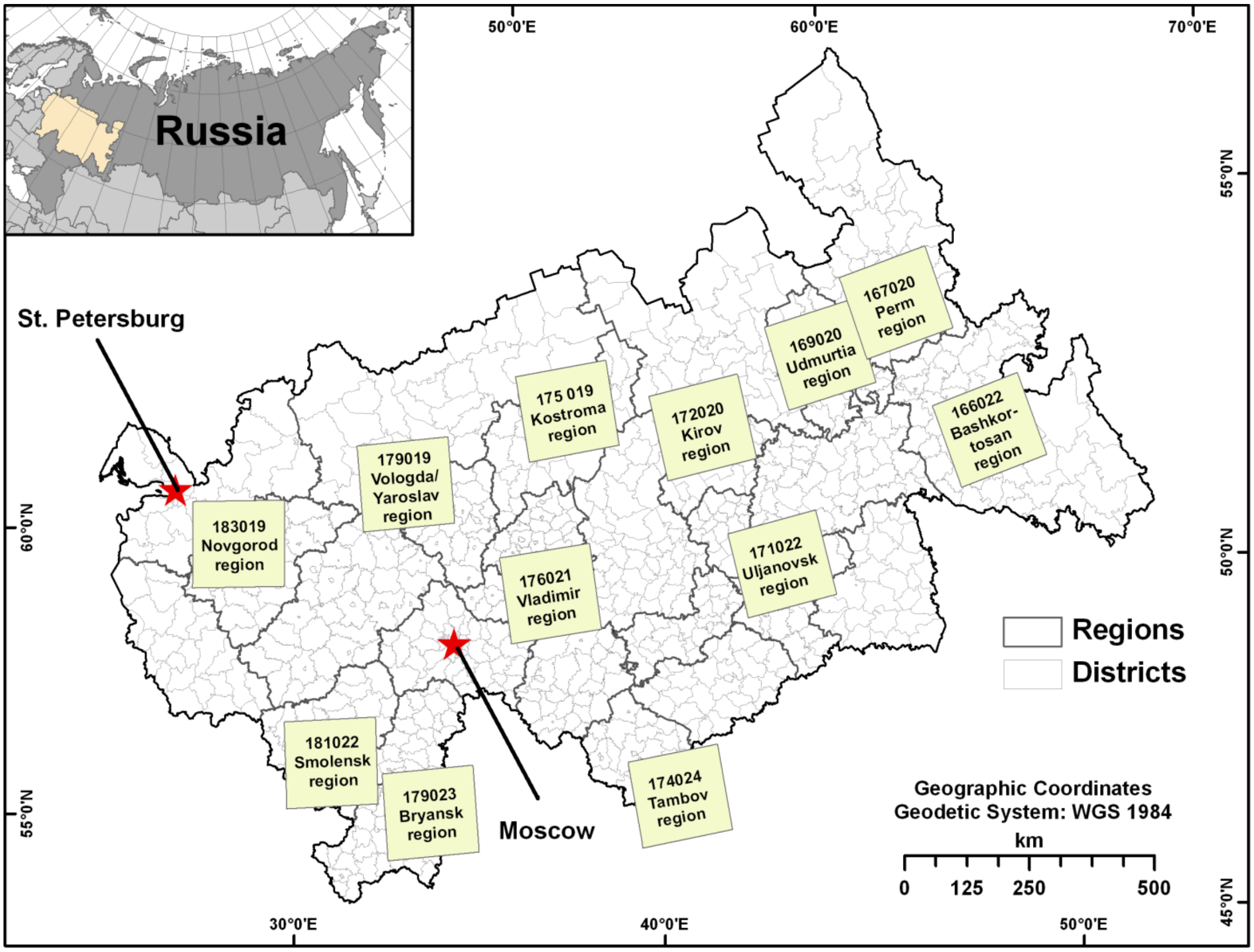

Russia
50°0'E
60°0'E
70°0'E
55°0'N
50°0'N
45°0'N
60°0'N
55°0'N
30°0'E
40°0'E
50°0'E
St. Petersburg
Moscow
183019 Novgorod region
179019 Vologda/ Yaroslav region
175 019 Kostroma region
172020 Kirov region
169020 Udmurtia region
167020 Perm region
166022 Bashkor-tosan region
176021 Vladimir region
171022 Uljanovsk region
181022 Smolensk region
179023 Bryansk region
174024 Tambov region
Regions
Districts
Geographic Coordinates
Geodetic System: WGS 1984
km
0
125
250
500

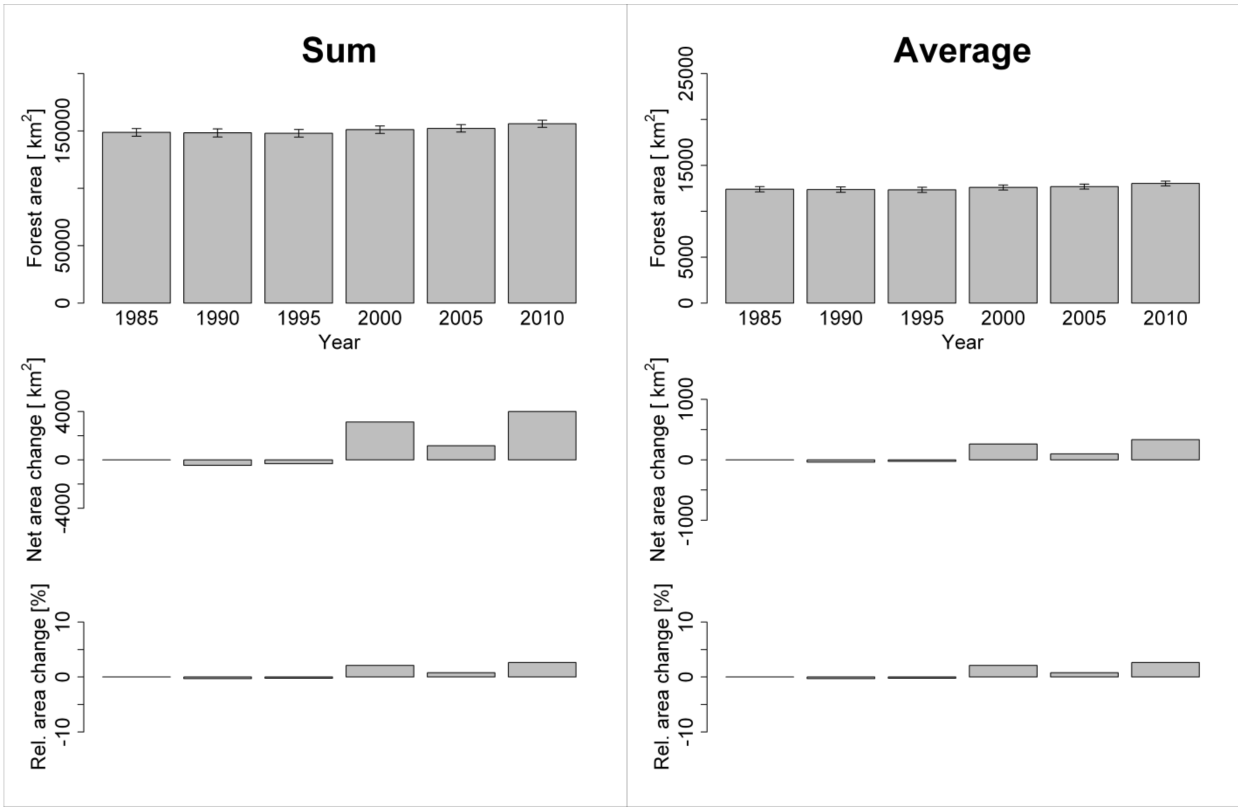

Sum
Average
Forest area [km2]
Net area change [km2]
Rel. area change [%]
Year
1985
1990
1995
2000
2005
2010

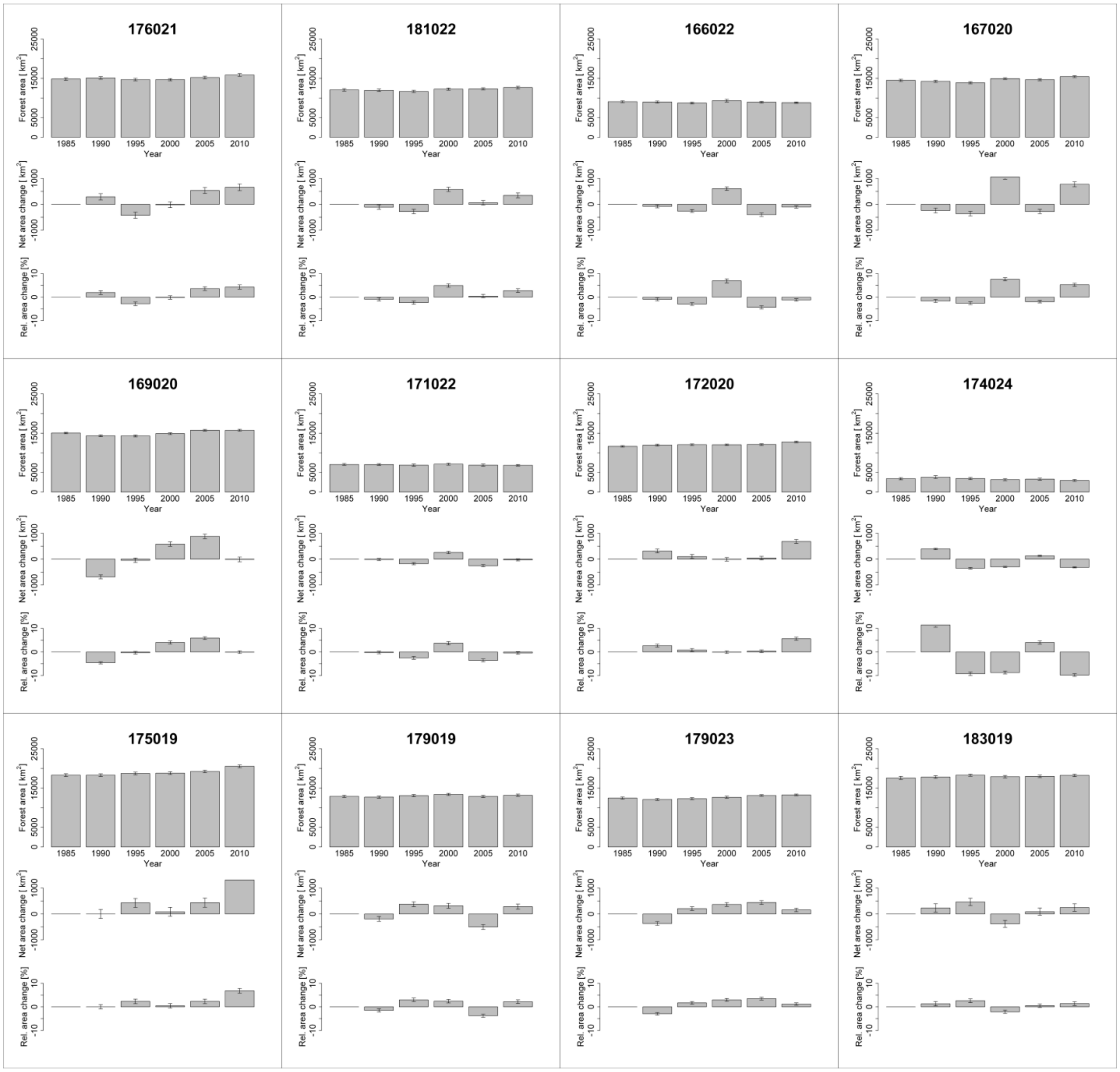
176021
181022
166022
167020
169020
171022
172020
174024
175019
179019
179023
183019
Forest area [km²]
Net area change [km²]
Rel. area change [%]
Year
1985
1990
1995
2000
2005
2010

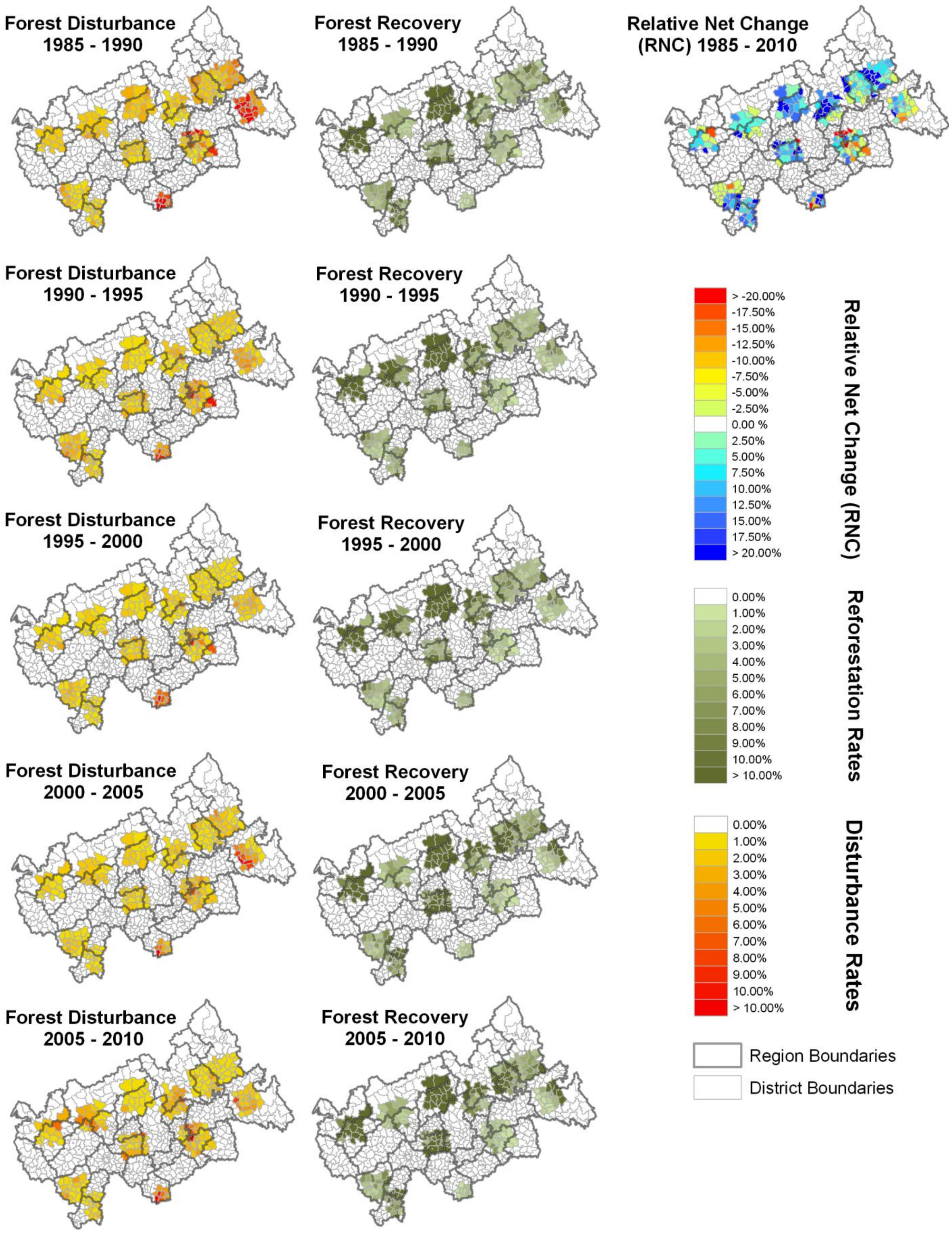

Forest Disturbance 1985 - 1990
Forest Recovery 1985 - 1990
Relative Net Change (RNC) 1985 - 2010
Forest Disturbance 1990 - 1995
Forest Recovery 1990 - 1995
Forest Disturbance 1995 - 2000
Forest Recovery 1995 - 2000
Forest Disturbance 2000 - 2005
Forest Recovery 2000 - 2005
Forest Disturbance 2005 - 2010
Forest Recovery 2005 - 2010
Relative Net Change (RNC)
> -20.00%
-17.50%
-15.00%
-12.50%
-10.00%
-7.50%
-5.00%
-2.50%
0.00 %
2.50%
5.00%
7.50%
10.00%
12.50%
15.00%
17.50%
> 20.00%
Reforestation Rates
0.00%
1.00%
2.00%
3.00%
4.00%
5.00%
6.00%
7.00%
8.00%
9.00%
10.00%
> 10.00%
Disturbance Rates
0.00%
1.00%
2.00%
3.00%
4.00%
5.00%
6.00%
7.00%
8.00%
9.00%
10.00%
> 10.00%
Region Boundaries
District Boundaries

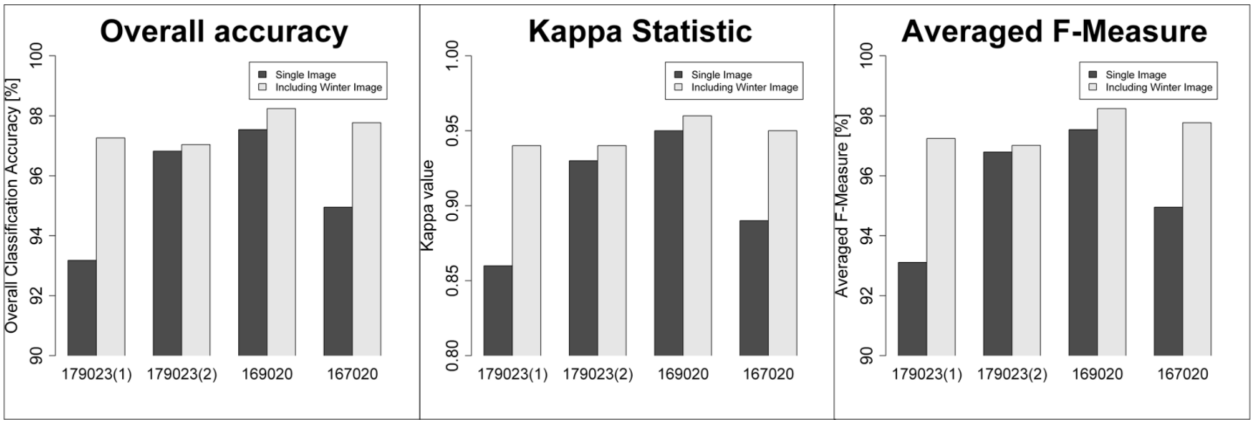
Overall accuracy
Overall Classification Accuracy [%]
Single Image
Including Winter Image
179023(1)
179023(2)
169020
167020
Kappa Statistic
Kappa value
Averaged F-Measure
Averaged F-Measure [%]

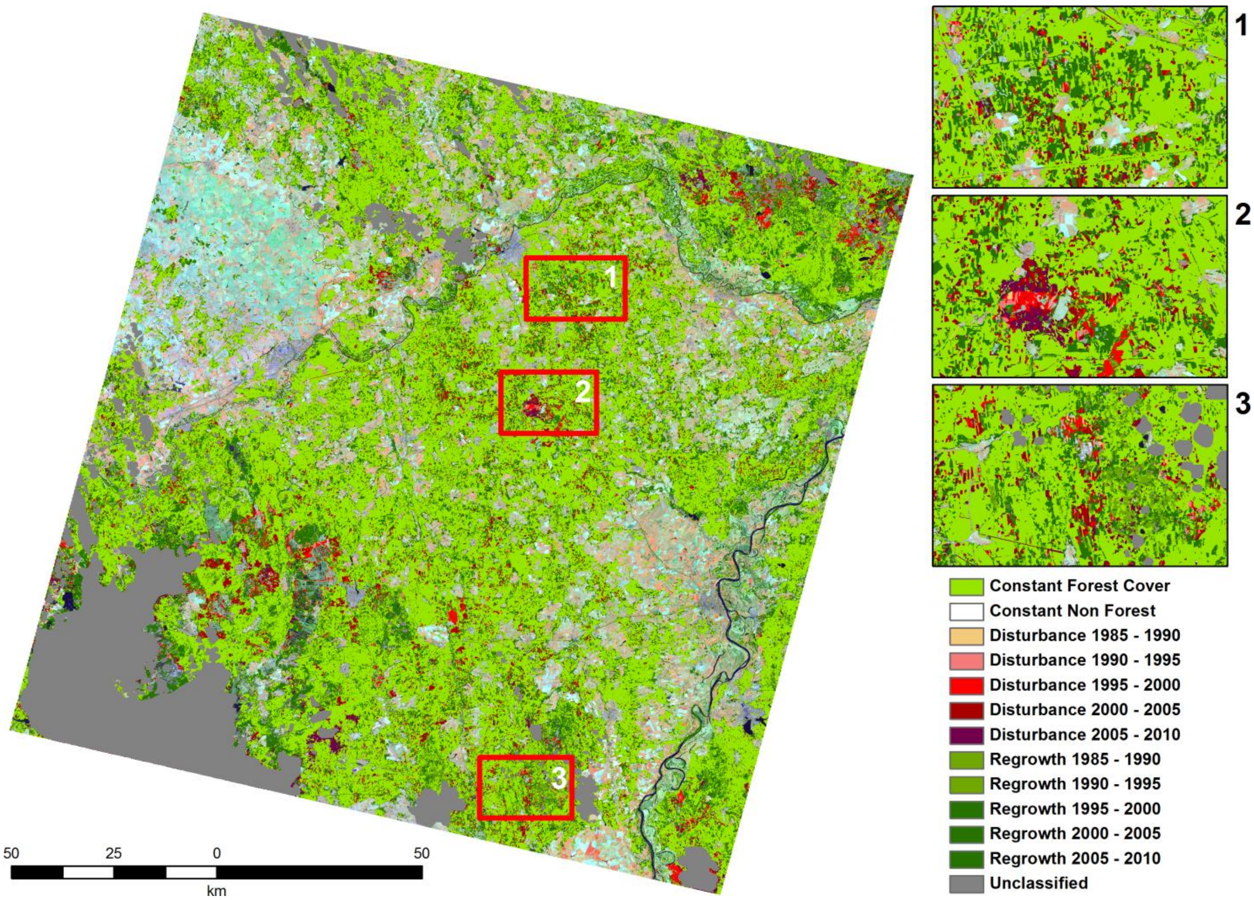
1
2
3
1
2
3
Constant Forest Cover
Constant Non Forest
Disturbance 1985 - 1990
Disturbance 1990 - 1995
Disturbance 1995 - 2000
Disturbance 2000 - 2005
Disturbance 2005 - 2010
Regrowth 1985 - 1990
Regrowth 1990 - 1995
Regrowth 1995 - 2000
Regrowth 2000 - 2005
Regrowth 2005 - 2010
Unclassified
50
25
0
50
km

Chapter 2: Landsat remote sensing of forest windfall disturbance

Co-Authors: Mutlu Ozdogan, Peter T. Wolter, Alexander Krylov, Nadezda Vladimirova, Volker C. Radeloff

Remote Sensing of Environment in review

Abstract:

Knowing if a forest disturbance is caused by timber harvest or a natural event is crucial for carbon cycle assessments, econometric analyses of timber harvesting, and other research questions. However, while remote sensing of forest disturbance in general is very well developed, discerning between different types of forest disturbances remains challenging. In this work, we developed an algorithm to separate windfall disturbance from clear-cut harvesting using Landsat data. The method first extracts training data primarily based on Tasseled Cap transformed bands and histogram thresholds with minimal user input. We then used a support-vector machine classifier to separate disturbed areas into 'windfall' and 'clear-cut harvests'. We tested our algorithm in the temperate forest zone of European Russia and the southern boreal forest zone of the United States. The forest-cover change classifications were highly accurate (~90%) and windfall classification accuracies were greater than 75% in both study areas. Accuracies were generally higher for larger disturbance patches. At the Russia study site about 60% of all disturbances were caused by windfall, versus 40% at

the U.S. study site. Given the similar levels of accuracy in both locations and the ease of application, the algorithm has the potential to fill a research gap in mapping wind disturbance using Landsat data in both temperate and boreal forests that are subject to frequent wind events.

Keywords:

Landsat, windfall, Forestness Index, Disturbance Index, Tasseled Cap Transformation

Introduction

Forests play an important role in the global carbon cycle and the provision of ecosystem services. Information on where and to what extent forest disturbances occur globally is thus a crucial necessity (Achard et al., 2002; Bonan 2008). Remote sensing can provide accurate and timely information regarding forest disturbance in many ecoregions at scales ranging from local to global and at many different temporal resolutions (Hansen and DeFries 2004; Healey et al. 2005; Achard et al. 2006; Potapov et al. 2009; Hansen et al. 2010;; Huang et al. 2010; Baumann et al. 2012; Potapov et al. 2012; Zhu et al. 2012). Data from Landsat Thematic Mapper (TM) and Enhanced Thematic Mapper Plus (ETM+) instruments have been used for many of these studies because of (1) the favorable combination of spatial, spectral and temporal resolution, (2) the free availability of the data (Wulder et al. 2012) and, (3) the long-term data record, which continues now thanks to the Landsat Data Continuity Mission (LDCM, Irons et al. 2012).

In most forest disturbance mapping studies that utilize Landsat data, the derived change products only identify areas of 'forest disturbance', but do not discriminate among different types of disturbances (e.g., Cohen et al. 1998; Coppin and Baur 1994; Ozdogan in press). This has already been identified as a gap in remote sensing based forest disturbance studies (e.g., Vogelmann et al. 2009; Masek et al. 2011; Hicke et al. 2012; Kasischke et al. 2013). The lack of attribution to the type of disturbance often makes it difficult to interpret forest disturbance maps, especially when these data are used as inputs to carbon budget assessments or econometric analyses. For example, many studies that seek to understand timber harvest trends are forced to equate forest disturbance with harvesting (e.g., Chomitz and Gray 1996; Wendland et al. 2011). As a result, natural disturbance is erroneously included in harvest estimates, which can lead to overestimation of harvested areas and dampen the significance of actual drivers of forest harvest. Inability to separate forest harvest from natural disturbances also affects studies that assess the effectiveness of protected areas in preventing logging (e.g., Hayes 2006; Andam et al. 2008; Wendland et al. in review). From the ecological point of view, information on the type of forest disturbance is important for biomass estimations and for the prediction of post-disturbance succession (Scheller and Mladenoff 2004; Kasischke et al. 2013). For example, more living biomass remains in place following a windfall event, compared to a clear-cut harvest, which can hinder the establishment of early successional species (Peterson 2000; Webb and Scanga 2001; Rich et al. 2010; Scheller et al. 2011).

The most common natural disturbances affecting forests are fire, insect defoliation and windfall (FAO 2005; FAO 2010). While remote sensing of fire-related disturbances and insect defoliation has received considerable attention in the past (e.g., French et al. 2008; Garcia-Haro et al. 2001; Patterson and Yool 1998; Pereira and Setzer 1993; Roder et al. 2008; Schroeder et al. 2011; Townsend et al. 2012; van Wagtendonk et al. 2004), only a handful of studies have focused on identifying and mapping windfall disturbances. In general, the existing studies can be categorized into two themes. The first category focuses on monitoring the impacts of tropical storms on forest structure using multispectral imagery or radar data (e.g. Nelson et al. 1994; Ramsey et al. 2009a,b;

Wang and Xu 2010; Negron-Suarez et al. 2010; Cheung et al. 2013). The second area of focus is severe storm (including tornados) damage on forests of continental interiors, which are characterized by smaller affected area but higher intensity disturbances, such as the Boundary Waters Blowdown in the Greater Border Lakes Region (USA) in 1999 (Rich et al 2010; Wolter et al. 2012). However, while these studies were successful in mapping the damage caused by each particular storm, they did not include developing a specialized, and potentially universal, method to separate wind-related change from other disturbances.

The Disturbance Index (DI, Healey et al. 2005) is an example of a universal method. The algorithm has been developed to detect areas of forest disturbance, and has been tested in a wide range of forest biomes including the Pacific Northwest (USA), the St. Petersburg and other locations in Russia, South-Sudan and Uganda and the conterminous United States (Healey et al. 2005; Masek et al. 2008; He et al. 2011; Gorsevski et al. 2012; Sieber et al. 2013). One reason for the success of the DI is its use of the Tasseled Cap transformation that convert Landsat bands into brightness', 'greenness', and 'wetness' measures to describe the variations in soil background reflectance, vegetation vigor, and vegetation senescence, respectively (Kauth and Thomas 1976; Crist and Kauth 1986). The success of the Tasseled Cap bands in the Disturbance Index across different study regions suggests that a windfall classification algorithm based on the same standardized bands might be successful as well across different regions throughout the world.

Our goal here was to develop an algorithm to distinguish windfall disturbance from forest harvests with Landsat data, exploiting the success of the DI for detecting wind-related forest damage in two different locations. Our specific objectives were to:

1. create a map of forest and forest disturbance using established methods from the literature,
2. develop an algorithm to separate the areas of forest-disturbance into windfall disturbance and clear-cut harvests,
3. test our algorithm in two study regions, (1) the temperate zone of European Russia and (2) the southern boreal forest zone of the United States.

Methods

Study Area

Our first study site is located in the temperate zone of European Russia (Landsat Path/Row 177/019, Figure 7 bottom right). Temperate coniferous, broadleaf, and mixed forests dominate the landscape with Norway spruce (Picea abies) and Scots pine (Pinus sylvestris) being the most abundant coniferous species. Major deciduous species include aspen (Populus tremula), grey alder (Alnus incana), and birch (Betula pendula). Commercial harvests are widespread in the region, because the Russian forestry sector is growing and western forest companies are increasing their investments in mills to exploit Russia's vast timber resources (Mutanen and Toppinen 2007). Besides commercial harvests, the region experiences frequent natural disturbance events. Specifically, the study region experienced two storms that occurred in October 2009 and

July 2010 (Koroleva and Ershov 2012), which were studied and mapped in detail by the Russian Forest Health Center (Krylov et al. 2012).

The second study site is located in the southern boreal forests in northern Minnesota (USA) (Landsat Path/Row 025/028, Figure 7, bottom left). The region is characterized by a mixture of glacial lakes and wetlands. Forest species in the region include early successional species, such as jack pine (Pinus banksiana), red pine (Pinus resinosa), or aspen (Populus tremuloides), as well as late successional species like white cedar (Thuja occidentalis) or balsam fir (Abies balsamea) (Frelich and Reich 1995; Rich et al. 2010). In 1999, the region experienced a large infrequent wind disturbances event, which is referred as the Boundary Waters Blowdown (or the Boundary Waters Canadian Derecho). The storm occurred between July 4th and 5th 1999 and lasted 22 hours. It travelled over 2000 km at an average pace of around 95 km/h, and with wind gusts of over 160 km/h. The storm caused over 1500 km2 of considerable forest damage (Price and Murphy 2002), and has been a research subject in the past (Rich et al. 2010; Wolter et al. 2012).

Image pre-processing

At both locations we analyzed Landsat data from the year before and the year after the windfall event. Our temporal frames were 1998-2000 for the U.S. site and 2009-2011 for the Russia site. Imagery for both study sites were pre-processed by converting digital numbers in to surface reflectance using the Landsat Ecosystem Disturbance Adaptive Processing System (LEDAPS) algorithm (Masek et al. 2006). Cloud-free images were available for both time points at the U.S. site, but not for the Russia site. Therefore, we selected images with the least amounts of clouds (hereafter called the base-image) and gap-filled them using other Landsat scenes from the same growing season (i.e., late May to August; 2009 and 2011, respectively, Table 3). Gap-filling was accomplished by first masking clouds and cloud shadows in each image using FMask (Zhu and Woodcock 2012), applying conservative threshold values to ensure that a maximum of clouds and cloud shadows were detected. Afterwards, we filled the gaps of our base-image using all other images from the respective growing season. We ensured that images located at the edge of a growing season (i.e., late May) were chosen last to fill gaps in the base-image. We thus minimized potential influences of a late spring onset that sometimes can lead to class confusions in forest/non-forest classifications. The result was a nearly cloud-free image composite for both time points (2009 and 2011).

Forest/Non-Forest classification

For both study sites, we classified the pre-disturbance image (1998 for the U.S. site, and 2009 for the Russia site) into 'forest' and 'non-forest' using a training data set generated automatically using the dark object approach (Huang et al. 2008). More specifically, we searched for the peak within a local histogram of Landsat's red band (Band 3). In the absence of non-vegetated dark objects, such as water or dark soil, pixels to the left of the peak can be considered forest pixels (Huang et al. 2008). We removed non-vegetated dark objects by applying a consistency check using the globally available

Moderate-Resolution Imaging Spectroradiometer (MODIS) vegetation continuous field product (VCF, Hansen et al. 2006) with a threshold value of 40%. Dark pixels passing this consistency check were then collected within a group of confident forest samples and used to calculate the Integrated Forestness Index (IFI):

$$IFI = \sqrt{\frac{1}{NB}\sum_{i=1}^{NB}\left(\frac{b_{pi} - \bar{b}_i}{SD_i}\right)^2}$$

where $\bar{b}_i$ and SD_i are the mean and standard deviation of the candidate forest pixels within that image for band i, b_{pi} is the spectral value for pixel p in band i, and NB is the number of bands (Huang et al. 2008). The index is an integrated Z-score depicting a pixel's probability of not being forest. Low IFI values indicate a higher likelihood of being forested areas and high IFI values a higher likelihood of other land cover classes (Huang et al. 2010). Using this information, we then delineated "non-forest" pixels by applying a threshold. Huang et al. (2008) provides a more comprehensive explanation on how to choose and modify this threshold to capture pixels with low IFI values that are non-forest areas, such as dark green agricultural fields. We also collected less pure pixels at class boundaries for each category by adjusting the IFI threshold for a pixel being assigned to either forest or non-forest depending on whether their neighboring pixel was previously labeled as forest or non-forest (Huang et al. 2008).

We used these training data in a Support Vector Machine (SVM) supervised classification. SVM are non-parametric classification algorithms that fit a linear hyperplane between two classes in a multi-dimensional space (Foody and Mathur

2004a). Our strategy to collect training samples of both 'pure' forest pixels and 'less pure' forest pixels (as well as non-forest pixels) favored the application of SVM, because the linear separation between classes is strongly dependent on pixels along class boundaries (Foody and Mathur 2004b). SVM use kernel functions to find the best fitting hyperplane, which require setting a kernel parameter for the kernel width (ɣ) and a regulation parameter (C). We chose the best parameter combination by comparing models that used a wide range of parameter combination and chose the parameters from the best fitting model (Janz et al. 2007).

Forest disturbance detection

We mapped forest disturbance in both locations using the Disturbance Index. The DI is a linear combination of normalized Tasseled-Cap bands. The idea behind the index is that disturbance sites exhibit higher brightness, and lower greenness and wetness values compared to undisturbed forests. The disturbance index is calculated as:

$$DI = B_r - (G_r + W_r)$$

where B_r, G_r, W_r are the Tasseled Cap bands, standardized around the scene's mean forest value. Positive values generally indicate disturbance areas (Healey et al. 2005). The advantage of the Disturbance Index is that it only requires setting a threshold, which is typically study region dependent. For the Russia site, we visually compared the results of multiple thresholds against sample sites of stand-replacing disturbance as well as windfall sites and identified DI=3.0 as providing the most accurate disturbance map. The same type of assessment for the U.S. site revealed that DI=2.5 identified disturbed areas best. In the final step we combined the initial forest/non-forest map with the areas of forest disturbance and created a change-map for 2009-2011 and 1998-2000, respectively. We then applied a majority filter and defined a minimum mapping unit of 5 pixels (roughly equivalent to 0.5 hectares) to eliminate isolated pixels that likely represented misclassifications.

Detecting windfall disturbance

Our windfall detection method was based on the assumption that only two forms of disturbances occurred on the landscape: windfall and harvests. To extract training data for each disturbance type, we visually examined the Landsat imagery to determine how wind-related disturbance may be spectrally different from clear-cut harvests. Based on these observations we postulated that, compared to harvests, a wind-related disturbance site would have:

a) Lower Tasseled Cap brightness values: The Tasseled Cap brightness is a measure of the soil proportion in the signal and sensitive to the abundance of shadows (Kauth and Thomas 1976). After a recent clear-cut harvest soil is often exposed and shadows are rare, leading to high brightness values. In contrast, after a windfall event, biomass often remains, reducing soil reflectance and maintaining shadows. This would result in lower brightness values for windfall disturbance than clear-cut harvests.
b) Higher Tasseled Cap wetness values: The Tasseled Cap wetness provides information about the moisture content of a site (Cohen and Spies 1992; Jin and

Sader 2005). Major over- and understory removal, typical for a clear-cut harvest, strongly reduces tasseled cap wetness (Ballard, 2000; Cohen and Goward 2004; Healey et al., 2005). Hence, a windfall disturbance will have on average a higher Tasseled Cap wetness value than a clear-cut harvest.

c) Lower short-wave infrared (SWIR) reflectance (Landsat band 5): Similar to the Tasseled Cap wetness index, TM band 5 is sensitive to the amount of water in vegetation, but through an inverse relationship (Schroeder et al. 2011). On average, a windfall disturbance site would be expected to have lower SWIR then a clear-cut harvest due largely to more shadows in a windfall site.

Using normalized pixel values around a mean of zero following a standard Z-transformation, a histogram of all disturbed pixels will exhibit three main 'areas'. For example, in the case of band-5 reflectance, the locations of importance in the histogram are 1) the center, in which the spectral characteristics of windfall disturbance and clear cuts are essentially the same; 2) the left side of the histogram, which is dominated by 'windfall' pixels; and 3) the right side of the histogram, which is dominated by 'clear-cut harvest' pixels (Figure 8). The nature of a normal distribution makes it convenient to target these areas. Specifically, we targeted areas to the left ('windfall') and to the right ('clear-cut') of one standard deviation from the mean, and extracted pixels located in these areas as training data for the 'windfall' and 'clear-cut harvest' categories. We then used the SVM to classify the disturbed areas, using the six multi-spectral bands from Landsat and the same parameter-search method as for the initial forest/non-forest classification.

In doing so, we were able to add information to our forest-change maps by attributing the cause of the forest disturbance. We postulated that a given cluster of disturbed pixels would have all been disturbed due the same cause, which especially in the case of windfall sites was confirmed during the validation process. Accordingly, we extracted all disturbance-labeled areas from our forest change map and converted these into vector-based polygons. These polygons were overlaid with our windfall classification map. Within each disturbance polygon, we then counted the number of pixels of each class (i.e., 'windfall' vs. 'clear-cut harvest') and assigned the final class label for the polygon based on the majority of the pixels in it.

Accuracy assessment

We assessed the accuracy of our methodology by evaluating (a) the accuracy of our forest-change map, and (b) the accuracy of windfall disturbance detection. For the forest-cover change maps, we randomly sampled 100 points from each of the three classes (i.e., 'constant forest', 'constant other', and 'disturbed'), and labeled each point manually using the Landsat composites and, where available, high-resolution imagery in Google-Earth. We then summarized the results in an error matrix, and calculated overall accuracy and the kappa statistics of the overall classification, as well as user's and producer's accuracy for each class (Congalton 1991; Foody 2002). To account for the possible sampling bias in the accuracy assessment, we area-weighted our classification accuracies (Card 1982) and adjusted the area estimates of our categories (Stehman 2012).

To estimate the performance of our proposed method in separating windfall from clear-cut harvests, we evaluated all disturbance sites to see whether or not they were assigned correctly to their expected class by visually inspecting the Landsat imagery and high-resolution Quickbird data. This analysis was supplemented with the following external datasets: for the Russia site, we had access to a hand-digitized validation dataset from 2010 from collaborators in the region. For the U.S. site, we used (a) a previously published Landsat-based classification of the region, which highlighted areas of windfall, fire, and logging disturbance (Wolter et al. 2012), and (b) a disturbance severity map created from IKONOS data (Rich et al. 2010). Both ancillary datasets did not cover our entire study region, but only areas in the northern half of the analyzed footprint (Wolter et al. 2012) and in the northwest of our study area (~ 121 km^2, Rich et al. 2010). We again generated an error-matrix to evaluate the accuracy of the classification of the polygons into 'windfall' and 'clear-cut harvest', and calculated the same accuracy measures.

Results

The forest change maps had high accuracies (Overall Accuracy 90.96% and Kappa value of 0.91 for the Russia change map; overall accuracy 89.33 % and Kappa value of 0.84 for the U.S. site). User's and producer's accuracies were higher for the stable classes compared to the disturbance class and higher at the Russia site compared to the U.S. site (Table 4). The accuracy for the windfall classification was 77.5% for the Russia site and 76.4% for the U.S. site. In both cases, commission errors for 'windfall' category were slightly higher than those for 'clear-cut harvest' (Table 5).

At the Russia site, 68.5% of the landscape (over 23,000 km^2) was classified as forest in 2009. By 2011, 475 km^2 of the forested area experienced a form of disturbance, corresponding to an annual change rate of about 1%. Of the 475 km^2 of affected forest area, over 300 km^2 (or 64%) were caused by two large windfall events in 2009 and 2010. Overall, we analyzed 7,028 disturbance polygons in Russia, 4,625 (or 65.8%) of which were characterized as 'windfall'.

For the U.S. site, results were similar: in 1998, over 76% of the investigated area was forested (nearly 13,000 km^2). By 2000, 395 km^2 were disturbed, corresponding to an annual disturbance rate of 1.5%. Roughly 171 km^2, or 43%, of the affected area was damaged by wind. Overall, we analyzed 5,977 unique disturbance polygons at the U.S. site, of which 3,735 (or 63%) were caused by a large storm in 1999 (Figure 9).

The point cloud featured two clusters, each of which contained observations of one disturbance type with very little ambiguity (i.e., 'windfall' or 'clear-cut harvest', Figure 10). Between the two study sites, the point cloud of the U.S. site exhibited a larger difference between the two disturbance types.

The classification accuracy of the disturbance polygons also varied by size. At the Russian site (Figure 11 top row) the lowest overall accuracy (just over 75%) was associated with the smallest disturbance polygons and then increased to an average of about 85% for disturbances of about 10 ha in size. After that size, the low number of polygons in each 0.5 ha-bin caused the data points containing to high variances to estimate a clear trend (Figure 11a). For windfall sites only, small disturbance sites were more accurately detected than larger ones. The accuracy for windfall sites dropped from on average 95% for small patches to 80% for patches of about 8 ha in size. Again, for patch sizes larger than 8 ha the number of polygons became too small to estimate a clear trend (Figure 11b). For clear-cut patches the classification accuracy was lowest (~55%) for the smallest patches close to our minimum mapping unit of 0.5 ha, but registered greater than 80% for patches of about 8 ha. For patches larger than 8 ha no clear trend was observable due to the low number of large disturbance patches (Figure 11c). At the U.S. study site the general patterns of accuracy were very similar to the Russia site (Figure 11d, e, f): For both disturbance types together, we found an increase in the classification accuracy from 70% for patches of 0.5 ha to over 95% for patches of about 7.5 ha in size (Figure 11d). For windfall disturbances, accuracies were high throughout the entire range of disturbance patches: they were highest for the smallest and the largest windfalls (>95%) but slightly lower for windfalls of about 7-8 ha in size (~95%, Figure 11e). However, here the trend was consistent across the entire range of patch sizes. For the clear-cut sites, the least accurate detection occurred for patches that were close to our minimum mapping unit of 0.5 ha. From there, the detection accuracy greatly improved with increasing patch size, yielding accuracies at about 80% for patches of about 5 ha in size (Figure 11f).

At the Russia site we also noticed that the first major windfall event was classified at a higher accuracy compared to the second one (Figure 12). Evaluating the spectral characteristics of these areas, we found that their band 5 reflectance values and

Tasseled Cap brightness values were above zero while their Tasseled Cap wetness values were below zero.

Discussion

We developed a novel algorithm to separate windfall disturbance from harvested areas based on Landsat data and tested the method successfully in two different locations – one in the temperate zone of European Russia and one in the southern boreal forests of the United States. The generation of the forest disturbance map applied previously published methods to detect forest disturbances. Using this disturbance map, we then developed and applied a rule set that determined whether the disturbance was caused by windfall or a harvest event. To our knowledge this is the first study that developed a method specifically for the purpose of separating windfall disturbance from clear-cut harvesting and tested its robustness in multiple study regions.

Our results showed that in both study sites the separation between windfall and clear-cut disturbance was possible in over 75% of the disturbed area. Given the small number of studies that simultaneously classify windfall and clear-cut harvests using Landsat data, only a limited comparison to previous work can be made. Compared to the studies of fire disturbance and clear-cut harvests (e.g., Pereira and Setzer 1993; Roder et al. 2008; Schroeder et al. 2011), our accuracies were generally lower. For example, Schroeder et al. (2011) achieved classification accuracies greater than 90%, while our results suggest a little over 75% success rate when detecting windfall. We believe that two major factors contribute to these differences. The first factor is related to the difference in the methods of the two studies. Contrary to our study Schroeder et al. (2011) gathered training data with considerable user input. In contrast, our algorithm did not require any user intervention during the training process. Compared to classifications that gather training data manually, automated methods often yield lower classification accuracies. As such, the automation inherent in our algorithm is probably more prone to errors but comes with the advantage of not requiring manually collected training data. The second reason is related to forest management practices, particularly partial harvests. Partial harvests typically remove mature trees from the canopy while leaving younger trees uncut (Wilson and Sader 2002), a management practice that is increasingly common particularly at the U.S. site. Partial harvests are known to impact Landsat's SWIR band (Olson 1994), a band that was highly important also in detecting windfall in our study. As such, it is possible that confusions between windfall and selective harvest lowered the overall detection accuracy, specifically by increasing the commission errors in our 'windfall' class. This highlights the need for a thorough understanding of harvesting practices before attributing disturbance types.

Our algorithm complements other efforts to process Landsat data with little or no user input (Healey et al. 2005; Huang et al. 2010). In the present study, we integrated two basic concepts that had not been previously combined to produce a forest-cover change map: the dark-object concept (Huang et al. 2008), and the Disturbance Index concept (Healey et al. 2005). Our disturbance attribution step was then based on the disturbance areas in the change map. We therefore stress that the attribution step, itself, can be combined with any other algorithm that detects forest disturbance using Landsat images.

Overall, the combination of the selected variables proved to be suitable in separating windfall disturbance from clear-cuts. Previous work on forest change detection suggests that both Landsat SWIR reflectance (band 5) and Tasseled Cap wetness values (a contrast of SWIR with the visible and near infrared bands) contain similar levels of information (Peddle et al. 1999; Cohen and Goward 2004; Healey et al. 2005; Chen and Vierling 2006; Schroeder et al. 2011). Similarly, SWIR and the Tasseled Cap Brightness often show a high degree of correlation (Cohen et al. 2003). However, initial tests using all permutations of the three bands during the training data collection suggested that the highest classification accuracy was achieved by using all three bands as opposed to using one band individually or in combination with another band. This might suggest that although correlated, each band contributes a unique source of information about windfall and harvest sites, so we suggest that even correlated information can be useful for improving classification accuracies.

Our results also suggest that the accuracy of the disturbance type classification increased with the size of a disturbed area. This size-related classification accuracy issue is potentially an artifact due to two aspects of our study design. First, mixed pixels along edges affect a small disturbance site more strongly than a larger site. Second, the generalization of disturbance sites at the polygon-level, posterior to the classification, may have introduced errors. Our decision to use the majority rule prior to delineating disturbance polygons might have affected particularly long and narrow disturbed patches. Despite these shortcomings, our algorithm represents a valuable contribution to forest disturbance mapping. Overall, we achieved mean classification accuracies of over 75%, and even higher values for larger disturbance patches. This suggests that for the vast majority of the disturbance area (83.3% at the Russia site, and 87.5% at the U.S. site), the classification results identified the main events that took place on the ground, i.e., widespread windfalls, correctly.

A number of uncertainties also remain. First, the windfall detection algorithm requires knowledge about a windfall event in the region of interest. Second, we were not able to test how the presence of fire or insect defoliation would affect our results. We can only speculate that a step-wise approach and the addition of fire-specific indices such as the Normalized Burn Ratio (NBR) could help isolate fire-affected pixel, which then could be used to sample training data. Third, we did not distinguish between different levels of windfall severity, which will likely impact the spectral signal (Rich et al. 2010). Fourth, the image composites at the Russian site might have introduced errors across the landscapes because of the different phenological stages. Though, the critical image dates (e.g., the May imagery) only covered a small proportion of the landscape and acquired climate records indicated that these errors were assumingly small. Fifth, we did not test how varying the threshold (i.e., we used one standard deviation away from the mean) of collecting windfall and clear-cut training data in the histogram would have affected our results, and we suspect that the threshold is sensitive to the proportion of 'windfall' and 'clear-cut' disturbance in the classification. Finally, at the Russia site, a second major windfall was largely missed by our algorithms (Figure 6).

While not having complete evidence due to missing ancillary information, two reasons potentially contribute to this omission. First, the 2010 storm event may have been a much stronger one compared to the 2009 event, causing more biomass to be removed from the site, making it spectrally more similar to a clear-cut harvest. The second, and in our opinion more likely, reason is salvage logging following the windfall. During salvage logging the damaged trees are removed from the site, rendering it spectrally similar to a clear-cut harvest. As such, the post-storm treatment of a site is a major factor impacting the correct classification of windfall disturbance using satellite imagery.

Knowing what caused a forest disturbance is valuable information for a variety of research questions that utilize forest disturbance maps. While the literature on remote sensing of fire- and insect-related disturbance is fairly rich, work on identifying windfall disturbance has not received much attention. Here, we developed a novel algorithm to generate training data and classify disturbance areas into 'windfall' and 'clear-cut harvest' disturbances. Our methodology requires minimal user input, and can be immediately applied to other Landsat based disturbance maps. The proposed method resulted in good classification accuracies, was effective in separating windfall and clear-cut harvest, and maintained similar accuracies across two different study regions. As with any other form of classification, the increased level of categorical information produced as a result of this work is of great value, especially for research that require information about changes in forest areas, such as econometric analyses that assess drivers of timber harvest and carbon management.

References

1. Achard, F., Eva, H.D., Stibig, H.J., Mayaux, P., Gallego, J., Richards, T., & Malingreau, J.P. (2002). Determination of deforestation rates of the world's humid tropical forests. *Science*, 297, 999-1002
2. Achard, F., Mollicone, D., Stibig, H.J., Aksenov, D., Laestadius, L., Li, Z.Y., Popatov, P., & Yaroshenko, A. (2006). Areas of rapid forest-cover change in boreal Eurasia. *Forest Ecology and Management*, 237, 322-334
3. Andam, K.S., Ferraro, P.J., Pfaff, A., Sanchez-Azofeifa, G.A., & Robalino, J.A. (2008). Measuring the effectiveness of protected area networks in reducing deforestation. *Proceedings of the National Academy of Sciences of the United States of America*, 105, 16089-16094
4. Ballard, T.M. (2000). Impacts of forest management on northern forest soils. *Forest Ecology and Management*, 133, 37-42
5. Baumann, M., Ozdogan, M., Kuemmerle, T., Wendland, K.J., Esipova, E., & Radeloff, V.C. (2012). Using the Landsat record to detect forest-cover changes during and after the collapse of the Soviet Union in the temperate zone of European Russia. *Remote Sensing of Environment*, 124, 174-184
6. Bonan, G.B. (2008). Forests and climate change: Forcings, feedbacks, and the climate benefits of forests. *Science*, 320, 1444-1449
7. Card, D.H. (1982). Using known map category marginal frequencies to improve estimates of thematic map accuracy. *Photogrammetric engineering and remote sensing*, 48, 431-439

8. Chen, X.X., & Vierling, L. (2006). Spectral mixture analyses of hyperspectral data acquired using a tethered balloon. *Remote Sensing of Environment*, 103, 338-350

9. Cheung, H.F., Pan, J.Y., Gu, Y.Z., & Wang, Z.Z. (2013). Remote-sensing observation of ocean responses to Typhoon Lupit in the northwest Pacific. *International Journal of Remote Sensing*, 34, 1478-1491

10. Chomitz, K. M. & D. A. Gray (1996). Roads, land use, and deforestation: A spatial model applied to belize. *World Bank Economic Review* 10(3): 487-512.

11. Cohen, W.B., & Spies, T.A. (1992). Estimating structural attributes of Douglas-fir/western hemlock forest stands from landsat and SPOT imagery. *Remote Sensing of Environment*, 41, 1-17

12. Cohen, W.B., Fiorella, M., Gray, J., Helmer, E., & Anderson, K. (1998). An efficient and accurate method for mapping forest clearcuts in the Pacific Northwest using Landsat imagery. *Photogrammetric engineering and remote sensing*, 64, 293-300

13. Cohen, W.B., Maiersperger, T.K., Gower, S.T., & Turner, D.P. (2003). An improved strategy for regression of biophysical variables and Landsat ETM+ data. *Remote Sensing of Environment*, 84, 561-571

14. Cohen, W.B., & Goward, S.A. (2004). Landsat's Role in Ecological Applications of Remote Sensing. *BioScience*, 54(6), 535-545

15. Congalton, R.G. (1991). A Review of Assessing the Accuracy of Classifications of Remotely Sensed Data. *Remote Sensing of Environment*, 37, 35-46

16. Coppin, P.R., & Bauer, M.E. (1994). Processing of Multitemporal Landsat TM Imagery to Optimize Extraction of Forest-Cover Change Features. *IEEE Transactions on Geoscience and Remote Sensing*, 32, 918-927

17. Crist, E.P., & Kauth, R.J. (1986). The Tasseled Cap De-Mystified. *Photogrammetric engineering and remote sensing*, 52, 81-86

18. de Beurs, K.M., & Townsend, P.A. (2008). Estimating the effect of gypsy moth defoliation using MODIS. *Remote Sensing of Environment*, 112, 3983-3990

19. FAO (2005). Global Forest Ressource Asessment 2005.

20. FAO (2010). Global Forest Ressource Assessment 2010.

21. Foody, G.M. (2002).Status of land cover classification accuracy assessment. *Remote Sensing of Environment*, 80, 185-201

22. Foody, G.M., & Mathur, A. (2004a). A relative evaluation of multiclass image classification by support vector machines. *IEEE Transactions on Geoscience and Remote Sensing*, 42, 1335-1343

23. Foody, G.M., & Mathur, A. (2004b). Toward intelligent training of supervised image classifications: directing training data acquisition for SVM classification. *Remote Sensing of Environment*, 93, 107-117

24. Frelich, L.E., & Reich, P.B. (1995). Spatial Patterns and Succession in a Minnesota Southern-Boreal Forest. *Ecological Monographs*, 65, 325-346

25. French, N.H.F., Kasischke, E.S., Hall, R.J., Murphy, K.A., Verbyla, D.L., Hoy, E.E., & Allen, J.L. (2008). Using Landsat data to assess fire and burn severity in the North

American boreal forest region: an overview and summary of results. *International Journal of Wildland Fire*, 17, 443-462

26. Garcia-Haro, F.J., Gilabert, M.A., & Melia, J. (2001). Monitoring fire-affected areas using Thematic Mapper data. *International Journal of Remote Sensing*, 22, 533-549

27. Gorsevski, V., Kasischke, E., Dempewolf, J., Loboda, T., & Grossmann, F. (2012). Analysis of the Impacts of armed conflict on the Eastern Afromontane forest region on the South Sudan — Uganda border using multitemporal Landsat imagery. *Remote Sensing of Environment*, 118, 10-20

28. Hansen, M., DeFries, R., Townshend, J.R., Carroll, M., Dimiceli, C., & Sohlberg, R. (2006). Vegetation Continuous Fields MOD44B, 2001 Percent Tree Cover, Collection 4. University of Maryland, College Park, Maryland, 2001

29. Hansen, M.C., & DeFries, R.S. (2004). Detecting long-term global forest change using continuous fields of tree-cover maps from 8-km advanced very high resolution radiometer (AVHRR) data for the years 1982-99. *Ecosystems*, 7, 695-716

30. Hansen, M.C., Stehman, S.V., & Potapov, P.V. (2010). Quantification of global gross forest-cover loss. *Proceedings of the National Academy of Sciences*, 107, 8650-8655

31. Hayes, T.M. (2006). Parks, people, and forest protection: An institutional assessment of the effectiveness of protected areas. *World Development*, 34, 2064-2075

32. He, L.M., Chen, J.M., Zhang, S.L., Gomez, G., Pan, Y.D., McCullough, K., Birdsey, R., & Masek, J.G. (2011). Normalized algorithm for mapping and dating forest disturbances and regrowth for the United States. *International Journal of Applied Earth Observation and Geoinformation*, 13, 236-245

33. Healey, S.P., Cohen, W.B., Yang, Z.Q., & Krankina, O.N. (2005). Comparison of Tasseled Cap-based Landsat data structures for use in forest disturbance detection. *Remote Sensing of Environment*, 97, 301-310

34. Hicke, J.A., Allen, C.D., Desai, A.R., Dietze, M.C., Hall, R.J., Hogg, E.H., Kashian, D.M., Moore, D., Raffa, K.F., Sturrock, R.N., & Vogelmann, J. (2012). Effects of biotic disturbances on forest carbon cycling in the United States and Canada. *Global Change Biology*, 18, 7-34

35. Huang, C., Davis, L.S., & Townshend, J.R.G. (2002). An assessment of support vector machines for land cover classification. *International Journal of Remote Sensing*, 23, 725 - 749

36. Huang, C., Goward, S.N., Masek, J.G., Gao, F., Vermote, E.F., Thomas, N., Schleeweis, K., Kennedy, R.E., Zhu, Z., Eidenshink, J.C., & Townshend, J.R.G. (2009). Development of time series stacks of Landsat images for reconstructing forest disturbance history. *International Journal of Digital Earth*, 2, 195 - 218

37. Huang, C., Goward, S.N., Masek, J.G., Thomas, N., Zhu, Z., & Vogelmann, J.E. (2010). An automated approach for reconstructing recent forest disturbance history using dense Landsat time series stacks. *Remote Sensing of Environment*, 114, 183-198

38. Huang, C.Q., Song, K., Kim, S., Townshend, J.R.G., Davis, P., Masek, J.G., & Goward, S.N. (2008). Use of a dark object concept and support vector machines to automate forest cover change analysis. *Remote Sensing of Environment*, 112, 970-985

39. Irons, J.R., Dwyer, J.L., & Barsi, J.A. (2012). The next Landsat satellite: The Landsat Data Continuity Mission. *Remote Sensing of Environment*, 122, 11-21

40. Janz, A., van der Linden, S., Waske, B., & Hostert, P. (2007). imageSVM - A user-orientated tool for advanced classification of hyperspectral data using Support Vector Machines. *Proceedings of the 5th EARSeL workshop on Imaging Spectroscopy*, Bruges, Belgium

41. Jin, S., & Sader, S.A. (2005). Comparison of time series tasseled cap wetness and the normalized difference moisture index in detecting forest disturbances. *Remote Sensing of Environment*, 94, 364-372

42. Kasischke, E.S., Amiro, B.D., Barger, N.N., French, N.H.F., Goetz, S.J., Grosse, G., Harmon, M.E., Hicke, J.A., Liu, S.G., & Masek, J.G. (2013). Impacts of disturbance on the terrestrial carbon budget of North America. *Journal of Geophysical Research-Biogeosciences*, 118, 303-316

43. Kauth, R.J., & Thomas, G.S. (1976). The Tasselled Cap - A Graphic Description of the Spectral-Temporal Development of Agricultural Crops as Seen by LANDSAT. *LARS Symposia*, Paper 159

44. Kennedy, R.E., Yang, Z., & Cohen, W.B. (2010). Detecting trends in forest disturbance and recovery using yearly Landsat time series: 1. LandTrendr -- Temporal segmentation algorithms. *Remote Sensing of Environment*, 114, 2897-2910

45. Key, C.H., & Benson, N. (1999). The Normalized Burn Ratio (NBR): A Landsat TM radiometric measure of burn severity. *http://www.frames.gov/rcs/3000/3356.html*

46. Krylov A.M., Malahova E.G., & N.A., V. (2012). Identification and assessment of forest areas damaged by windfalls in 2009–2010 by means of remote sensing (in Russian). *Proceedings of the St. Petersburg Forest Technical Academy*, 197-207

47. Koroleva, N.V. & Ershov, D.V. (2012). Assessment of an error of determination of areas windfalls using space images of high spatial resolution of Landsat-TM (in Russian). *Actual problems in remote sensing of the Earth from Space*, 9, 80-86

48. Masek, J.G., Vermote, E.F., Saleous, N.E., Wolfe, R., Hall, F.G., Huemmrich, K.F., Feng, G., Kutler, J., & Teng-Kui, L. (2006). A Landsat surface reflectance dataset for North America, 1990-2000. *IEEE Geoscience and Remote Sensing Letters*, 3, 68-72

49. Masek, J.G., Huang, C., Wolfe, R., Cohen, W., Hall, F., Kutler, J., & Nelson, P. (2008). North American forest disturbance mapped from a decadal Landsat record. *Remote Sensing of Environment*, 112, 2914-2926

50. Masek, J.G., Cohen, W.B., Leckie, D., Wulder, M.A., Vargas, R., de Jong, B., Healey, S., Law, B., Birdsey, R., Houghton, R.A., Mildrexler, D., Goward, S., & Smith, W.B. (2011). Recent rates of forest harvest and conversion in North America. *Journal of Geophysical Research-Biogeosciences*, 116

51. Negron-Juarez, R., Baker, D.B., Zeng, H.C., Henkel, T.K., & Chambers, J.Q. (2010). Assessing hurricane-induced tree mortality in U.S. Gulf Coast forest ecosystems. *Journal of Geophysical Research-Biogeosciences*, 115

52. Nelson, B.W., Kapos, V., Adams, J.B., Wilson, J.O., & Braun, O.P.G. (1994). Forest Disturbance by Large Blowdowns in the Brazilian Amazon. *Ecology*, 75, 853-858

53. Olsson, H. (1994). Changes in satellite-measured reflectances caused by thinning cuttings in Boreal forest. *Remote Sensing of Environment*, 50, 221-230

54. Ozdogan, M. Automated forest disturbance mapping with Support Vector Machines and incomplete training data. *PLOS ONE,* In press.

55. Patterson, M.W., & Yool, S.R. (1998). Mapping Fire-Induced Vegetation Mortality Using Landsat Thematic Mapper Data: A Comparison of Linear Transformation Techniques. *Remote Sensing of Environment*, 65, 132-142

56. Peddle, D.R., Hall, F.G., & LeDrew, E.F. (1999). Spectral mixture analysis and geometric-optical reflectance modeling of boreal forest biophysical structure. *Remote Sensing of Environment*, 67, 288-297

57. Pereira, M.C., & Setzer, A.W. (1993). Spectral characteristics of fire scars in Landsat-5 T images of Amazonia. *International Journal of Remote Sensing*, 14, 2061-2078

58. Peterson, C.J. (2000). Damage and recovery of tree species after two different tornadoes in the same old growth forest: a comparison of infrequent wind disturbances. *Forest Ecology and Management*, 135, 237-252

59. Potapov, P., Hansen, M.C., Stehman, S.V., Pittman, K., & Turubanova, S. (2009). Gross forest cover loss in temperate forests: biome-wide monitoring results using MODIS and Landsat data. *Journal of Applied Remote Sensing*, 3

60. Potapov, P.V., Turubanova, S.A., Hansen, M.C., Adusei, B., Broich, M., Altstatt, A., Mane, L., & Justice, C.O. (2012).Quantifying forest cover loss in Democratic Republic of the Congo, 2000–2010, with Landsat ETM+ data. *Remote Sensing of Environment*, 122, 106-116

61. Price, C., & Murphy, B. (2002). Lightning activity during the 1999 Superior Derecho, *Geophysical Research Letters*, 29, 21-42

62. Ramsey, E., Rangoonwala, A., Middleton, B., & Lu, Z. (2009a). Sattelite Optical and Radar used to track Wetland Forest impact and short-term recovery from Hurricane Katrina. *Wetlands*, 29, 66-79

63. Ramsey, E., Werle, D., Lu, Z., Rangoonwala, A., & Suzuoki, Y. (2009b). A Case of Timely Satellite Image Acquisitions in Support of Coastal Emergency Environmental Response Management. *Journal of Coastal Research*, 25, 1168-1172

64. Rich, R.L., Frelich, L., Reich, P.B., & Bauer, M.E. (2010). Detecting wind disturbance severity and canopy heterogeneity in boreal forest by coupling high-spatial resolution satellite imagery and field data. *Remote Sensing of Environment*, 114, 299-308

65. Roder, A., Hill, J., Duguy, B., Alloza, J.A., & Vallejo, R. (2008). Using long time series of Landsat data to monitor fire events and post-fire dynamics and identify driving factors. A case study in the Ayora region (eastern Spain). *Remote Sensing of Environment*, 112, 259-273

66. Scheller, R.M., & Mladenoff, D.J. (2004). A forest growth and biomass module for a landscape simulation model, LANDIS: design, validation, and application. *Ecological Modelling*, 180, 211-229

67. Schroeder, T.A., Wulder, M.A., Healey, S.P., & Moisen, G.G. (2011). Mapping wildfire and clearcut harvest disturbances in boreal forests with Landsat time series data. *Remote Sensing of Environment*, 115, 1421-1433

68. Stehman, S.V. (2012). Impact of sample size allocation when using stratified random sampling to estimate accuracy and area of land-cover change. *Remote Sensing Letters*, 3, 111-120

69. Stueve, K.M., Perry, C.H., Nelson, M.D., Healey, S.P., Hill, A.D., Moisen, G.G., Cohen, W.B., Gormanson, D.D., & Huang, C.Q. (2011b). Ecological importance of intermediate windstorms rivals large, infrequent disturbances in the northern Great Lakes. *Ecosphere*, 2, art2

70. Townsend, P.A., Singh, A., Foster, J.R., Rehberg, N.J., Kingdon, C.C., Eshleman, K.N., & Seagle, S.W. (2012). A general Landsat model to predict canopy defoliation in broadleaf deciduous forests. *Remote Sensing of Environment*, 119, 255-265

71. Van Wagtendonk, J.W., Root, R.R., & Key, C.H. (2004). Comparison of AVIRIS and Landsat ETM+ detection capabilities for burn severity. *Remote Sensing of Environment*, 92, 397-408

72. Vogelmann, J.E., Tolk, B., & Zhu, Z. (2009). Monitoring forest changes in the southwestern United States using multitemporal Landsat data. *Remote Sensing of Environment*, 113, 1739-1748

73. Wang, F.G., & Xu, Y.J. (2010). Comparison of remote sensing change detection techniques for assessing hurricane damage to forests. *Environmental Monitoring and Assessment*, 162, 311-326

74. Webb, S.L., & Scanga, S.E. (2001). Windstorm Disturbance without patch dynamics: Twelve Years of Change in a Minnesota forest. *Ecology*, 82, 893-897

75. Wendland, K.J., Lewis, D.J., Alix-Garcia, J., Ozdogan, M., Baumann, M., & Radeloff, V.C. (2011). Regional- and district-level drivers of timber harvesting in European Russia after the collapse of the Soviet Union. *Global Environmental Change*, 21, 1290-1300
76. Wendland, K.J., Baumann, M., Lewis, D.J., Sieber, A., & Radeloff, V.C. Protected area effectiveness in European Russia during and after the collapse of the Soviet Union. *In review*
77. Wilson, E.H., & Sader, S.A. (2002). Detection of forest harvest type using multiple dates of Landsat TM imagery. *Remote Sensing of Environment*, 80, 385-396
78. Wolter, P.T., Sturtevant, B.R., Miranda, B.R., Lietz, S.M., Townsend, P.A., & Pastor, J. (2012). Forest land cover change (1975-2000) in the Greater Border Lakes region. Research Map NRS-3. Newtown Square, PA: U.S. Department of Agriculture, Forest Service, Northern Research Station., 17 p (http://dx.doi.org/10.2737/RDS-2012-0007).
79. Wulder, M.A., Masek, J.G., Cohen, W.B., Loveland, T.R., & Woodcock, C.E. (2012). Opening the archive: How free data has enabled the science and monitoring promise of Landsat. *Remote Sensing of Environment*, 122, 2-10
80. Zhu, Z., & Woodcock, C.E. (2012). Object-based cloud and cloud shadow detection in Landsat imagery. *Remote Sensing of Environment*, 118, 83-94
81. Zhu, Z., Woodcock, C.E., & Olofsson, P. (2012).Continuous monitoring of forest disturbance using all available Landsat imagery. *Remote Sensing of Environment*, 122, 75-91

Figure Captions

Figure 7: Locations where the windfall classification method was tested. Study site 1 is located in the temperate zone of European Russia; study site 2 is located in the Greater Border Lake Region in northeast Minnesota (USA).

Figure 8: Schematic representation training data collection strategy for the windfall classification. The data in the histogram represent values of the validation data of the Russian study site for the band-5 reflectance.

Figure 9: Classification results for the Russia site (left) and the U.S. site (right). For both study locations, examples are presented of areas characterized primarily by windfall disturbance (177019A and 026027A), and areas primarily characterized by clear-cut harvest (177019B and 026027B).

Figure 10: Validation of the training data to classify disturbance areas into 'windfall' and 'clear-cut harvest' in the spectral feature space in which they were generated.

Figure 11: Proportion of correctly classified disturbance patches by patch size for the two classes, 'windfall' and 'clear-cut harvest', and the two classes combined. The top row represents the Russian site (footprint 177019), the bottom row the U.S. site (footprint 026027). The data presented are binned data with a bin width of 0.5 ha. Every bin was subdivided into six groups with 0.09 ha increments in patch size (i.e.,

increments of one Landsat pixel). The point represent the mean proportion correctly classified polygons across sub-groups in each bin, the error bars represent the standard deviation. The colors represent the number of polygons in every bin.

Figure 12: Misclassified disturbance site. Classification results suggest that the disturbance is caused by harvest. Validation data reveal that the site is caused by windfall.

Tables

Table 3: Image acquisition dates for the Landsat imagery used in this analysis. The images for footprint Path/Row 177/019 are ranked in the order they were used to create the image composite.

Path/Row 177/019			Path/Row 026/027		
Year in Analysis	Acquisition date	Sensor	Year in Analysis	Acquisition date	Sensor
2009	2009-07-11	TM5	1998	1998-09-16	TM5
	2009-08-23	ETM+			
	2009-07-30	TM5			
	2009-06-12	TM5			
	2009-05-19	TM5			
2011	2011-06-02	TM5	2000	2000-07-03	TM5
	2011-06-26	ETM+			
	2011-07-12	ETM+			
	2011-07-20	TM5			
	2011-05-25	ETM+			
	2011-08-05	TM5			

Table 4: Area-weighted classification accuracies for our Landsat-based change-maps. Presented are the overall accuracies, kappa, user's and producer's accuracies for the three classes 'Constant Forest (F)', 'Constant Non-Forest (NF)' and 'Disturbance (D)'.

Landsat Path/Row	Overall Accuracy [%]	Kappa	User's Accuracy [%]			Producer's Accuracy [%]		
			F	NF	D	F	NF	D
177019	90.96	0.91	91.00	91.00	88.00	95.40	84.07	66.28
026027	89.33	0.84	88.00	88.00	92.00	95.88	77.14	33.35

Table 5: Accuracy measures for the separation of the disturbance polygons into 'windfall' (W) and 'clear-cut harvest' (CC). Presented are the overall accuracy, the kappa statistics as well as user's and producer's accuracy.

Landsat Path/Row	Overall Accuracy [%]	Kappa	User's Accuracy [%]		Producer's Accuracy [%]	
			W	CC	W	CC
177019	77.52	0.55	71.87	87.34	90.80	64.11
026027	76.39	0.55	62.95	98.80	98.86	61.54

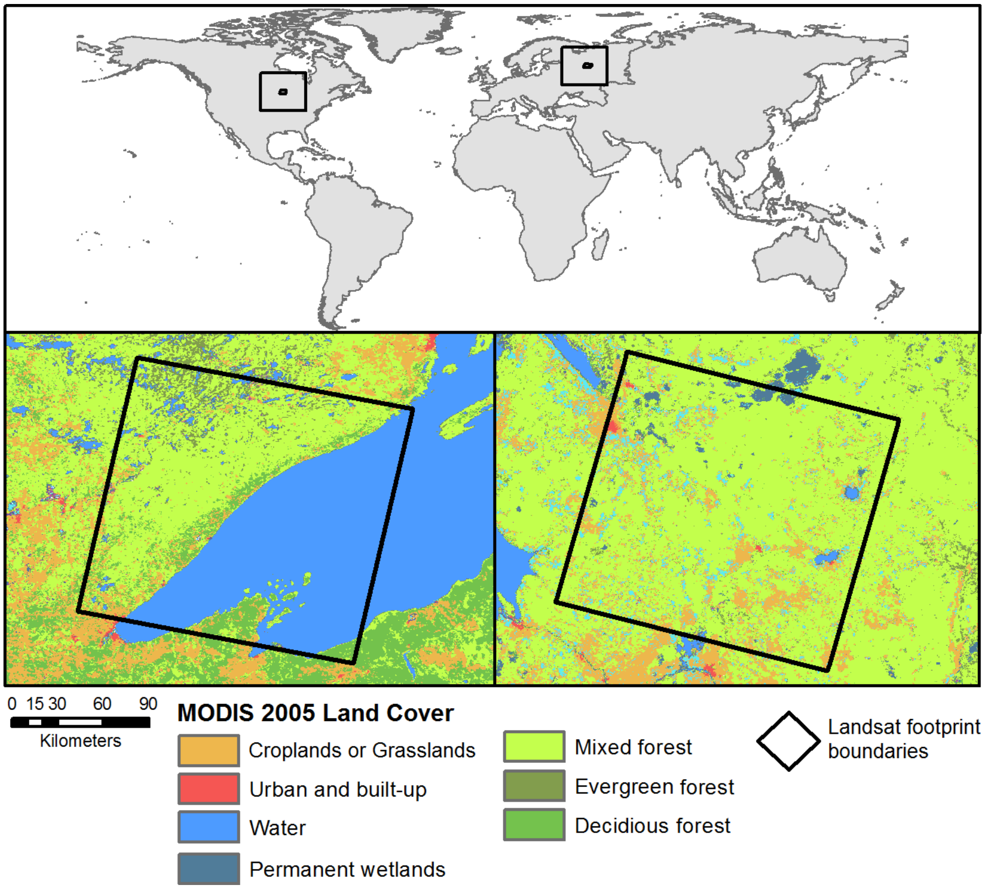
0 15 30 60 90
Kilometers
MODIS 2005 Land Cover
Croplands or Grasslands
Urban and built-up
Water
Permanent wetlands
Mixed forest
Evergreen forest
Decidious forest
Landsat footprint boundaries

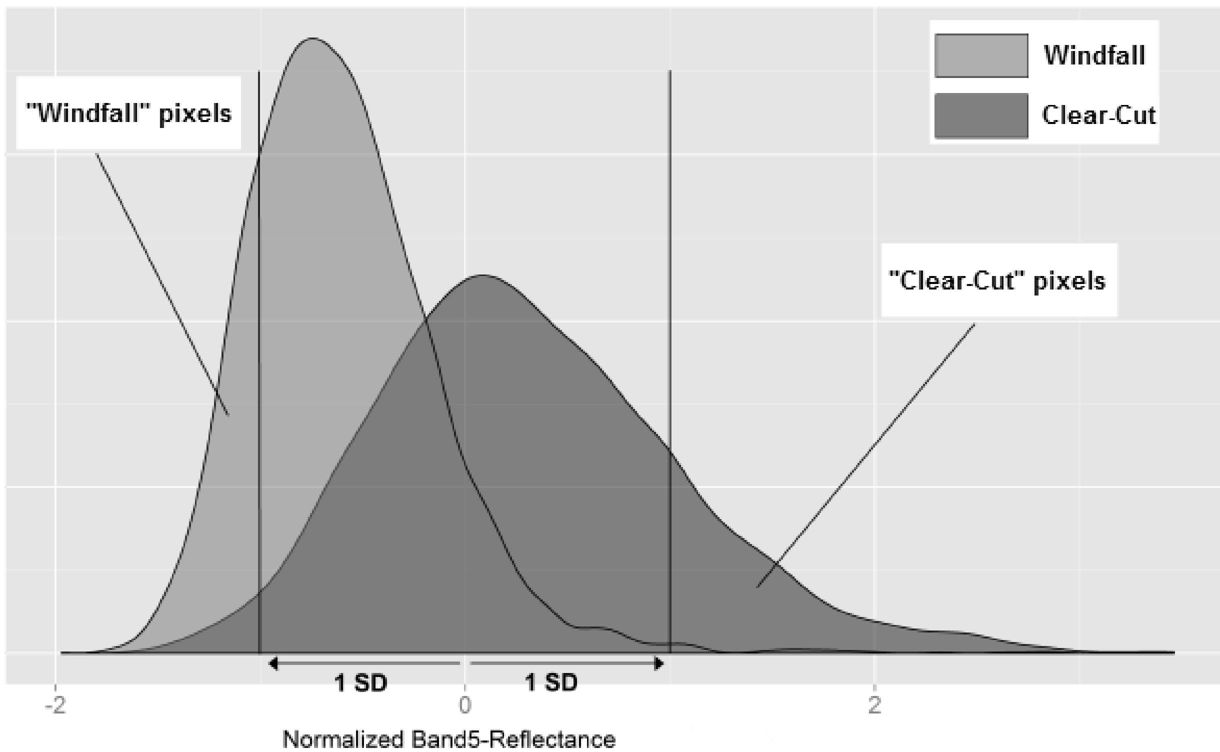
"Windfall" pixels
Windfall
Clear-Cut
"Clear-Cut" pixels
1 SD
1 SD
-2
0
2
Normalized Band5-Reflectance

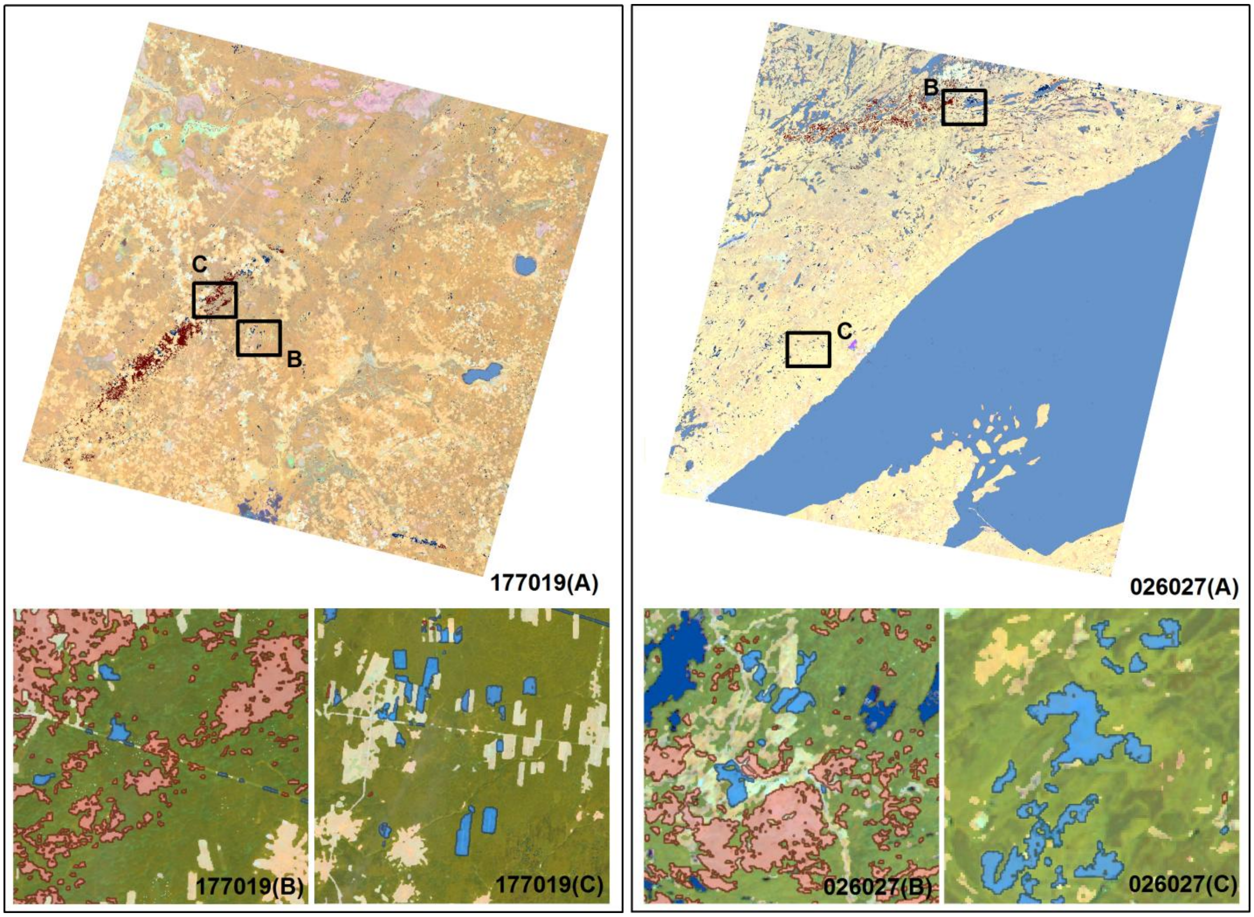
C
B
177019(A)
B
C
026027(A)
177019(B)
177019(C)
026027(B)
026027(C)

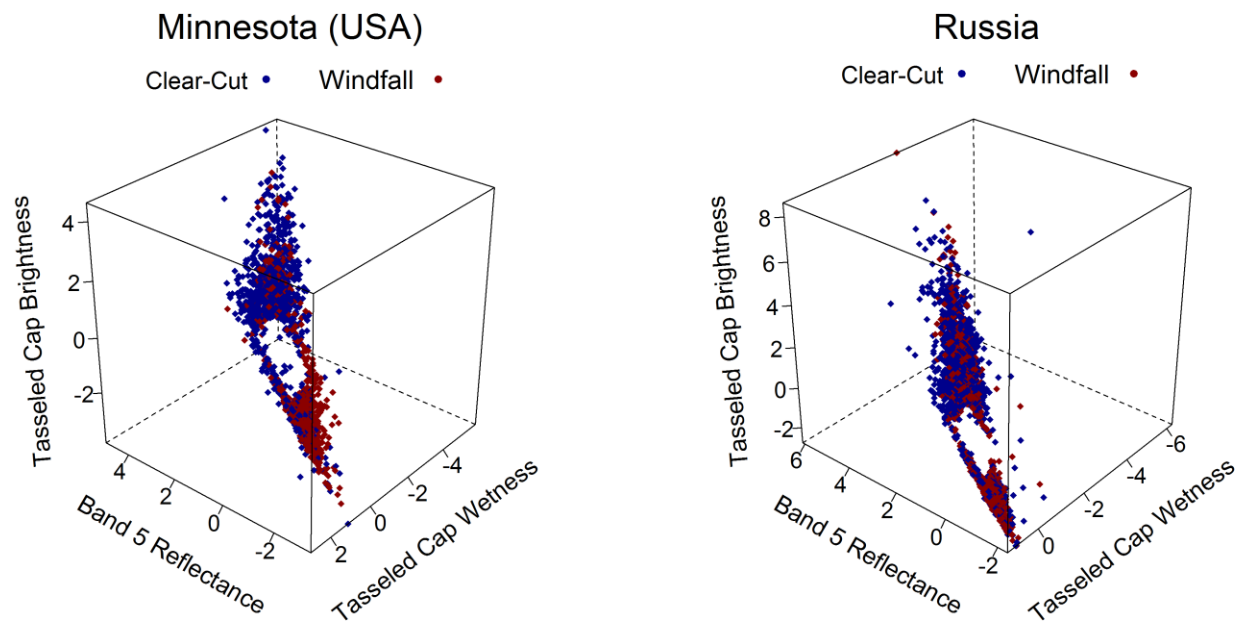
Minnesota (USA)
Clear-Cut
Windfall
Tasseled Cap Brightness
Band 5 Reflectance
Tasseled Cap Wetness
Russia
Clear-Cut
Windfall
Tasseled Cap Brightness
Band 5 Reflectance
Tasseled Cap Wetness

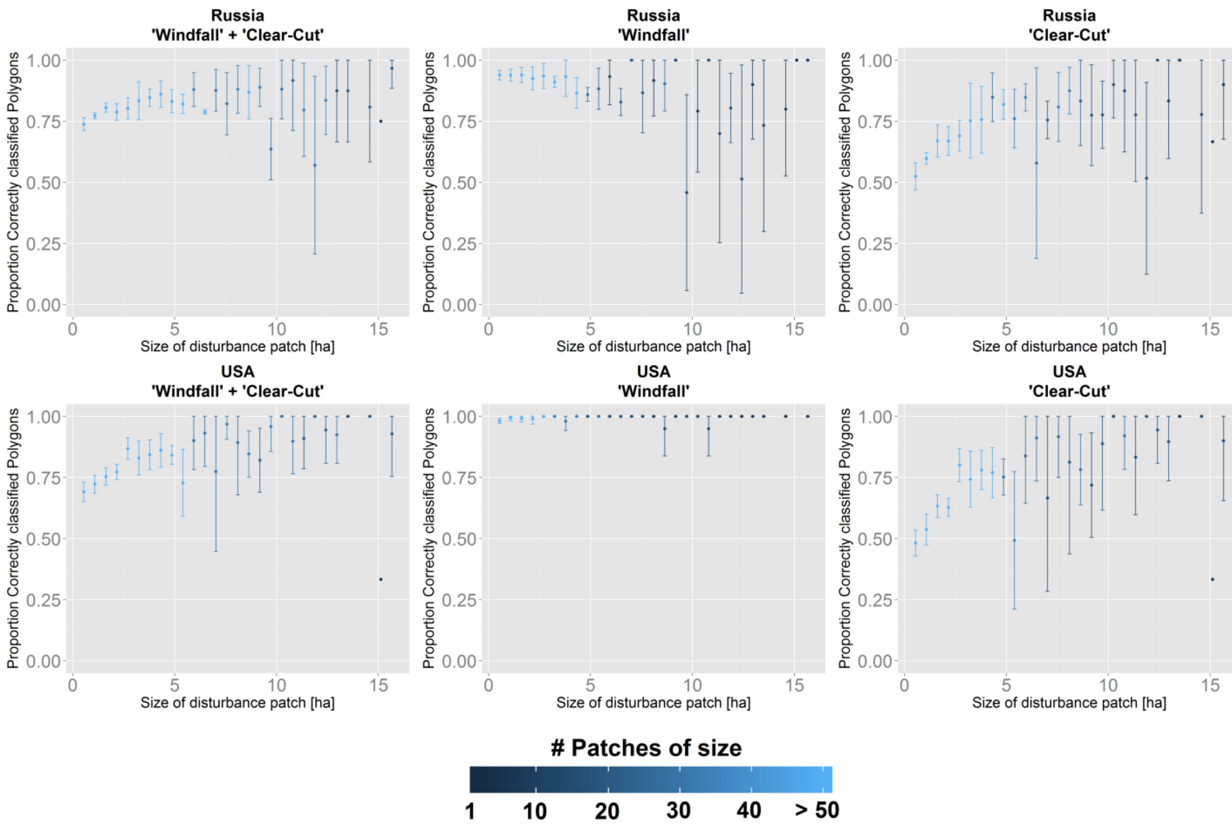
Russia
'Windfall' + 'Clear-Cut'
Russia
'Windfall'
Russia
'Clear-Cut'
USA
'Windfall' + 'Clear-Cut'
USA
'Windfall'
USA
'Clear-Cut'
Proportion Correctly classified Polygons
Size of disturbance patch [ha]
Patches of size
1
10
20
30
40
> 50

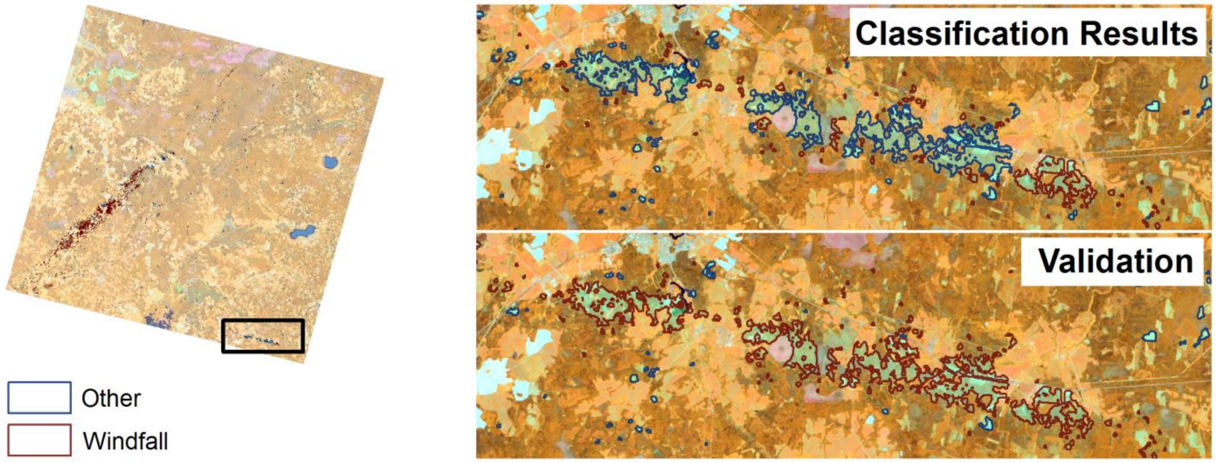
Classification Results
Validation
Other
Windfall

Chapter 3: Modeling green-leaf phenology using Dynamic Time Warping and all available Landsat data

Co-Authors: Mutlu Ozdogan, Andrew D. Richardson, Volker C. Radeloff

In preparation for *Remote Sensing of Environment*

Abstract:

Green leaf phenology is an important measure that describes the development of vegetation over a year and thus offers ways to characterize the interaction between climate and the biosphere. Remote sensing has been a popular tool to characterize phenology over large areas but the tradeoff between temporal frequency and spatial resolution has limited their use for detailed studies. For example the existing phenology products from the Moderate Resolution Imaging Spectroradiometer (MODIS) sensor are made at coarse 500m spatial resolution and are not applicable in cases such as detailed classification of mixed forests. Landsat imagery offer a higher spatial resolution but limited image availability over the growing season has prevented phenology products to be routinely generated from Landsat imagery. Here, we present a method that uses all available Landsat imagery between 2002 and 2012 to generate a daily Landsat vegetation index product. We used Dynamic Time Warping (DTW) and MODIS vegetation index time series data to detect the interannual differences in phenology and used this information to re-align the Landsat images. The result was a synthetic very dense daily time series of Landsat observations. Using the dense time series we then modeled a Landsat phenology. We performed this method across eight different study regions and multiple years. We compared the MODIS reference time series and ground-based camera data from the PhenoCam-network based on phenological transition dates (green-up (GU), start-of-season (SoS), maturity (Mat), senescence (Sen), end-of-season (EoS) and dormancy (Dorm)). Results for the MODIS comparison show a strong agreement. Dates of GU, SoS and Mat showed an agreement of >90%, Dorm and EoS dates over 80% and Sen date over 75%. The agreement between the Landsat and PhenoCam time series showed generally lower agreements, but GU and SoS dates were still over 75%. Results also suggest a systematic shift between the time series and a varying effect of the study site and the year of analysis. Our study suggests that using multi-year imagery it is possible to describe a year of green-leaf phenology at much finer spatial detail than what has been available to date. This highlights the potential for making fine scale phenology maps using the rich Landsat data archives over large areas and multiple years.

Keywords

Landsat, Dynamic Time Warping, green leaf PhenoCam, Phenology, MODIS, EVI

Introduction

Characterizing green leaf phenology is an important measure to describe the development of vegetation over the year and thus offers ways to characterize the interaction between climate and the biosphere (Wolfe et al. 2005; Zhang et al. 2006). Remote sensing from satellites allows for the observation of green leaf phenology across large spatial scales because of the standardized and repeated measurements (Asner et al. 2000; Knudby 2004; Paruelo et al. 1997; Roetzer et al. 2000; Tucker et al. 1986). For example, the Moderate Resolution Image Spectroradiometer (MODIS) data are widely used to characterize green leaf phenology across the globe as a standard MODIS product (Zhang et al. 2006; Zhang et al. 2003; Ganguly et al. 2010; Hufkens et al. 2012). For many applications including ecosystem net primary production (Goward et al. 1985) and annual evapotranspiration (Sun et al. 2004), that are applied over large areas, the spatial resolution of MODIS phenology data (500m-1,000m) is adequate to describe the biophysical processes. However, other applications such as characterization of bird migrations by the phenological state of vegetation (Wood et al. 2012, Wood and Pidgeon in press) or the habitat selection by red deer (Schaefer et al. 2008) might benefit from a higher spatial resolution. Likewise, successful mapping of tree species in forested landscapes requires an appropriate description of variation in green-leaf phenology at the stand level throughout the year, which is often done by using multi-date imagery (Wolter et al. 1995; Wolter and Townsend 2011; Isaacson et al. 2012). This is because the timing of green-up during the spring and browndown during the fall can vary substantially across different species (Lechowicz 1984; Richardson et al. 2006) as well as within the same species (Crawley & Akheteruzzaman 1988; Luqez et al. 2008).

Landsat satellites provide images at a higher spatial resolution (30m) than MODIS. With now over 40 years of continuous terrestrial observation Landsat satellites provide an unprecedented archive (Loveland and Dwyer 2012). Over the last five years the free and open access to the Landsat archive triggered a proliferation of new products (Woodcock et al. 2008; Wulder et al. 2012). For example, Landsat observations have been used to describe long-term averages of green leaf phenology in New England (USA) (Fisher et al. 2006) and to describe the interannual variability in phenology (Melaas et al. 2013). Despite these new developments in Landsat image processing for phenology, to date a product that describes green leaf phenology within a single year has not yet been available from Landsat data. Here we developed a method to describe the green leaf phenology of a single year at the spatial resolution of Landsat imagery.

One reason why a phenology product is not yet available from Landsat is that, while the spatial (30m) and the spectral resolution of Landsat satellites are ideal to describe green leaf phenology, the temporal resolution (i.e., the number of images per year that are available for the same location) is limited. While every point on the planet can technically be observed on a 16-day repeat cycle, cloud contamination, inconsistent archives or other technical issues cause that for many regions of the world a true 16-day repeat cycle is not achieved. This has limited our ability to extract phenologically meaningful observations in a single year. With the opening of the Landsat archives however, there are now exciting new opportunities to overcome the issue of inadequate temporal resolution. Here, we combined all available Landsat data within a single time series to model green leaf phenology.

When combining multi-year imagery into a time-series set, representing a single year, the challenge is to remove the effect of differences in green leaf phenology between years. In other words, contrary to highlighting phenological differences across years (Melaas et al. 2013) the goal is to eliminate the between-year variation in vegetation phenology to create a synthetic one-year observations of Landsat data. Dynamic Time Warping (DTW) can help to overcome the between-year differences. DTW was originally developed for speech recognition (Sakoe and Chiba 1978), but there is an increasing number of applications of DTW in remote sensing questions, particularly for those involving time-series problems. For example, DTW was used to detect similar cane sugar fields across different regions in Brazil based on Advanced Very High Resolution Radiometer (AVHRR) time series (Romani et al. 2010). Other applications have been more of technical in nature, focusing on the development of segmentation pre-processing methods for the simplified representation of satellite image time series (Weber et al. 2012), image clustering to overcome the issue of irregularly distributed image time series in land-cover classifications (Petitjean et al. 2012), or re-aligning a handful of Landsat observations based on the phenology observed by MODIS and AVHRR data (Huseby et al. 2005). In this work we applied a similar idea to Huseby et al. (2005). However, contrary to Huseby et al (2005) we re-aligned all available Landsat imagery between 2002 and 2012 to simulate daily Landsat EVI observations for a single year.

The aim of DTW is to stretch and compress two time series locally to ultimately make them as similar as possible (Giorgino 2009; Petitjean et al. 2011). The underlying idea is that, while the two time series are potentially very different at a certain day of the year, their overall evolution is very similar. For example, in case of the phenological variation throughout the year, the green-up stage might be slightly offset in different years. However, in every year there will be a green-up stage in natural vegetation canopies and this green-up stage will always precede the maturity stage of the vegetation. In other words, across multiple different years, the phenological evolution over the year will almost always follow a curve reminiscent of a double logistic function, but the parameters of the function will vary across years (Huseby et al. 2005). Thus, given a reference time series data describing vegetation activity (e.g., for the year 2005) and the time series vegetation data of a second, different year (e.g., 2007), the goal is to find for each day in the 2007-data the corresponding day of year in the reference time series. We call the corresponding days of the two time series 'Day-of-Year-matches' (DOY_m), which can be interpreted, for example, that May 15th of the year 2007 corresponds phenologically to May 25th of the reference year (2005). Thus, using DTW we translated the chronological time series into a phenological time series (Huseby et al. 2005).

One main criterion to apply DTW is to have a sufficiently accurate measure to describe the phenology of the two time series. In this work, we used the MODIS Enhanced Vegetation Index (EVI) to find the DOY_m for each day of a year. Using MODIS EVI, we then re-organized a Landsat time series, consisting of all available

Landsat images between 2002 and 2012 to create a new synthetic time series with high temporal resolution and extracted corresponding green leaf phenology data of any year.

Generating a new synthetic dataset inevitably raises questions and concerns regarding its ecological meaning and accuracy. The challenge hereby is to find a benchmark dataset that describes the same phenomenon as the synthetic dataset, but has an independent acquisition strategy. Data from the PhenoCam network fulfill this requirement. They can be used to quantitatively monitor seasonal development of vegetation on the ground at a very high temporal resolution (Richardson et al. 2006; Richardson et al. 2007), and can be linked to remote sensing estimates of phenology such as the timing of spring and autumn, and growing season length (Elmore et al. 2012; Hufkens et al. 2012; White et al. 2009). Here, we compared the ground-based PhenoCam time series pictures to our synthetic Landsat time series using multiple different phenological 'keydates' (e.g., the green up date, the maturity date etc.) that describe the development, maturity, and the senescent of natural vegetation canopies.

Our main goal was to generate a Landsat product that characterizes the phenological evolution of a single year using all available Landsat data between 2002 and 201. Specifically, our objectives were to:

1. use dynamic time warping to create a synthetic, high temporal resolution Landsat time series,
2. use the time series to create a green-leaf phenology product from Landsat,

3. compare the generated Landsat phenology to PhenoCam digital camera time series and the MODIS EVI reference time series based on phenological 'keydates'.

Methods

Study area and datasets

To test the new approach, we chose PhenoCam sites with data over several years with limited or no missing observations (Table 6). We then acquired the corresponding Landsat and MODIS datasets. The datasets were (a) all Landsat images between 2002 and 2012 with cloud coverage of less than 70%, (b) MODIS 8-day surface reflectance composites (MOD09A1 Version 5) between 2002 and 2012 and (c) the PhenoCam photos for the selected years which we analyzed in our study (Table 6).

Dynamic Time Warping to create a Landsat phenology

In a first step we calculated MODIS EVI time series of each year between 2002 and 2012. To do this, we used the 8-day-MODIS surface reflectance values (MOD09A1), of which we calculated the Enhanced Vegetation Index following equation (1):

$$EVI = G \cdot \frac{\rho_{NIR} - \rho_{red}}{\rho_{NIR} + C_1 \cdot \rho_{red} - C_2 \cdot \rho_{blue} + L}$$

where ρ are the atmospherically corrected surface reflectance values, G=2.5, L=1, $C1$=6, $C2$=7.5 are coefficients that describe the aerosol resistance term ($C1$, $C2$), a canopy background adjustment factor (L), and a gain factor (G, Huete et al. (2002)). We then fitted a double logistic function to MODIS EVI time series to estimate the EVI for each day of a target year (Zhang et al. 2006; Zhang et al. 2003). We modified the double logistic function by adding several parameters that controlled the phase of green-up and senescence, as well as a summer green-down parameter to fully capture the phenological dynamics (Elmore et al. 2012; Melaas et al. 2013). We thus estimated the daily EVI (EVI_d) for each year following equation (2):

$$EVI_d(t) = m_1 + (m_2 - m_7 \cdot t) \cdot \left(\frac{1}{1 + e^{m_3 - m_4 \cdot t}} - \frac{1}{1 + e^{m_5 - m_6 \cdot t}}\right)$$

where t is the day of year, m_1 is the minimum EVI and m_2 the amplitude of EVI during the year, $m_{3,4}$ and $m_{5,6}$ are parameters to control the phase of green-up ($m_{3,4}$) and senescence ($m_{5,6}$), and m_7 the summer green-down param parameter (Elmore et al. 2012; Fisher et al. 2006; Melaas et al. 2013). We extracted parameters m_1 and m_2 from the MODIS-EVI time series, the remaining parameters we estimated using the method of least squares by applying the Levenberg-Marquard algorithm (Moré 1978).

In the next step, we selected a reference time series based on the years of interest (i.e., the years that we had PhenoCam observations available). We then calculated the alignment between all available Landsat EVI data and the MODIS reference time series using DTW. In principle, DTW compares two time series with each other and optimally deforms one of the two input time series to the other (Giorgino 2009; Petitjean et al. 2012; Romani et al. 2010). To align the two time series (e.g., the phenology of the year 2004 (P^{04}) to the phenology of the year 2005 (P^{05})), we build a *365*-by-*365* matrix, in which each element (i, j) described the Euclidean distance between two days of the time series P_i^{04} and P_j^{05}. We then calculated all warping-paths $WP = (w_1, w_2, \dots, w_k)$ as the sum of the matrix elements defining the mapping between P^{04} and P^{05} . The optimal warping path was then the path that minimized the overall path-cost through the matrix following equation (3):

$$DTW(P^{04}, P^{05}) = min\left\{\frac{\sqrt{\sum_{k=1}^{K} w_k}}{K}\right\}.$$

We also defined three additional restrictions for the final warping path: (a) the warping path had to start at $w_1 = (1{,}1)$ and end at $w_k = (365{,}365)$ and find for every day in P^{04} a DOY_m in P^{05}, (b) the elements of a warping path must be adjacent to another element of the matrix (continuity), and (c) the points must be monotonically spaced in time (monotonicity) (Giorgino 2009; Romani et al. 2010). The result of this procedure was a vector that contained all DOY_m between P^{04} and P^{05}.

We then applied the DOY_m to the Landsat images from any other year other than the reference year, and assembled them within one dense time series. Every Landsat image of the new time series went then into a pre-processing chain, that involved (a) converting digital numbers into surface reflectance values using the Landsat Ecosystem Disturbance Adaptive Processing System (LEDAPS, Masek et al. 2006), and (b) removing clouds and cloud shadows using Fmask (Zhu and Woodcock 2012). Once the pre-processing was complete, we calculated for every Landsat image the EVI following eq. (1), and generated for every pixel a green leaf phenology curve using eq. (2) and the same parameter estimation strategy.

In the final step, we extracted ecologically important phenological transition dates including the days of (a) the green-up [*GU*], (b) the start of the season [*SoS*], (c) maturity [*Mat*], (d) senescence [*Sen*], (e) the end of the season [*EoS*] and (f) the dormancy [*Dorm*]. These dates (hereafter: referred to as keydates) are extracted by calculating the first and second derivatives of the double-logistic function (Figure 13).

Time-series comparison

After the generation of the dense Landsat time series, we compared our results with (a) a time-series from the PhenoCam-webcam located at our study sites, and (b) the MODIS-EVI time series of the reference year (i.e., the year we time-warped the Landsat images to). To generate the time-series observations from the PhenoCam data, we downloaded all pictures for the site of interest for the reference year from the PhenoCam website. Within each picture, we defined a region of interest that maximized the area of canopy that was consistent across every picture and at the same time excluded sky, understory and forest floor (Richardson et al. 2009; Richardson et al. 2007). We then extracted the DN values of all three channels (red, green and Blue) of each digital picture and calculated the Excess Green Index ExG_M (Hufkens et al. 2012; Sonnentag et al. 2012):

$$ExG_M = 2 \cdot G - (R - B)$$

where *R, G, B* are the are the brightness levels of the green, red and blue channels. We used the freely available MATLAB tool that is available on the PhenoCam-network website (http://phenocam.sr.unh.edu/webcam/). Finally, we fitted a double logistic function to the ExG_M , applying the same parameter estimation method and calculated the keydates corresponding to the PhenoCam data.

Results

Merging all available Landsat data from three sources (e.g. TM5, ETM+, ETM+-SLC-off) between 2002 and 2012 to represent one single year increased the data availability an average of 24.9 times the actual number of observations for that year, with an average of 274 images per year. Qualitatively, applying DTW to re-align Landsat data resulted in Landsat EVI time series that was much more similar to the reference EVI time series from MODIS (Figure 14).

Comparing the Landsat time series and MODIS observations, all keydates showed a higher correlation coefficient compared to the keydate-comparison between Landsat and the PhenoCam data, and this was consistent across all keydates. The correlation coefficients between Landsat and MODIS for each keydate were *GU*=0.97, *SoS*=0.96, *Mat*=0.91, *Sen*=0.76, *EoS*=0.81 and *Dorm*=0.84. Between Landsat and PhenoCam, we found these correlation coefficients to be *GU*=0.80, *SoS*=0.76, *Mat*=0.60, *Sen*=0.03, *EoS*=0.52, *Dorm*=0.55 (Figure 15).

The average differences between estimated keydates were comparatively lower between the Landsat and MODIS time series than between the Landsat and PhenoCam time series (Figure 16). Across study sites and years of analysis, on average all keydates were estimated to occur later in Landsat compared to MODIS: Specifically, the difference in *GU* between Landsat and MODIS was +1.34 days (standard deviation of 2.8 days), *SoS* date +1.23 days (2.21), *Mat* date +1.35 days (3.34 days) and *Sen* date +2.85 days (4.54). Only the *Dorm* date was estimated earlier in Landsat (mean of -0.26 days, standard deviation 3.78 days). For each keydate individually, we found the smallest difference for the *GU* date at the 'Mammothcave' study site and the largest difference at the 'Cary-Institute' study site (-0.44 days vs. +7 days). For the *SoS* date 'Mammothcave' showed the smallest difference and 'Morgan-Monroe' the largest (-1.44 days vs. +4.5 days), the difference in the *Mat* date was smallest at the 'Harvard-Forest' site and largest at 'Morgan-Monroe' (0.25 days vs. 7.75 days), the difference in *Sen* date was on average largest at the 'Mammothcave' site and smallest at 'Arbutuslake' (+10.2 days vs. -0.33 days). The difference in the *EoS* date was largest at the 'Mammothcave' site and smallest at the 'Arbutuslake' site (+6.4 days vs. 0.66 days), and in case of the *Dorm* date we found the largest difference at the 'Cary-Institute' site and the smallest at the 'Bartlett' site (-8.6 days vs. 0.25 days).

For the Landsat-PhenoCam comparison, the differences were comparatively larger and in all cases the keydates were estimated later in the Landsat time series. Specifically, *GU* had a mean difference of +6.82 days (standard deviation 5.24days), *SoS* +10.07 days (6.71), *Mat* +13.9 days (9.27), *Sen* +7.5 days (8.07), *EoS* +2.75 days (6.47) and *Dorm* +10.03 days (8.21). For the different keydates individually the largest and smallest differences were: *GU* date +18 days ('Cary-Institute') vs. +3.25 days ('Bartlett'), *SoS* date +21 days ('Cary-Institute') vs. +5.88 days ('Mammothcave'), *Mat* date +26 days ('Cary-Institute') vs. +6.4 days ('Mammothcave'), *Sen* date +17.6 days ('Cary-Institute') vs. +3 days (‘Arbututslake’), *EoS* date +10.5 days (‘Bartlett’) vs. -2.5 days (‘Morgan-Monroe’), and *Dorm* date 0 days (‘Harvard-Forest’) vs. +21 days (Morgan-Monroe’) (Figure 15).

Discussion

Remote sensing is a useful tool to characterize green leaf phenology across large spatial scales. Several ecological applications such as the estimation of annual evapotranspiration benefit from MODIS derived phenology, available only at 500m spatial resolution. However, other applications such as the characterization of bird migration or the classification of mixed forests would benefit from phenological information at the resolution of Landsat satellites. Here, we described a method that combines Landsat images of multiple years into a single year dense time series. Using Dynamic Time Warping (DTW) to account for interannual differences, we provide a product describing green leaf phenology at the spatial resolution of Landsat satellites.

Our results suggest that by using MODIS EVI time series and DTW to re-align Landsat imagery of multiple years it was possible to generate a temporally very dense time series of Landsat observations. This confirms findings in a study region in Norway using a mix of MODIS and Advanced Very High Resolution Radiometer (AVHRR) NDVI time series (Huseby et al. 2005). However, while Huseby et al. (2005) only used a handful of Landsat imagery, in this study we took advantage of all available Landsat imagery between 2002 and 2012. The use of all available imagery allowed us to create a Landsat dense time series for an entire year, which makes our analysis different from other existing studies that characterized autumn senescence by realigning Landsat imagery (Isaacson et al. 2012). While it is difficult to validate the efficacy of our approach in a quantitative way, the post-DTW time series of Landsat EVI data is much more similar than the pre-warping EVI data to the MODIS EVI time series observations for the same year.

On the other hand, while the overall shape of the time series of greenness observations between Landsat, PhenoCam and MODIS appear very similar, our results suggest certain level of disagreement for the key phenological dates (or keydates), extracted from the same datasets. For example, there is a strong agreement between those keydates extracted from the re-aligned Landsat data and MODIS, but the differences were larger between the Landsat and the PhenoCam and these findings were consistent across locations (Figure 16). Several sources of error are responsible for these differences. First, general differences in how the data are recorded and evaluated may have biased our results. Specifically the camera field of view (FOV) associated with the oblique looking digital pictures strongly affects the agreement between MODIS and PhenoCam at the larger scale (Hufkens et al. 2012). We believe that this effect also shows up in our study. The comparison of Landsat and MODIS intuitively seems 'closer and more intuitive' compared to the Landsat-PhenoCam evaluation, which would explain the relatively higher differences in 'keydates' between the Landsat and PhenoCam time series. Second, the overall differences in how the images (i.e., the different types of satellite images and the digital camera images) were acquired and processed produce uncertainties that ultimately yield the differences between the fitted functions. Thus, we suggest interpreting the observed differences between the time series in our study with caution, as it is impossible to say that one index, or one time series, is 'better' or 'worse' than the other (Richardson et al. 2007). The Landsat green leaf phenology presented here should therefore be seen as an additional measure of green leaf phenology at a finer spatial resolution that complements the existing products from MODIS and PhenoCam. The Landsat green leaf phenology presented here should therefore be seen as an additional measure of green leaf phenology at a finer spatial resolution that complements the existing products from MODIS and PhenoCam.

Our results also suggested that in the Landsat-PhenoCam comparison all keydates were estimated earlier in the PhenoCam time series compared to the Landsat time series. We are not entirely sure as to what causes these larger differences as we anticipated Landsat to be more sensitive to understory greenup, which almost always happens earlier in temperate forest ecosystems. For example, PhenoCam cameras, with the oblique and user-determined view, capture overstory more than the understory. However, Landsat observes the same location from the nadir view angle (or "straight down") and as such assumingly is relatively more sensitive to understory compared to the PhenoCam. Thus, one would assume that especially during the first half of the season keydates to be estimated earlier in Landsat compared to PhenoCam, but our results suggest the opposite. Nevertheless, while not neglecting these observational differences between Landsat and PhenoCam datasets, we note that the primary goal of this study was to create a phenology product from Landsat that was comparable to those from MODIS. With the small differences in keydates between Landsat and

MODIS and the limited influence of the factors 'year' and 'study site', we suggest that the phenology created from Landsat presented here is a useful product that allows for a spatially detailed description of the phenological evolution during the year.

A number of uncertainties also remain. First, we did not test how changes in land cover, for example a clear cut harvest event, may affect the results presented here. Second, our approach, as it is currently implemented, is not an independent approach, but will always require information about yearly 'reference' phenologies from other data sources. Here, we used one data source (i.e., MODIS) but other sensors such as AVHRR could potentially yield similar results and would further allow using Landsat imagery acquired prior to 2002. Third, the slight radiometric differences between Landsat TM5 and ETM+ images might have introduced some noise in our synthetic time series. Fourth, our study is limited to forested landscapes and does not consider agricultural areas, leaving it somewhat uncertain how the approach would perform in agricultural applications.

Green leaf phenology is an important measure to describe the vegetation dynamics throughout a year. Characterizing green leaf phenology at a high spatial resolution might help to map mixed forest stands more accurately or to improve our understanding of other ecological questions such as the interplay of phenological evolution and bird migration. Here, we present an approach to model green leaf phenology at the resolution of Landsat satellites. Our results show that there is substantial agreement between the Landsat phenology and the MODIS reference phenology as well as the phenology on the ground from PhenoCam data. In the short run, this makes the presented green-leaf phenology product being a considerable alternative to existing remote sensing based products, though at a much higher spatial resolution. In the long run, however, the product has the potential to pave the road towards a spatially more detailed of phenological studies and thus to a better understanding on the interaction between the biosphere and climate.

References

1. Asner, G.P., Townsend, A.R., & Braswell, B.H. (2000). Satellite observation of El Nino effects on Amazon forest phenology and productivity. *Geophysical Research Letters*, 27, 981-984
2. Crawley, M.J., & Akhteruzzaman, M. (1988). Individual variation in the phenology of oak trees and its consequences for herbivorous insects. *Functional Ecology*, 2, 409-415
3. Elmore, A.J., Guinn, S.M., Minsley, B.J., & Richardson, A.D. (2012). Landscape controls on the timing of spring, autumn, and growing season length in mid-Atlantic forests. *Global Change Biology*, 18, 656-674
4. Fisher, J.I., Mustard, J.F., & Vadeboncoeur, M.A. (2006). Green leaf phenology at Landsat resolution: Scaling from the field to the satellite. *Remote Sensing of Environment*, 100, 265-279
5. Ganguly, S, Friedl, MA, Tan, B, Zhang, XY, Verma, M. (2010). Land surface phenology from MODIS: Characterization of the Collection 5 global land cover dynamics product. *Remote Sensing of Environment*, 114(8), 1805-1816.
6. Giorgino, T. (2009). Computing and Visualizing Dynamic Time Warping Alignments in R: The dtw Package. *Journal of Statistical Software*, 31, 1-24
7. Goward, S.N., Tucker, C.J., & Dye, D.G. (1985). North-American Vegetation Patterns Observed with the Noaa-7 Advanced Very High-Resolution Radiometer. *Vegetatio*, 64, 3-14

8. Huete, A., Didan, K., Miura, T., Rodriguez, E.P., Gao, X., & Ferreira, L.G. (2002). Overview of the radiometric and biophysical performance of the MODIS vegetation indices. *Remote Sensing of Environment*, 83, 195-213
9. Hufkens, K., Friedl, M., Sonnentag, O., Braswell, B.H., Milliman, T., & Richardson, A.D. (2012). Linking near-surface and satellite remote sensing measurements of deciduous broadleaf forest phenology. *Remote Sensing of Environment*, 117, 307-321
10. Huseby, R.B., Aurdal, L., Eikvil, L., Solberg, R., Vikhamar, D., & Solberg, A. (2005). Alignment of growth seasons from satellite data. *2005 International Workshop on the Analysis of Multi-Temporal Remote Sensing Images* (IEEE Cat. No. 05EX1064), 213-216
11. Isaacson, B., Serbin, S., & Townsend, P. (2012). Detection of relative differences in phenology of forest species using Landsat and MODIS. *Landscape Ecology*, 27, 529-543
12. Knudby, A. (2004). An AVHRR-based model of groundnut yields in the peanut basin of senegal. *International Journal of Remote Sensing*, 25, 3161-3175
13. Lechowicz, M.J. (1984). Why do Temperate decidious Trees leaf out at different Times - Adaptation and Ecology of Forest Communities. *American Naturalist*, 124, 821-842
14. Loveland, T.R., & Dwyer, J.L. (2012). Landsat: Building a strong future. *Remote Sensing of Environment,* 122, 22-29
15. Luquez, V., Hall, D., Albrectsen, B.R., Karlsson, J., Ingvarsson, P., & Jansson, S. (2008). Natural phenological variation in aspen (Populus tremula): the SwAsp collection. *Tree Genetics & Genomes*, 4, 279-292

16. Masek, J.G., Vermote, E.F., Saleous, N.E., Wolfe, R., Hall, F.G., Huemmrich, K.F., Feng, G., Kutler, J., & Teng-Kui, L. (2006). A Landsat surface reflectance dataset for North America, 1990-2000. *Geoscience and Remote Sensing Letters, IEEE,* 3, 68-72

17. Melaas, E.K., Friedl, M.A., & Zhu, Z. (2013). Detecting interannual variation in deciduous broadleaf forest phenology using Landsat TM/ETM+ data. *Remote Sensing of Environment*, 132, 176-185

18. Moré, J. (1978). The Levenberg-Marquardt algorithm: Implementation and theory. In G.A. Watson (Ed.*), Numerical Analysis* (pp. 105-116): Springer Berlin Heidelberg

19. Paruelo, J.M., Epstein, H.E., Lauenroth, W.K., & Burke, I.C. (1997). ANPP estimates from NDVI for the Central Grassland Region of the United States. *Ecology*, 78, 953-958

20. Petitjean, F., Inglada, J., & Gancarski, P. (2012). Satellite Image Time Series Analysis Under Time Warping*. IEEE Transactions on Geoscience and Remote Sensing*, 50, 3081-3095

21. Petitjean, F., Ketterlin, A., & Gancarski, P. (2011). A global averaging method for dynamic time warping, with applications to clustering. *Pattern Recognition*, 44, 678-693

22. Richardson, A.D., Bailey, A.S., Denny, E.G., Martin, C.W., & O'Keefe, J. (2006). Phenology of a northern hardwood forest canopy. *Global Change Biology*, 12, 1174-1188

23. Richardson, A.D., Braswell, B.H., Hollinger, D.Y., Jenkins, J.P., & Ollinger, S.V. (2009). Near-surface remote sensing of spatial and temporal variation in canopy phenology. *Ecological Applications,* 19, 1417-1428

24. Richardson, A.D., Jenkins, J.P., Braswell, B.H., Hollinger, D.Y., Ollinger, S.V., & Smith, M.L. (2007). Use of digital webcam images to track spring green-up in a deciduous broadleaf forest. *Oecologia*, 152, 323-334

25. Roetzer, T., Wittenzeller, M., Haeckel, H., & Nekovar, J. (2000). Phenology in central Europe - differences and trends of spring phenophases in urban and rural areas. *International Journal of Biometeorology*, 44, 60-66

26. Romani, L.A.S., Goncalves, R.R.V., Zullo, J., Traina, C., Jr., & Traina, A.J.M. (2010). New DTW-based method to similarity search in sugar cane regions represented by climate and remote sensing time series. In, Geoscience and Remote Sensing Symposium (IGARSS), 2010 *IEEE International* (pp. 355-358)

27. Sakoe, H., & Chiba, S. (1978). Dynamic-Programming Algorithm Optimization for Spoken Word Recognition. *IEEE Transactions on Acoustics Speech and Signal Processing*, 26, 43-49

28. Schaefer, J.A., Morellet, N., Pepin, D., & Verheyden, H. (2008). The spatial scale of habitat selection by red deer. *Canadian Journal of Zoology-Revue Canadienne De Zoologie*, 86, 1337-1345

29. Sonnentag, O., Hufkens, K., Teshera-Sterne, C., Young, A.M., Friedl, M., Braswell, B.H., Milliman, T., O'Keefe, J., & Richardson, A.D. (2012). Digital repeat

photography for phenological research in forest ecosystems. *Agricultural and Forest Meteorology*, 152, 159-177

30. Sun, R., Gao, X., Liu, C.M., & Li, X.W. (2004). Evapotranspiration estimation in the Yellow River Basin, China using integrated NDVI data. *International Journal of Remote Sensing*, 25, 2523-2534
31. Tucker, C.J., Fung, I.Y., Keeling, C.D., & Gammon, R.H. (1986). Relationship between Atmospheric Co2 Variations and a Satellite-Derived Vegetation Index. *Nature*, 319, 195-199
32. Weber, J., Petitjean, F., & Gancarski, P. (2012). Towards efficient satellite image time series analysis: Combination of dynamic time warping and quasi-flat zones. In, Geoscience and Remote Sensing Symposium (IGARSS), 2012 *IEEE International* (pp. 4387-4390)
33. White, M.A., de Beurs, K.M., Didan, K., Inouye, D.W., Richardson, A.D., Jensen, O.P., O'Keefe, J., Zhang, G., Nemani, R.R., van Leeuwen, W.J.D., Brown, J.F., de Wit, A., Schaepman, M., Lin, X.M., Dettinger, M., Bailey, A.S., Kimball, J., Schwartz, M.D., Baldocchi, D.D., Lee, J.T., & Lauenroth, W.K. (2009). Intercomparison, interpretation, and assessment of spring phenology in North America estimated from remote sensing for 1982-2006. *Global Change Biology*, 15, 2335-2359
34. Wolfe, D.W., Schwartz, M.D., Lakso, A.N., Otsuki, Y., Pool, R.M., & Shaulis, N.J. (2005). Climate change and shifts in spring phenology of three horticultural woody perennials in northeastern USA. *International Journal of Biometeorology*, 49, 303-309

35. Wolter, P.T., Mladenoff, D.J., Host, G.E., & Crow, T.R. (1995). Improved Forest Classification in the Northern Lake-States using Multitemporal Landsat Imagery. *Photogrammetric engineering and remote sensing*, 61, 1129-1143

36. Wolter, P.T., & Townsend, P.A. (2011). Multi-sensor data fusion for estimating forest species composition and abundance in northern Minnesota. *Remote Sensing of Environment*, 115, 671-691

37. Wood EM, Pidgeon AM. Tree phenology, migratory songbirds, and climate variation: a precautionary approach suggests managing for tree heterogeneity. *Studies in Avian Biology*, in press.

38. Wood, E.M., Pidgeon, A.M., Liu, F., & Mladenoff, D.J. (2012). Birds see the trees inside the forest: The potential impacts of changes in forest composition on songbirds during spring migration. *Forest Ecology and Management*, 280, 176-186

39. Woodcock, C.E., Allen, R., Anderson, M., Belward, A., Bindschadler, R., Cohen, W., Gao, F., Goward, S.N., Helder, D., Helmer, E., Nemani, R., Oreopoulos, L., Schott, J., Thenkabail, P.S., Vermote, E.F., Vogelmann, J., Wulder, M.A., & Wynne, R. (2008). Free access to Landsat imagery. *Science*, 320, 1011-1011

40. Wulder, M.A., Masek, J.G., Cohen, W.B., Loveland, T.R., & Woodcock, C.E. (2012). Opening the archive: How free data has enabled the science and monitoring promise of Landsat. *Remote Sensing of Environment*, 122, 2-10

41. Zhang, X.Y., Friedl, M.A., & Schaaf, C.B. (2006). Global vegetation phenology from Moderate Resolution Imaging Spectroradiometer (MODIS): Evaluation of global

patterns and comparison with in situ measurements. *Journal of Geophysical Research-Biogeosciences*, 111

42. Zhang, X.Y., Friedl, M.A., Schaaf, C.B., Strahler, A.H., Hodges, J.C.F., Gao, F., Reed, B.C., & Huete, A. (2003). Monitoring vegetation phenology using MODIS. *Remote Sensing of Environment*, 84, 471-475

43. Zhu, Z., & Woodcock, C.E. (2012). Object-based cloud and cloud shadow detection in Landsat imagery. *Remote Sensing of Environment*, 118, 83-94

Figure Captions

Figure 13: Example of the three phenology-profiles (Landsat, PhenoCam and MODIS) and the estimation strategy of the keydates. The top row represents the EVI/ExGm time series, whereas the middle and bottom row represent the first and second derivative of the phenology-profiles. The keydates are (chronologically with the year): green-up date (GU, red line), Start-of-Season date (SoS, blue line), Maturity date (Mat, orange line), Senescence date (Sen, green line), the End-of-Season date (EoS, light blue line), and Dormancy date (Dorm, yellow line). The example represents the Mammothcave study site for the year 2012.

Figure 14: Comparison of the Landsat-time series ‘unwarped’ vs. ‘warped’, the example is the Mammothcave study site for the year 2012. The red dots are Landsat EVI values from 2012, the grey dots indicate Landsat EVI data from all other years that got time-warped to the reference year. The black line represents the MODIS EVI from the reference year 2012.

Figure 15: Scatterplots and correlation coefficients to assess the differences in the keydates between Landsat and PhenoCam time series (top), and Landsat and MODIS time series (bottom). All points represent one year of analysis at one study site. The colors represent the different study sites.

Figure 16: Differences in estimated keydates at the different study sites. The top row represents the Landsat-MODIS comparison, the bottom row the Landsat-PhenoCam comparison. The points describe the mean difference in estimated keydates across all years that were analyzed at each particular study sites. The error bars show the standard deviation of the keydate estimations.

Figure 17: Example of daily EVI time series between 2003 and 2012 at the Mammothcave study site. The EVI maps represent a 500x500 pixel subset around the location of the PhenoCam on day of year 200. The EVI curves represent the modeled phenology for Landsat and PhenoCam at the PhenoCam location.

Figure 18: Comparison of the MODIS phenology and the newly generated Landsat phenology. Presented are the estimated keydates GU, SoS, Mat (left column top to bottom) and Sen, EoS and Dorm (right column). In addition, the phenology at the approximate location of the PhenoCam is presented. The example shows the case of the Mammothcave study region for the year 2012

Tables

Table 6: Study sites and datasets, used in the study. Years indicate the years with complete phenology in the PhenoCam-data.

Study Site Name	Years	Landsat Path/Row (# images)	MODIS footprint	Characterization
Bartlett	2008, 2009, 2011, 2012	012/029 (257)	h12 v04	Mixed forest, deciduous species dominant, some understory
Mammothcave	2003, 2004, 2005, 2006, 2008, 2009, 2011, 2012	021/034 (254)	h11 v05	Decidious forest, amount of understory unclear
Harvard-Forest	2009, 2010, 2011, 2012	013/030 (215)	h12 v04	Mostly deciduous, some coniferous, understory present
Cary-Institute	2010, 2011, 2012	014/031 (268)	h12 v04	Mostly deciduous, view from side, amount of understory unclear
Arbutuslake	2009, 2010, 2012	015/029 (242)	h12 v04	Mostly deciduous, in background more coniferous, only little understory
Morgan-Monroe	2009, 2010, 2011, 2012	021/033 (285)	h11 v05	Dominant deciduous, little understory
Univ. Michigan Biolog. Station	2010, 2011, 2012	021/028 (257)	h12 v04	Mostly deciduous, some coniferous in the foreground, understory

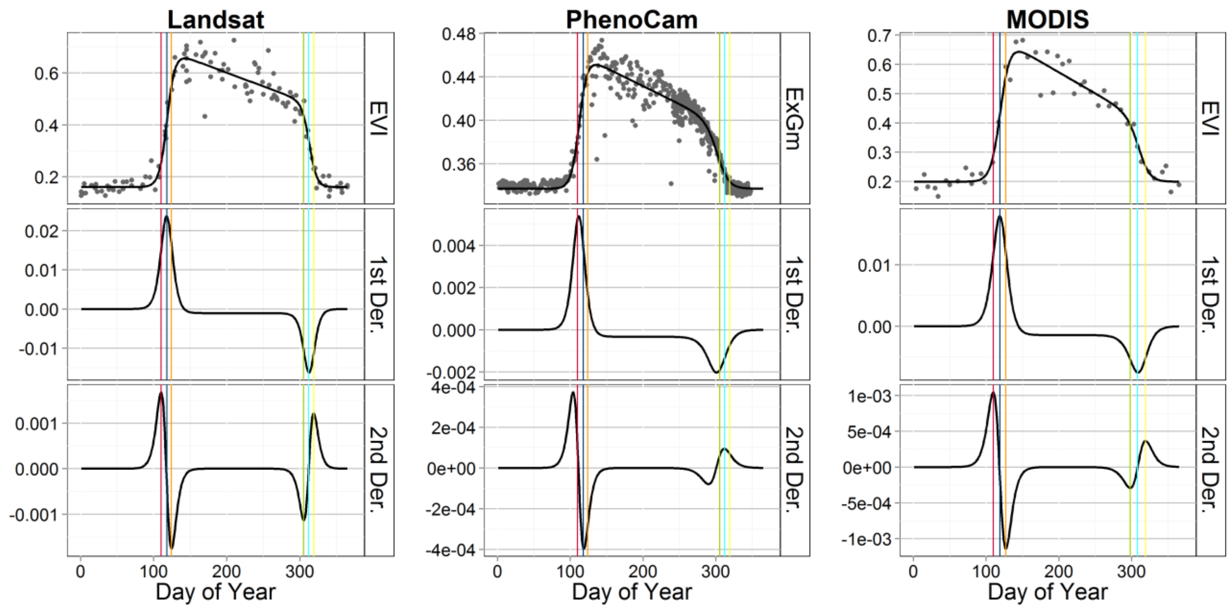

Landsat
PhenoCam
MODIS
EVI
ExGm
EVI
1st Der.
2nd Der.
Day of Year

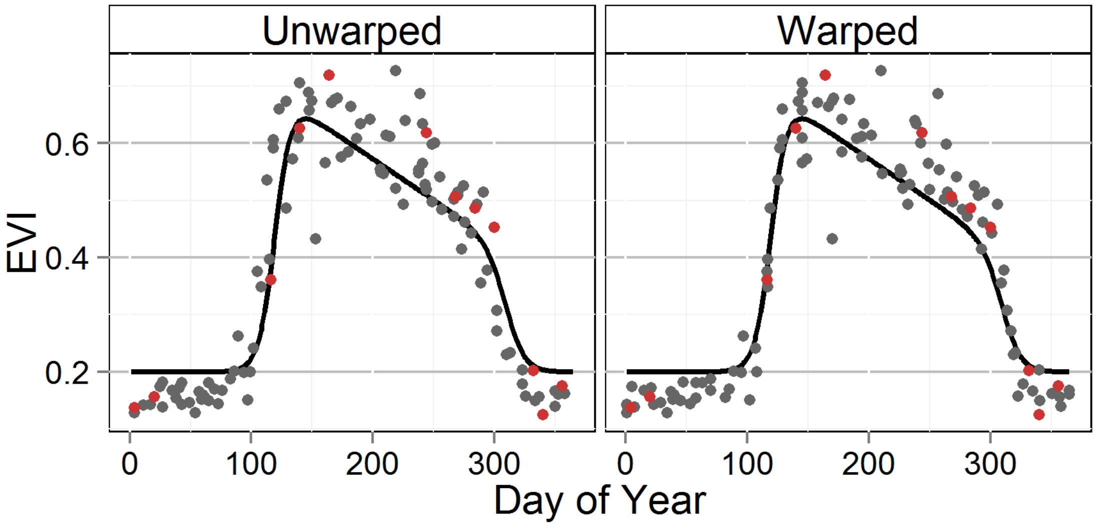
Unwarped
Warped
EVI
0.6
0.4
0.2
0
100
200
300
Day of Year

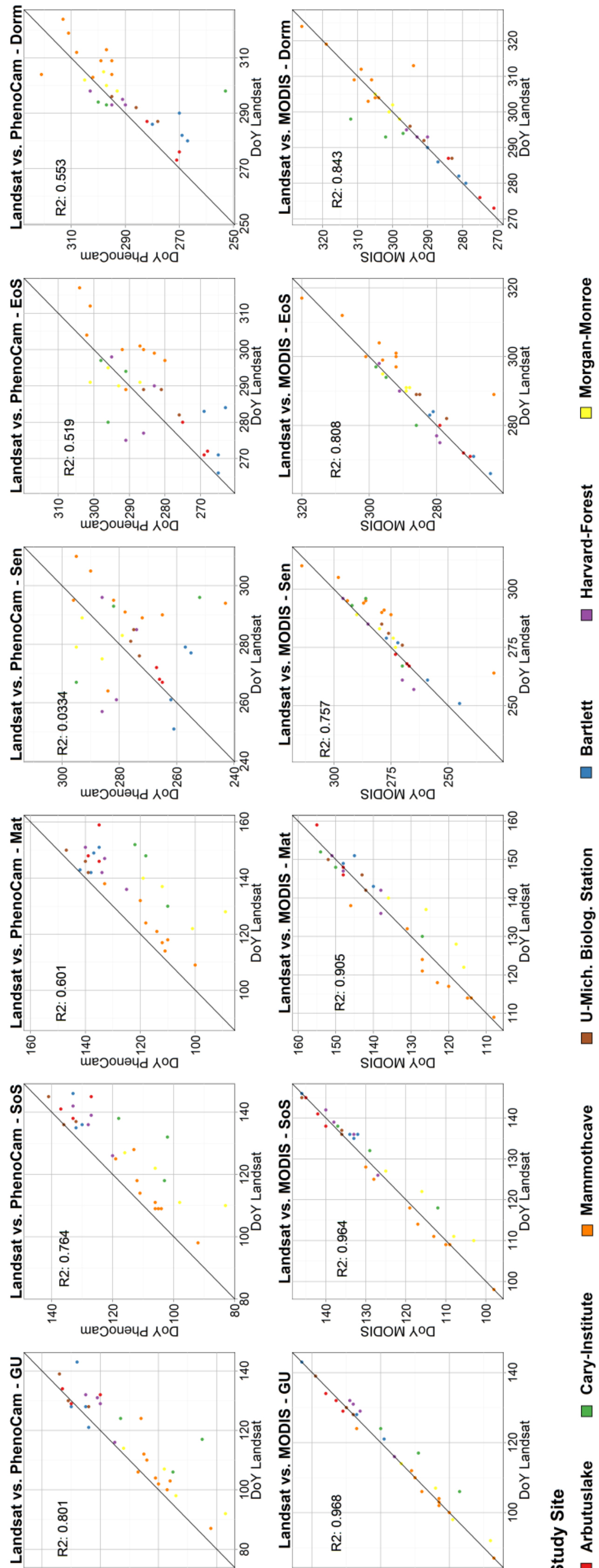
Landsat vs. PhenoCam - GU
R2: 0.801
Landsat vs. PhenoCam - SoS
R2: 0.764
Landsat vs. PhenoCam - Mat
R2: 0.601
Landsat vs. PhenoCam - Sen
R2: 0.0334
Landsat vs. PhenoCam - EoS
R2: 0.519
Landsat vs. PhenoCam - Dorm
R2: 0.553
Landsat vs. MODIS - GU
R2: 0.968
Landsat vs. MODIS - SoS
R2: 0.964
Landsat vs. MODIS - Mat
R2: 0.905
Landsat vs. MODIS - Sen
R2: 0.757
Landsat vs. MODIS - EoS
R2: 0.808
Landsat vs. MODIS - Dorm
R2: 0.843
DoY PhenoCam
DoY MODIS
DoY Landsat
Study Site
Arbutuslake
Cary-Institute
Mammothcave
U-Mich. Biolog. Station
Bartlett
Harvard-Forest
Morgan-Monroe

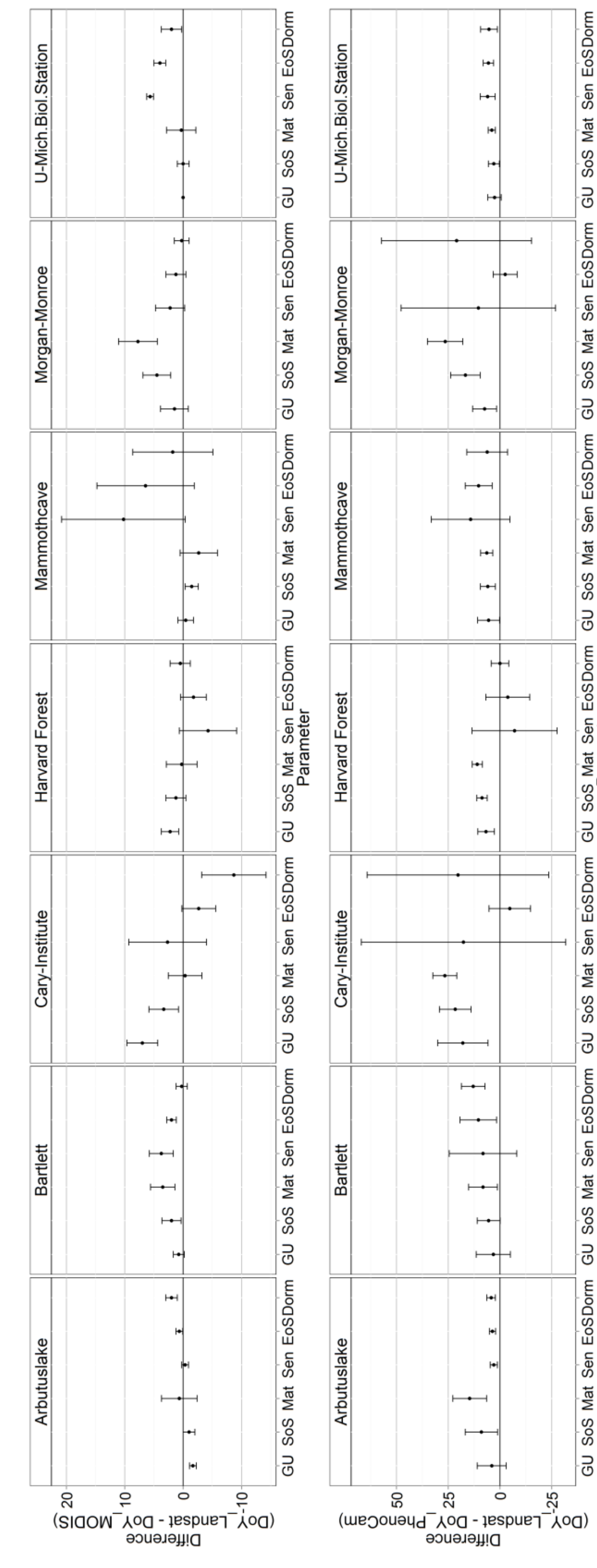
Arbutuslake
Bartlett
Cary-Institute
Harvard Forest
Mammothcave
Morgan-Monroe
U-Mich.Biol.Station
GU SoS Mat Sen EoSDorm
Parameter
Difference
(DoY_Landsat - DoY_MODIS)
20
10
0
-10
(DoY_Landsat - DoY_PhenoCam)
50
25
0
-25

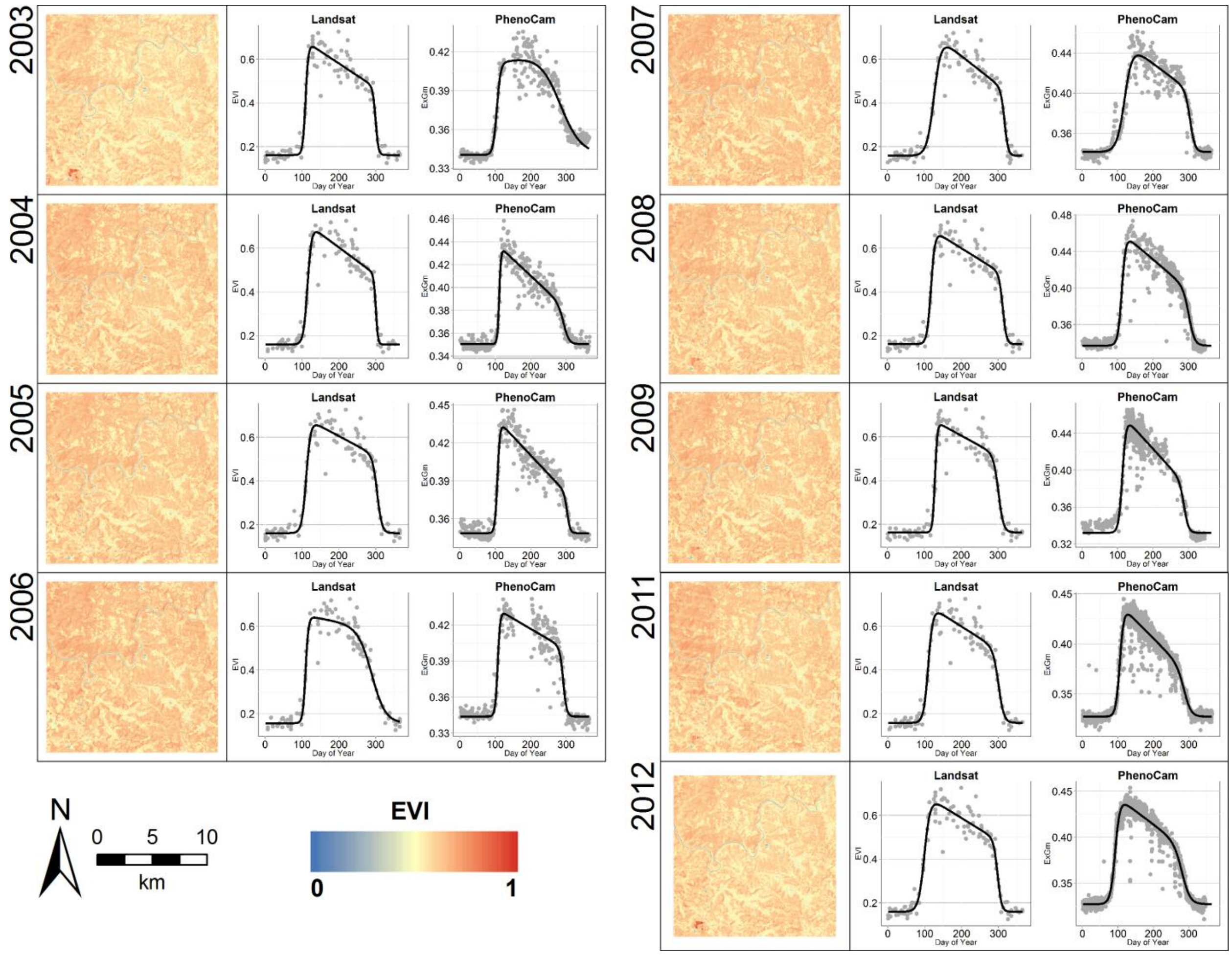
2003
2004
2005
2006
2007
2008
2009
2011
2012
Landsat
PhenoCam
Day of Year
EVI
ExGm
N
0 5 10
km
EVI
0
1

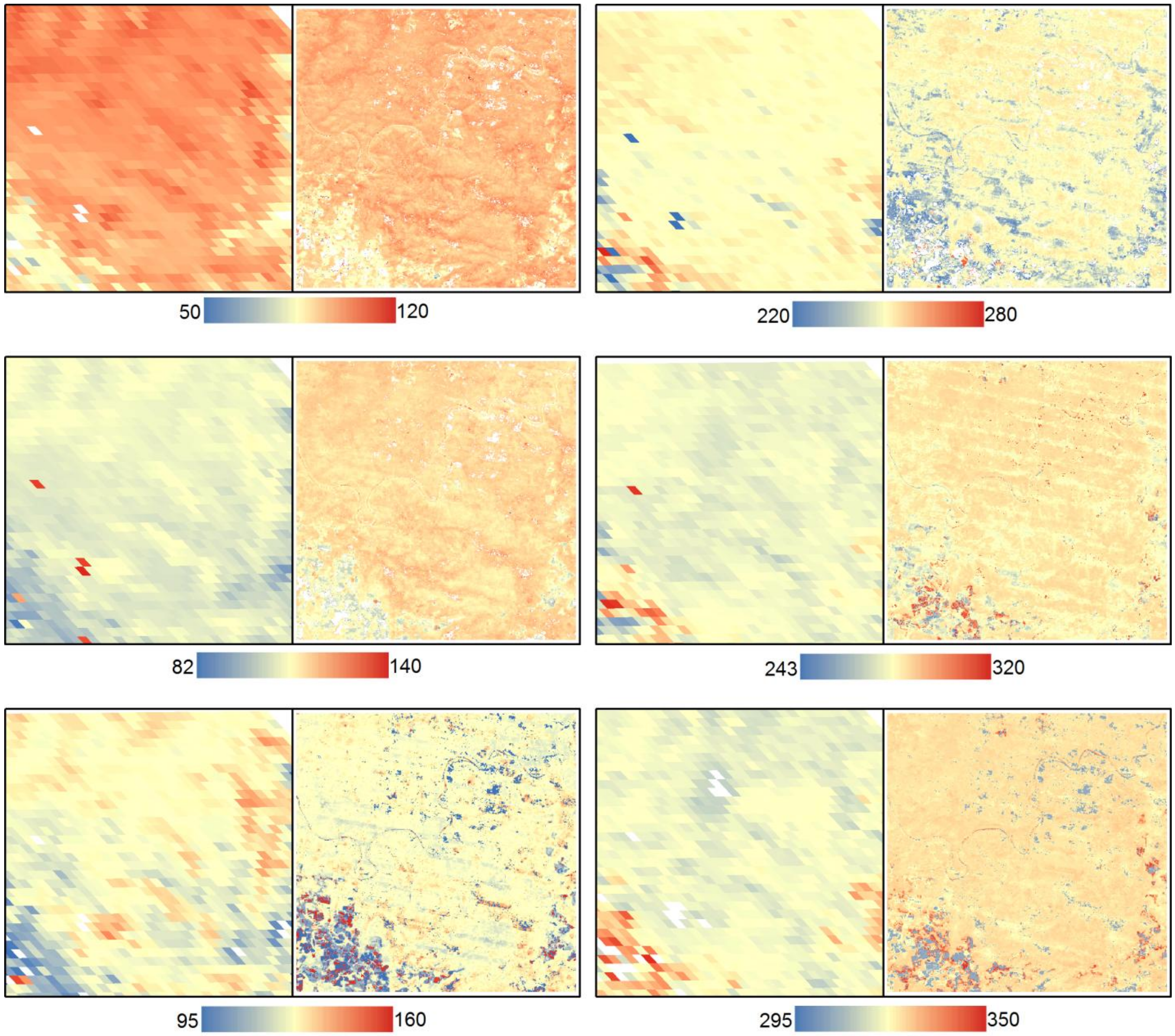
50
120
220
280
82
140
243
320
95
160
295
350

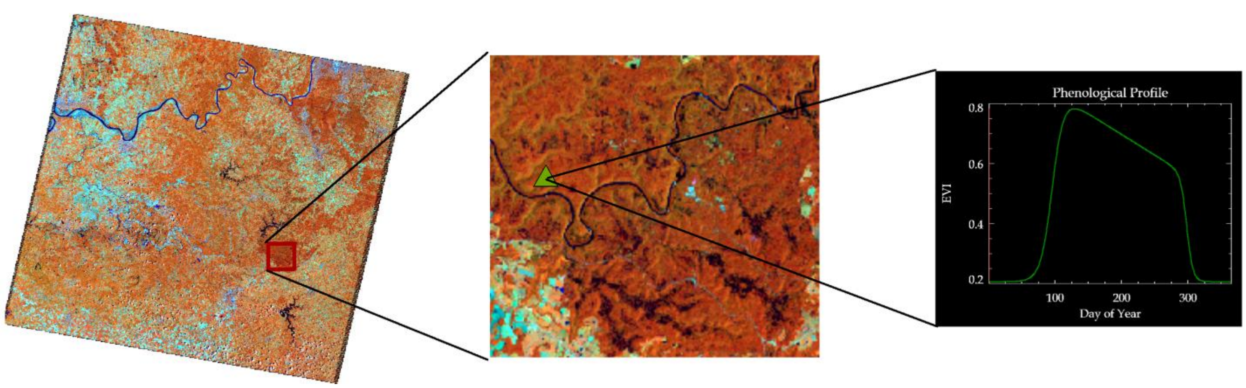
Phenological Profile
0.8
0.6
0.4
0.2
EVI
100
200
300
Day of Year